CNS pharmacology of NKCC1 inhibitors*

Loescher, Wolfgang

2022-03-01

Loescher , W & Kaila , K 2022 , ' CNS pharmacology of NKCC1 inhibitors* ' , Neuropharmacology , vol. 205 , 108910 . https://doi.org/10.1016/j.neuropharm.2021.108910

http://hdl.handle.net/10138/343598
https://doi.org/10.1016/j.neuropharm.2021.108910

Neuropharmacology 205 (2022) 108910

Contents lists available at ScienceDirect

Neuropharmacology

journal homepage: www.elsevier.com/locate/neuropharm

CNS pharmacology of NKCC1 inhibitors☆

Wolfgang Löscher [a,b,*], Kai Kaila [c,**]

[a] Dept. of Pharmacology, Toxicology, and Pharmacy, University of Veterinary Medicine Hannover, Germany
[b] Center for Systems Neuroscience Hannover, Germany
[c] Molecular and Integrative Biosciences and Neuroscience Center (HiLIFE), University of Helsinki, Finland

ARTICLE INFO

Keywords:
NKCC1
Bumetanide
Epilepsy
Neonatal
Prodrugs
Autism
Brain injury

ABSTRACT

The Na–K–2Cl cotransporter NKCC1 and the neuron-specific K–Cl cotransporter KCC2 are considered attractive CNS drug targets because altered neuronal chloride regulation and consequent effects on GABAergic signaling have been implicated in numerous CNS disorders. While KCC2 modulators are not yet clinically available, the loop diuretic bumetanide has been used in clinical studies to treat brain disorders and as a tool for NKCC1 inhibition in preclinical models. Bumetanide is known to have anticonvulsant and neuroprotective effects under some pathophysiological conditions. However, as shown in several species from neonates to adults (mice, rats, dogs, and by extrapolation in humans), at the low clinical doses of bumetanide approved for diuresis, this drug has negligible access into the CNS, reaching levels that are much lower than what is needed to inhibit NKCC1 in cells within the brain parenchyma. Several drug discovery strategies have been used over the last ~15 years to develop brain-permeant compounds that, ideally, should be selective for NKCC1 to eliminate the diuresis mediated by inhibition of renal NKCC2. The strategies employed to improve the pharmacokinetic and pharmacodynamic properties of NKCC1 blockers include evaluation of other clinically approved loop diuretics; development of lipophilic prodrugs of bumetanide; development of side-chain derivatives of bumetanide; and unbiased high-throughput screening approaches of drug discovery based on large chemical compound libraries. The main outcomes are that (1), non-acidic loop diuretics such as azosemide and torasemide may have advantages as NKCC1 inhibitors vs. bumetanide; (2), bumetanide prodrugs achieve significantly higher brain levels of the parent drug and have lower diuretic activity; (3), the novel bumetanide side-chain derivatives do not exhibit any functionally relevant improvement of CNS accessibility or NKCC1 selectivity vs. bumetanide; (4) novel compounds discovered by high-throughput screening may resolve some of the inherent problems of bumetanide, but as yet this has not been achieved. Thus, further research is needed to optimize the design of brain-permeant NKCC1 inhibitors. Another major challenge is to identify the mechanisms whereby various NKCC1-expressing cellular targets of these drug within (e.g., neurons, oligodendrocytes or astrocytes) and outside the brain parenchyma (e.g., blood-brain barrier, choroid plexus, endocrine and immune system), as well as molecular off-target effects, might contribute to their reported therapeutic and adverse effects.

1. Introduction

The electroneutral Na–K–2Cl cotransporter isoform NKCC1 (Fig. 1A, B) belongs to the Na^+-dependent subgroup of solute carrier 12 (SLC12) family of secondary-active ion transporters (Russell, 2000; Markadieu and Delpire, 2014; Mahadevan and Woodin, 2020).). Altered neuronal

Abbreviations: AQP, aquaporin; ASD, autism spectrum disorder; BBB, blood-brain barrier; CA, carbonic anhydrase; $[Cl^-]i$, intracellular Cl^- concentration; CSF, cerebrospinal fluid; DIMAEB, dimethylaminoethyl ester of bumetanide; DS, Down syndrome; GDP, giant depolarizing potential; HEK, human embryonic kidney; HPA, hypothalamic-pituitary-adrenal; HPD, hippocampal paroxysmal discharge; KCC, K–Cl cotransporter; KO, knockout; MCT, monocarboxylate transporter; NKCC, Na–K–2Cl cotransporter; OAT, organic anion transporter; OATP, organic anion-transporting polypeptide; OSR1, oxidative stress-responsive kinase; PB, phenobarbital; PBO, piperonyl butoxide; SE, status epilepticus; SLC, solute carrier; SPAK, Ste20-related proline-alanine-rich kinase; TLE, temporal lobe epilepsy; TM, transmembrane helix; TSC, tuberous sclerosis complex; WNK, with no lysine kinase.

☆ We dedicate this work to our late colleague, Dr. Peter W. Feit, who discovered bumetanide and contributed significantly to several of the studies reviewed here.

* Corresponding author. Dept. of Pharmacology, Toxicology, and Pharmacy, University of Veterinary Medicine Hannover, Germany.
** Corresponding author.
E-mail addresses: wolfgang.loescher@tiho-hannover.de (W. Löscher), kai.kaila@helsinki.fi (K. Kaila).

https://doi.org/10.1016/j.neuropharm.2021.108910
Received 21 June 2021; Received in revised form 25 November 2021; Accepted 26 November 2021
Available online 6 December 2021

chloride regulation leading to an increased intracellular Cl^- concentration ($[Cl^-]_i$) has been implicated in numerous CNS disorders, including neonatal seizures, acquired epilepsy, autism, cerebral edema after ischemic and traumatic brain injury, as well as in swelling-related neurodegeneration and neuropathic pain (Kahle et al., 2008; Kaila et al., 2014a,b; Puskarjov et al., 2014; Huang et al., 2019a; Auer et al., 2020a; Savardi et al., 2021). Thus, NKCC1 (encoded by *SLC12A2*), which takes up chloride ions, and the neuron-specific K–Cl cotransporter, KCC2 (*SLC15A2*), which extrudes chloride (Fig. 2A), are highly interesting pharmacological targets for basic research as well as for CNS drug development. While as yet no drugs are clinically available that modulate KCC2, bumetanide (Fig. 1C) is a relatively specific inhibitor of NKCC1 at low concentrations (depending on the preparation, ~0.2–10 μmol/l) (Russell, 2000). However, in addition to blocking NKCC1, bumetanide is a potent FDA-approved diuretic, which acts by blocking the isoform NKCC2 (*SLC12A1*), located in the loop of Henle in the kidneys (Roush et al., 2014; Oh and Han, 2015).

Bumetanide is widely used to inhibit NKCC1 in both experimental and clinical studies, although its clinical use in the treatment of brain disorders is off-label (see also Kharod et al., 2019). Bumetanide has been shown to exert antiseizure and neuroprotective actions in vitro or when applied directly to the brain parenchyma (see below). There is limited evidence that systemically applied (per os, i.p, or i.v.) bumetanide might be beneficial in some CNS disorders, particularly in autism spectrum disorders (ASD); however, two recent phase 3 clinical trials assessing bumetanide in the treatment of ASD in children and adolescents showed no effectiveness (section 5).

It is of utmost importance to recognize that bumetanide has negligible CNS accessibility (section 2.5), which was first demonstrated already in 1993 by cerebrospinal fluid (CSF) drug analysis in dogs (Javaheri et al., 1993). This fact has been totally ignored in much of the work done during the last 3 decades. Indeed, clinically relevant doses

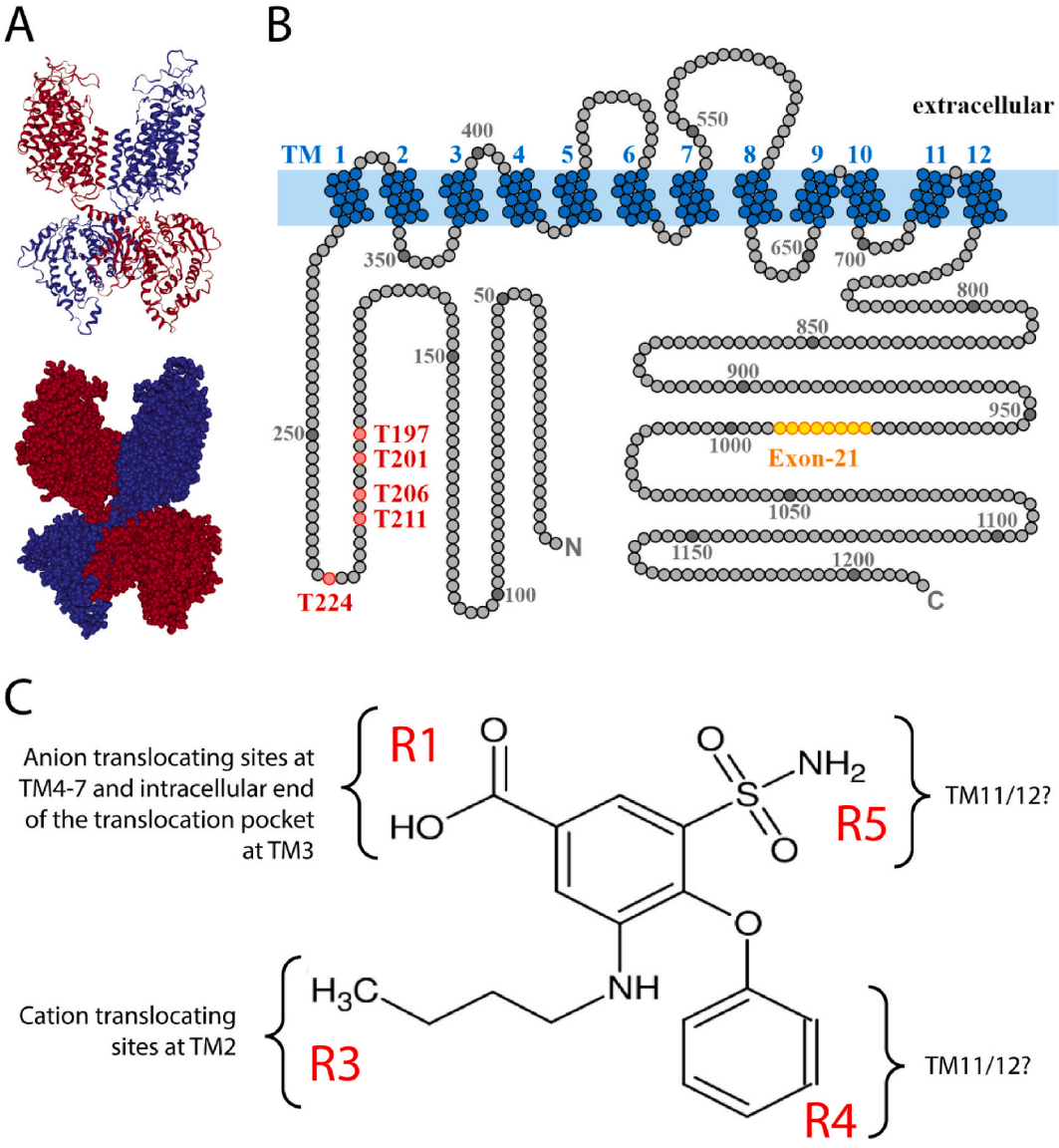

Fig. 1. NKCC1 protein structure and binding sites of bumetanide. (A) The dimer structure of NKCC1 shown as 3D ribbon model (upper) and a space-filling model (lower), with the two monomers shown in different colours (red, blue). (B) Schematic representation of NKCC1 secondary structure showing the 12 transmembrane domains (TM) and the intracellular N- and C-terminal domains. Phosphorylation sites are indicated in red, and the alternatively spliced region (which is present in the NKCC1a but not in the NKCC1b isoform) encoded by exon 21 is highlighted in yellow. Adapted from Virtanen et al. (2020). (C) Molecular structure of bumetanide and its binding sites in NKCC1 and NKCC2. Bumetanide is assumed to possess four potential binding groups (R1, R3, R4, R5). Assignment of binding groups is based on the work of Isenring et al. (1998a,b) and Somasekharan et al. (2012). Adapted from Hannaert et al. (2002). The structure-activity data on bumetanide side-chain derivatives described in section 3.3 substantiate the conclusions implicit in this figure.

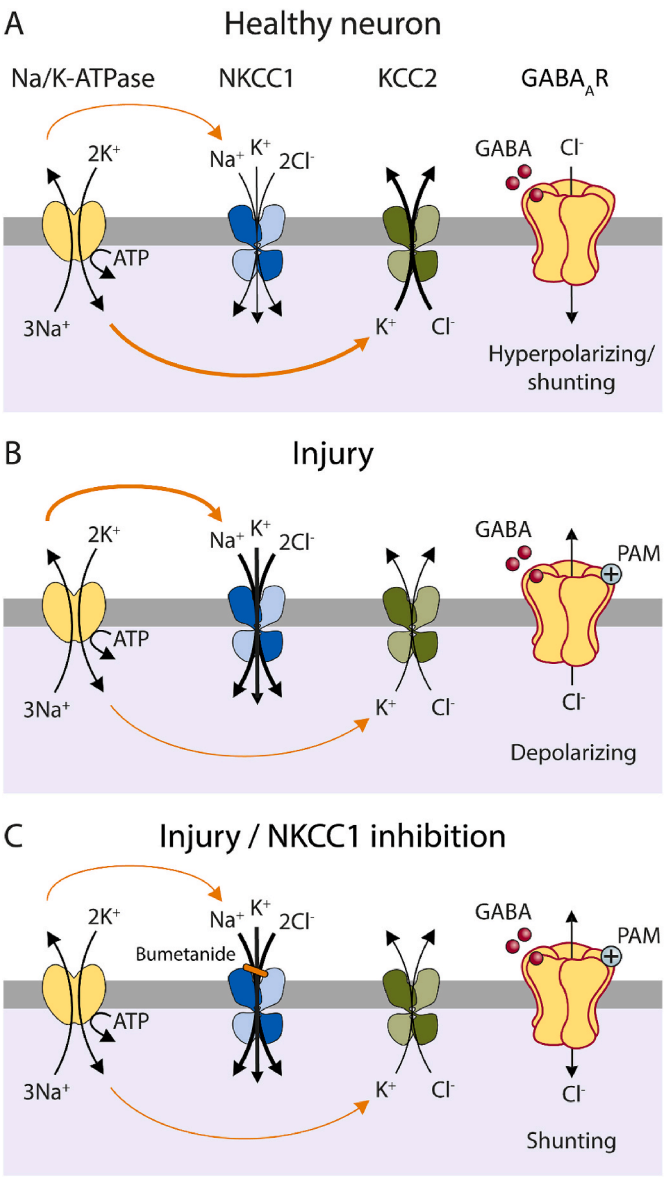

Fig. 2. Model of the shift from hyperpolarizing to depolarizing GABA action in CNS neurons caused by changes in the expression levels of postsynaptic NKCC1 and KCC2 upon brain injury. (A) NKCC1 and KCC2 are secondary active transporters that, under physiological conditions, mediate neuronal Cl^- uptake, and extrusion, respectively. Net ion transport by NKCC1 and KCC2 is fueled by the Na^+ and K^+ chemical gradients generated by the Na–K ATPase (not illustrated). The ion stoichiometry of NKCC1 and KCC2 renders them electrically silent (electroneutral). In healthy cortical neurons of human neonates and adults, Cl^- extrusion via KCC2 is highly active and able to maintain a hyperpolarizing Cl^- current during the inhibitory shunting action of $GABA_A$ receptor activation (for discussion, see Kaila et al., 2014a). (B) After brain injury, KCC2 is often promptly down-regulated along with functional up-regulation of NKCC1, and the direction of the Cl^- current is reversed leading to depolarizing GABA responses. Under these conditions, the application of positive allosteric modulators (PAMs) of $GABA_A$ receptors (e.g., barbiturates, benzodiazepines, and others) can lead to aggravation of seizures promoted by the depolarizing and sometimes frankly excitatory Cl^- current. (C) Pharmacologic block of NKCC1 by bumetanide or other NKCC1 inhibitors attenuates or abolishes the depolarizing drive of $GABA_A$-mediated Cl^- current, and subsequent application of positive modulators of $GABA_A$ receptors will at least partly restore shunting inhibition. This topic is extensively discussed in the text.

(~0.1–0.3 mg/kg) applied in numerous rodent models of CNS disorders are much too low to achieve bumetanide levels in the brain that would be high enough to significantly inhibit NKCC1 in neurons (or in glia; see below). This is also a major problem in the interpretation of the results of all clinical trials on bumetanide in humans, ranging from neonatal asphyxia seizures to epilepsy and neuropsychiatric diseases (see section 5). In rats and mice, the consequences of the low CNS accessibility, which is attributable to poor blood-brain barrier (BBB) permeability, are accentuated by the fast metabolism of the drug (section 2.5). However, there are regions in the brain with a 'leaky' BBB, which may permit much more effective bumetanide tissue penetration (but see section 5). This is a characteristic of areas involved in neuroendocrine signaling. Our discussions below on the extremely low BBB permeability of bumetanide and related compounds are mainly focused on cortical and hippocampal areas, in which most of the work of NKCC1 blockers has been done.

In addition to an enhanced BBB permeability, achieving an increased molecular target selectivity for NKCC1 vs. NKCC2 has been a goal in drug discovery programs to reduce or abolish the NKCC2-mediated diuretic activity of the compounds. Acute and chronic diuresis are not merely inconvenient side effects of bumetanide and related drugs. Drug-induced diuresis will have an effect on hydration and water consumption of the organism; and on extracellular space (ECS) volume in the brain which, in turn, affects neuronal excitability and seizure propensity (section 5). Moreover, systems-level water homeostasis has numerous connections to endocrine mechanisms via vasopressinergic and other CNS-wide signaling mechanisms (Bankir et al., 2017). Diuresis as such has quite obviously a major effect in clinical trials, making fully 'blind' experiments impossible, unless another diuretic compound plus an inert placebo would be used. In fact, we are not aware of any prospective clinical trials on bumetanide actions with this kind of a three-tier design.

There are major conundrums regarding the CNS actions of bumetanide. First of all, it has become clear that *the expression levels of NKCC1 in neurons are very low compared to numerous other cell types in the brain* (section 4). And, as will be discussed below, the drug and some of its poorly BBB-permeable derivatives have been reported to exert beneficial actions in some animal models of brain disorders, including epilepsy, neonatal seizures, autism, and anxiety, even when applied in vivo at doses which are insufficient to inhibit NKCC1 in any cell type located in the brain parenchyma. Thus, bumetanide applied in vivo apparently has *targets outside the brain* that mediate some of its beneficial CNS actions (section 5). For example, bumetanide applied i.p. reduced experimental neuroinflammation but, in stark contrast, injection of the drug directly into the brain had the opposite effect (Tóth et al., 2021). In line with the latter observation, several studies have reported deleterious actions of bumetanide, including a proconvulsant effect in the amygdala kindling model of temporal lobe epilepsy (TLE) (Töpfer et al., 2014). The overall picture of bumetanide actions becomes even more complex in light of data showing that, when applied directly into brain tissue, the drug can also exert neuroprotective and antiepileptogenic actions, as shown in a model of TLE in rats (Kourdougli et al., 2017, section 4).

All the distinct modes and sites of action described above must be taken into account when examining and (re-)evaluating the effects of conventional NKCC1 blockers. It is obvious that novel, brain-permeant drugs which target NKCC1 within brain tissue would be valuable not only for possible clinical applications but also as pharmacological tools in basic research. Much of our present discussions are centered on these topics. We raise numerous major points in this review to challenge some of the fundamental but frequent misconceptions on the actions of NKCC1 blockers, many (but not all) of which are related to ignorance on the pharmacokinetic limitations of these compounds; and to the lack of cellular target specificity, not only within but also outside the CNS. Here, it is prudent to note that while we have shown in numerous studies that bumetanide, applied in vivo, is devoid of a robust antiseizure action itself in rodents but acts in some models to potentiate the effects of phenobarbital (PB), particularly in epileptic rodents (Töllner et al.,

2014; Töpfer et al., 2014; Töllner et al., 2015a; Erker et al., 2016; Brandt et al., 2018; Hampel et al., 2021b; Johne et al., 2021a,b [cf., Table S1]), we do not yet understand the mechanism underlying the above actions. Thus, one of the major aims of this review is to promote novel experimental approaches based on solid information on the available pharmacokinetic and pharmacodynamic properties of bumetanide and related NKCC1 blockers.

2. NKCC1 and bumetanide: physiology and pharmacology

2.1. NKCC1 as a putative drug target within and outside the brain

There is general agreement regarding the idea that many if not most neuropsychiatric diseases have their roots in brain development (Thapar et al., 2017; Ismail and Shapiro, 2019). Thus, following the identification of the Cl^- transporters NKCC1 and KCC2 as the key molecules involved in the shift of GABA action from depolarizing to hyperpolarizing (Fig. 2A and B) (Rivera et al., 1999; Hübner et al., 2001a; Virtanen et al., 2021), lots of attention has been paid to the roles of these two transporters in CNS disorders.

In immature neurons, active accumulation of Cl^- by NKCC1 leads to an inwardly-directed, depolarizing driving force of currents (channel-mediated efflux of Cl^-) across the anion-permeable $GABA_A$ receptors. During neuronal maturation, there is a gradual shift from depolarizing to hyperpolarizing $GABA_A$ receptor responses, which is the basis of efficient postsynaptic inhibition in most CNS neurons (Kaila, 1994; Kaila et al., 2014a). This developmental shift in GABA action is attributable to a progressive increase in the expression of KCC2 (see also Spoljaric et al., 2019) with a time course that depends not only on the type of neuron but also on the species in question (Rivera et al., 1999; Virtanen et al., 2020). Thus, in laboratory rats and mice, GABA actions in hippocampal and neocortical neurons become hyperpolarizing by the end of the second postnatal week. In contrast, and in line with other species-specific differences in pre- and postnatal milestones in brain development, GABA is hyperpolarizing already in the healthy term newborn human cortex as evidenced by the high level of expression of KCC2 and by the properties of the EEG (Vanhatalo et al., 2005; Sedmak et al., 2016; Virtanen et al., 2021). This is obviously a fundamental insight for relevant cross-species calibration (e.g. rodent-to-human) of developmental time in translational studies, including pharmacological ones (see Pospelov et al., 2020).

That immature neurons have a high NKCC1-dependent $[Cl^-]_i$ was originally deduced based on depolarizing GABA responses recorded in vitro, which were abolished by bumetanide (Ben-Ari et al., 2007). More recently, similar observations have been made in vivo (Murata and Colonnese, 2020). Notably, in vitro preparations such as hippocampal slices from neonatal rodents generate bumetanide-sensitive network responses, known as Giant Depolarizing Potentials (GDPs), which are driven by NKCC1-mediated depolarizing GABA actions in pyramidal neurons of the hippocampal CA3 area (Ben-Ari et al., 1989, 2007; Sipilä et al., 2005). Whether GDPs have a strict counterpart in vivo is a matter of conjecture, but recording *these events in brain tissue* in vitro *offers a very useful assay for an initial drug screening of putative neuronal NKCC1 blockers* (Töllner et al., 2014; Brandt et al., 2018).

In addition to the neurodevelopmental aspects of KCC2 and NKCC1 expression, a highly interesting observation (soon after the discovery of the developmental GABA shift) was that hippocampal kindling (as used in well-established models of TLE) led to a BDNF-dependent decrease in the expression of KCC2 with a delay of only a few hours (Rivera et al., 2002; Kaila et al., 2014a). This finding was instrumental in understanding the evolvement of the neuronal trauma-related *depolarizing shift in the $GABA_A$ reversal potential* (E_{GABA}) that is seen, for instance, in TLE and brain injury, in which hyperpolarizing GABA actions become depolarizing and dependent on NKCC1 (Fig. 2B) (Cohen et al., 2002; Huberfeld et al., 2007; Lu et al., 2008; Barmashenko et al., 2011; Wang et al., 2017). The dependence of certain kinds of epileptiform events on NKCC1, such as the interictal events in human TLE, is evidently based on their sensitivity to bumetanide in *ex vivo* tissue (Huberfeld et al., 2007). This finding and subsequent research readily explained earlier results on the 'paradoxical' depolarizing actions of GABA in the epileptic human brain (Köhling et al., 1998; Kaila et al., 2014b, 2022).

To make an intermediary summary: it was the above two major lines of research - one on the developmental GABA shift, and the opposite one seen upon neuronal trauma - that originally set the scene for most of the ensuing and current work on NKCC1 and KCC2 in brain disorders and diseases. In particular, the idea emerged that pharmacological inhibition of NKCC1 might be a valuable therapeutic strategy in a wide spectrum of CNS disorders (see section 5; Kahle et al., 2008; Ben-Ari, 2017; Schulte et al., 2018). Therefore, the actions of bumetanide have raised enormous interest (see also Kharod et al., 2019). For similar reasons, there has been a lot of interest also in putative KCC2 activators (Gagnon et al., 2013; Kahle et al., 2014; Delpire, 2021).

In the CNS, KCC2 is exclusively expressed in neurons (Virtanen et al., 2021) and outside the CNS in endocrine cells of the pancreatic islet (Kursan et al., 2017). In contrast to this, as described in the Introduction, NKCC1 is expressed by virtually all cell types in the brain, including the vasculature, BBB, and choroid plexus. The same is true for NKCC1 expression patterns outside the brain where it is located in a large variety of distinct tissues and cell types. Thus, NKCC1 has numerous physiological functions, including regulation of cell volume, secretion of the endolymph in the inner ear, Cl^--driven fluid secretion in many exocrine glands, regulation of vascular tone, and many more (Markadieu and Delpire, 2014; Delpire and Gagnon, 2018; Virtanen et al., 2020). This, however, does not make NKCC1 obsolete as a possible drug target, as evidenced for instance by work on drugs targeting ubiquitous carbonic anhydrase (CA) isoforms with comparable, wide-ranging cellular patterns of expression (Lemon et al., 2021; Pospelov et al., 2021; Supuran, 2021). Notably, at the time when most of the research programs on designing novel bumetanide derivatives were started (see below), the cellular heterogeneity of NKCC1 expression patterns in the brain was not known, and NKCC1 was thought to be primarily expressed by neurons.

2.2. The structural properties of NKCC1

A cDNA encoding NKCC1 was first cloned from the shark rectal gland in 1994 (Xu et al., 1994). Recently, the 3D structure of several cation-chloride cotransporters, including that of human NKCC1, have been determined by single-particle cryo-electron microscopy (cryo-EM) (Yang et al., 2020; see also Zhang et al., 2021). This has vastly expanded our knowledge on the functional properties of these ion transporters. Like all the other members of the SLC12 family, NKCC1 assembles into a dimer (Fig. 1A), with the first ten transmembrane helices (TM) harboring the transport pore and TM11-TM12 lining the dimer interface (Fig. 1B). Human NKCC1 comprises 1212 amino acids yielding a core molecular size of 131.4 kDa. The large regulatory cytoplasmic C-terminal domain of NKCC1 contains a 16-amino acid fragment encoded by exon 21 (Fig. 1B), which can be spliced alternatively yielding two splice variants, NKCC1a and NKCC1b, whereof the latter is devoid of the 16-amino acid fragment. Exon 21 possesses a sequence that targets NKCC1 to the basolateral membrane of epithelial cells. A notable exception is the choroid plexus epithelium, where NKCC1 is highly expressed in the apical membrane (Delpire and Gagnon, 2018), which makes it difficult to target with bumetanide. Based on data from the human brain, NKCC1b was initially thought to be the major NKCC1 splice variant in the brain (Vibat et al., 2001), but recent data on the mouse brain show the opposite, with NKCC1a levels about three times higher than NKCC1b (Gregoriades et al., 2019). However, we do not know yet which splice isoform is preferentially expressed in central neurons. The cellular specificity of the expression of NKCC1a and NKCC1b isoforms is an important issue, since these two isoforms may have different subcellular localizations and post-translational modifications, resulting in different functional properties concerning membrane trafficking and ion translocation (Virtanen et al., 2020).

NKCC1 and KCC2 are activated oppositely by phosphorylation (except for one site, S940, targeted by protein kinase C in KCC2): the former is activated while the latter is inactivated (Kahle et al., 2013; Chi et al., 2021). NKCC1 has several potential phosphorylation sites within its terminal N- and C-domains (Fig. 1B), which play a critical role in regulating its transport activity (Markadieu and Delpire, 2014; Delpire and Gagnon, 2018; Zhang et al., 2021). There are key residues in both intracellular (N- and C-) termini which are targeted by several regulatory pathways, especially by the WNK (with no lysine kinase; a Cl^- sensor), SPAK (Ste20-related proline-alanine-rich kinase), and OSR1 (oxidative stress-responsive kinase) kinase cascade (Markadieu and Delpire, 2014; Shekarabi et al., 2017; Delpire and Gagnon, 2018). Thus, when dealing with NKCC1 pharmacology, it is important to note that this molecule can be targeted directly, and also by drugs that act on the above phosphorylation cascades (see section 3.7). However, the latter topic is presently addressed only in connection with one bumetanide-related compound, STS66 (also known as BUM66; see section 3.7).

2.3. A brief history of bumetanide

Bumetanide is an FDA-approved, widely used and very potent ("high-ceiling") diuretic drug with 500-fold greater affinity for NKCCs than for KCCs (Schlatter et al., 1983; Alvarez-Leefmans, 2012). It is a sulfamoylbenzoic acid derivative (Fig. 1C), first synthesized by Peter W. Feit in 1969 at Leo Pharma in Denmark (Feit, 1971). At the time of the development of bumetanide in the 1960s, its exact target in the kidney was not known. Bumetanide was discovered in systematic structure-activity studies of a large series of diuretically active 3-amino-5-sulfamoylbenzoic acid derivatives (Feit, 1971), which was followed by the synthesis of several series of compounds related both in chemical structure and diuretic profile (Nielsen and Feit, 1978; Feit, 1981, 1990). Notably, rodents metabolize bumetanide and its derivatives too rapidly to allow quantitative assessment of their diuretic potency (Olsen, 1977; Töpfer et al., 2014). Therefore, dogs were used for the original screening of diuretically active aminobenzoic acid compounds, which eventually led to the discovery of bumetanide (Feit, 1971, 1981, 1990; Frey, 1975; Nielsen and Feit, 1978). Thus, sulfamoylbenzoic acid diuretics were synthetized long before their cellular and molecular mechanisms of action were elucidated (Feit, 1981). The potency of bumetanide exceeded that of the clinically established loop diuretics furosemide and ethacrynic acid in dogs as well as in humans (Cohen, 1981). This work also indicated that the dog is a valuable translational model for structure-activity studies on loop diuretics acting via inhibition of renal NKCC2.

In 1979, Frizzell et al. proposed that the diuretic effect of loop diuretics was mediated by inhibition of Na–Cl cotransport in the kidney. This prompted Palfrey et al. (1980) to study the effect of various aminobenzoic acid derivatives, including bumetanide and some of its derivatives on a cation co-transport system in avian erythrocytes, which was later identified as NKCC1 (Flatman and Creanor, 1999). The data showed a good correlation between diuretic potency in the dog assay and inhibitory efficacy in the avian cotransporter. A similar correlation analysis was not available for mammalian NKCCs until our study on several bumetanide derivatives (Lykke et al., 2015). Using the *Xenopus* oocyte as a heterologous expression system for studying drug effects on human NKCC2 (hNKCC2), a significant correlation between inhibition of hNKCC2a (the major splice variant of hNKCC2 in the kidney) and diuretic potency in dogs was found.

2.4. Molecular modeling of bumetanide and its binding sites in NKCC cotransporters

Molecular modeling of bumetanide and its binding sites in NKCC cotransporters indicated an aromatic central ring associated with four potentially active groups at positions R1, R3, R4, and R5 as illustrated in Fig. 1C (Hannaert et al., 2002). Three of these groups (R1, R3, R5) are also found in the structure of furosemide (Hannaert et al., 2002). The phenoxy group in position R4 of bumetanide confers higher lipophilicity to the compound and is not shared by furosemide. Furosemide and bumetanide displayed similar inhibitory action on rat NKCC1 and NKCC2, so it was suggested that NKCC1 and NKCC2 have a similar protein conformation to bind the R1, R3, R4, and R5 diuretic residues, as shown in Fig. 1C (Hannaert et al., 2002).

Bumetanide binding is competitive with one of the two substrate chloride ions, which suggests that bumetanide and other loop diuretic drugs bind within the transport pocket of NKCCs (Forbush and Palfrey, 1983). A more recent study on the functional role of TM3 in human NKCC1, using cysteine and tryptophan-scanning mutagenesis, indicated that TM3 makes up one face of a translocation pathway that opens to the extracellular surface (Zhang et al., 2021). This confirmed the hypothesis that bumetanide binds within the translocation cavity (Somasekharan et al., 2012). In line with the above findings, we found that extracellular but not intracellular application of bumetanide blocks hNKCC1 in the heterologous *Xenopus laevis* oocyte expression assay (Brandt et al., 2018).

Further experimental mutations in NKCC1 TMs would most likely affect drug actions by disturbing conformational rates and ion-transport equilibria of NKCC1. Thus, more direct work at the structural level is needed to understand the molecular pharmacology of bumetanide's inhibitory action on NKCC1. Cryo-EM based structures of NKCC1 (e.g., Chew et al., 2019; Yang et al., 2020) will allow a direct evaluation of the molecular modeling shown in Fig. 1C. Indeed, in their work on the structure of human NKCC1a, Zhang et al. (2021) recently reported that

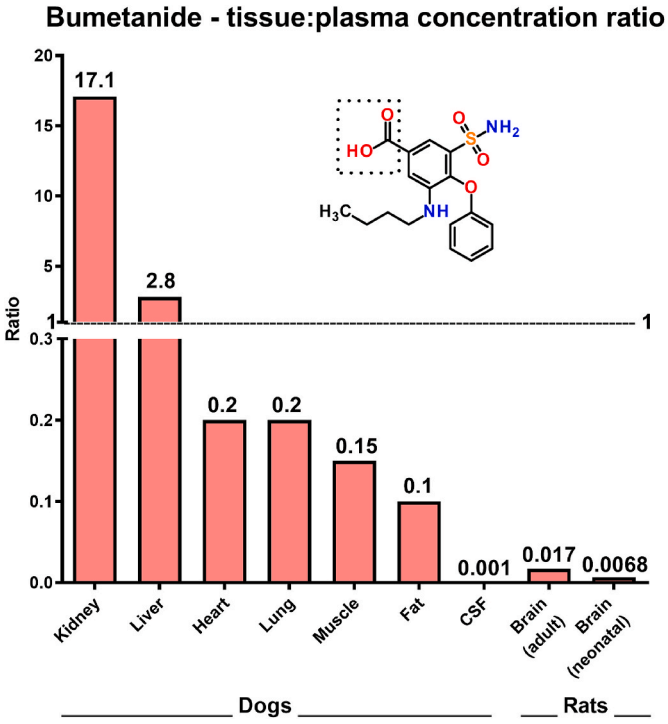

Fig. 3. Tissue distribution of bumetanide after systemic administration in dogs and rats. Because of the carboxylic group of bumetanide (indicated by the hyphenated box in the chemical structure of this drug), bumetanide is highly ionized in the blood, which limits its diffusion into most tissues, except for the kidney and liver, in which bumetanide is taken up by active transport. Drug levels are even lower in cerebrospinal fluid (CSF) and brain as a result of blood-CSF and blood-brain barriers. Peak concentrations of the drug are achieved in highly variable time windows in various organs and tissues, with that fastest time-to-peak of only 2 min in the brain, which is followed by a fast and prompt decay (see Fig. 4A). Data are from Cohen et al. (1976), Javaheri et al. (1993), Brandt et al. (2010), and Li et al. (2011).

Table 1
Brain levels of bumetanide and its derivatives following systemic administration of different doses in rodents. Data are grouped according to dose level (in mg/kg). See Puskarjov et al. (2014) for minimal NKCC1 inhibitory concentrations of bumetanide. Note that based on the data shown, systemic doses of at least 2 mg/kg bumetanide are needed to obtain NKCC1 inhibitory drug levels in the brain. However, also note that the majority of studies that determined brain drug levels in tissue homogenates did not correct for unspecific binding to brain lipids and proteins, although only the free (unbound) drug can interact with NKCC1 (see Brandt et al., 2018). Furthermore, it is important to note that bumetanide very rapidly enters the brain following parenteral administration, reaching maximal brain levels (C_{max}) already 2 min after i.v. with rapid decline thereafter (Hampel et al., 2021a); thus, determination at only one relatively late time point (e.g., 30 min) underestimates C_{max} and may explain, at least in part, the large differences in brain bumetanide levels across studies from different laboratories. Abbreviations: C_{max}, maximal brain concentration; P, postnatal day.

Compound	Dose	Species	Age/ sex	Health status	Time of decapitation after drug administration	Average brain level	Percent of plasma concentration reaching the brain (brain: plasma ratio x 100)	Minimal NKCC1 inhibitory concentrations (100–300 nM) of bumetanide reached?	Reference
Bumetanide	0.15 mg/ kg i.p.	Rat	P10/ male	Normal	0.5 h	0.51 ng/g (1.4 nM) (at 10 min 0.76 ng/ g [2.11 nM])	0.43%	No	Cleary et al. (2013)
Bumetanide	0.15 mg/ kg i.p.	Rat	P10/ male	15 min after hypoxia/ neonatal seizures	0.5 h	0.68 ng/g (1.8 nM)	0.5%	No	
Bumetanide	0.3 mg/ kg i.p.	Rat	P10/ male	Normal	0.5 h	0.94 ng/g (2.6 nM) (at 10 min 1.2 ng/g [3.4 nM])	0.55%	No	Cleary et al. (2013)
Bumetanide	0.3 mg/ kg i.p.	Rat	P10/ male	15 min after hypoxia/ neonatal seizures	0.5 h	1.07 ng/g (2.9 nM)	0.5%	No	Cleary et al. (2013)
Bumetanide	0.3 mg/ kg i.v.	Rat	P11/ both sexes	~10 min after asphyxia/ neonatal seizures	~1 h	10 ng/g (27 nM)	3.6%	No	Johne et al., 2021b
Bumetanide	0.3 mg/ kg i.p.	Rat	Adult/ male	Normal	0.5 h	~1.4 ng/g (3.8 nM)	0.68%	No	Li et al. (2011)
Bumetanide	0.5 mg/ kg i.p. once daily for 3 weeks	Rat	P10/ both sexes	Normal	0.5 h after last drug injection	1.7 ng/g (4.7 nM)	0.46%	No	Wang et al. (2015)
Bumetanide	0.5 mg/ kg i.p. once daily for 3 weeks	Rat	P10/ both sexes	Hypoxia/ neonatal seizures 3 weeks before brain level determination	0.5 h after last drug injection	2.2 ng/g (6 nM)*	0.77	No	Wang et al. (2015)
Bumetanide	2 mg/kg i.v.	Mouse	Adult	Normal	5 min (time of C_{max})[a]	~60 ng/g (160 nM)	~0.5%	Yes[b]	Savardi et al. (2020)
Bumetanide	10 mg/kg i.v.	Rat	Adult/ female	Normal	0.25 h (time of C_{max})[a]	53 ng/g (150 nM) (piriform cortex and amygdala)	1.4%	Yes[b]	Töllner et al. (2014)
Bumetanide	10 mg/kg i.v.	Rat	Adult/ female	Normal	0.25 h (time of C_{max})[a]	11.8 ng/g (320 nM) (hippocampus)	1.67%	Yes[b]	Töpfer et al. (2014)
Bumetanide	10 mg/kg i.v. (bolus) follo-wed by i.v. infusion with 6 mg/kg/ h over 5 h	Rat	Adult/ male	Normal	Hippocampal dialysate was collected at 20 min intervals during bumetanide administration; whole tissue levels were determined at the end of the 5-h infusion period	1370 ng/g [3760 nM] in hippocampal tissue; only 132 ng/ml (=360 nM) in dialysate (= 9.6% of whole tissue level)	~6% for whole tissue but only ~0.01% for dialysate (extracellular) levels	Yes (also in the extracellular fluid)	Donovan et al. (2015)
Bumetanide	10 mg/kg i.v.	Mouse	Adult/ female	Normal	0.5 h	330 ng/g (910 nM)	1,6%	Yes[b]	Töllner et al. (2014)
Bumetanide	10 mg/kg i.v.	Mouse	Adult/ female	Normal	0.5 h	270 ng/g (740 nM)	1.8%	Yes[b]	Töpfer et al. (2014)
Bumetanide	10 mg/kg i.v.	Mouse	Adult/ female	Normal	0.25 h	380 ng/g (1040 nM)	1.1%	Yes[b]	Römermann et al. (2017)
Bumetanide		Mouse		Normal			1.5%	Yes[b]	

(*continued on next page*)

Table 1 (*continued*)

Compound	Dose	Species	Age/ sex	Health status	Time of decapitation after drug administration	Average brain level	Percent of plasma concentration reaching the brain (brain: plasma ratio x 100)	Minimal NKCC1 inhibitory concentrations (100–300 nM) of bumetanide reached?	Reference
	10 mg/kg i.v.		Adult/ female		2 min (time of C_{max})	1030 ng/g (2830 nM)			Hampel et al. (2021a)
Bumetanide	10 mg/kg i.v.	Rat	P11/ both sexes	~10 min after asphyxia/ neonatal seizures	~1 h	190 ng/g (520 nM)	2.5%	Yes[b]	Johne et al. (2021a)
Bumetanide	15 mg/kg i.p.	Rat	Adult/ female	Normal	0.5 h	150 ng/g (410 nM) (piriform cortex)	1.7%	Yes[b]	Brandt et al. (2010)
DIMAEB (prodrug of bumetanide)	13 mg/kg i.v.	Rat	Adult/ female	Normal	0.5 h	280 ng/g bumetanide (770 nM)*	2.9%*	Yes[b]	Töllner et al. (2014)
DIMAEB (prodrug of bumetanide)	13 mg/kg i.v.	Mouse	Adult/ female	Normal	0.5 h	990 ng/g (2720 nM)*	3.1%*	Yes[b]	Töllner et al. (2014)
DIMAEB (prodrug of bumetanide)	13 mg/kg i.v.	Rat	P11/ both sexes	~10 min after asphyxia/ neonatal seizures	~1 h	150 ng/g (410 nM)	3.1%	Yes[b]	Johne et al. (2021a)
Bumepamine	10 mg/kg i.v.	Mouse	Adult/ female	Normal	0.5 h	3420 ng/g	142% (indicating brain accumulation)	Bumepamine does not inhibit NKCC1 directly	Brandt et al. (2018)
Bumepamine	10 mg/kg i.v.	Rat	P11/ both sexes	~10 min after asphyxia/ neonatal seizures	~1 h	2010 ng/g	207% (indicating brain accumulation)	Bumepamine does not inhibit NKCC1 directly	Johne et al. (2021a)
STS66 (BUM66)	10 mg/kg i.v.	Mice	Adult/ female	Normal	0.5 h	2800 ng/g	93%	IC_{50} of STS66 is ~40 μM	Luo et al. (2020); and unpublished data (see text)
ARN23746	2 mg/kg i.v.	Mouse	Adult	Normal	5 min (time of C_{max})[a]	~120 ng/g (290 nM)	~4.3%	IC_{50} of ARN23746 is ~20 μM	Savardi et al. (2020)

*Significantly higher than in controls.

[a] Earlier time points were not included; in the Hampel et al. (2021a) study, peak brain levels were determined already 2 min after i.v. injection.

[b] Brain level not corrected for unspecific binding to brain proteins and lipids, which is 83% for bumetanide in the mouse brain (see Brandt et al., 2018) and 77% in the rat brain (Donovan et al., 2016); however, in vivo Donovan et al. (2015) detected only 9.6% of hippocampal bumetanide levels in hippocampal dialysates of rats, indicating that the extracellular (functionally relevant) concentration of bumetanide in the brain is lower than expected from in vitro dialysis studies.

mutations at the intracellular end of the translocation pore dramatically reduced the affinity for bumetanide. Because bumetanide is likely to inhibit NKCC1 from an extracellular site by binding within the translocation cavity (see above), its high ionization is not a problem for use in vitro, or for acting on CNS targets in vivo that are not protected by the BBB (e.g., NKCC1 expressed on the luminal membrane of the cerebral vascular endothelium). However, because the bumetanide fraction that is not bound to plasma protein is only ~2–3% of the total, substantially higher plasma concentrations are needed to achieve a transient half-maximal inhibition of NKCC1 in vivo compared to in vitro conditions, where plasma protein binding and the BBB do not limit neuronal target access (Puskarjov et al., 2014).

2.5. Pharmacodynamic and pharmacokinetic limitations in the use of bumetanide as a CNS drug

Bumetanide, which is often and erroneously thought to be the only clinically available NKCC-selective drug (see section 3.1), exerts its diuretic effect by inhibiting sodium transport in the thick ascending limb of the loop of Henle via inhibition of NKCC2. NKCC2 was long thought to be solely located in the kidney, but more recent studies have shown that it is expressed in several other tissues, including the gastrointestinal tract (Zhu et al., 2011), pancreas (Alshahrani et al., 2012), and the rat and human inner ear, most likely acting together with NKCC1 in the regulation of endolymph volume (Kakigi et al., 2009; Nishimura et al., 2009; Akiyama et al., 2010). Bumetanide inhibits NKCC1 and NKCC2 with similar potency, so it will inhibit the two transporters in a variety of tissues. This explains, for instance, the ototoxicity of bumetanide, particularly in neonates (Pressler et al., 2015; Ding et al., 2016; Soul et al., 2021).

Inhibition of NKCC1 (most likely NKCC1a) in the inner ear is involved in the ototoxicity of bumetanide (Ding et al., 2016; Kharod et al., 2019). In NKCC1 knockout mice, hearing and balance are strongly affected, pointing to both cochlear and vestibular defects (Gagnon and Delpire, 2013). Histology of the cochlea revealed an absence of endolymph as well as loss of hair cells and supporting outer phalangeal cells in the organ of Corti (Gagnon and Delpire, 2013). Bumetanide and other loop diuretics induce unique pathological changes in the cochlea such as the formation of edematous spaces in the epithelium of the stria vascularis, which leads to a rapid decrease of the endolymphatic potential and eventual loss of the cochlear microphonic potential, summating potential, and compound action potential (Ding et al., 2016). Coadministration of bumetanide and aminoglycoside antibiotics such as gentamycin increases the risk of ototoxicity (Ding et al., 2016), which, at least in part, explains the ototoxicity of bumetanide in clinical trials on neonatal seizures (Pressler et al., 2015; Soul et al., 2021; Löscher and

Table 2
NKCC1 inhibitors and structurally related compounds that have been characterized in vitro and in vivo. In vivo data are from rodents (rats or mice).

Compound	Metabolism to bumetanide in rodents?	Brain:plasma ratio of bumetanide in rodents	Brain:plasma ratio of parent compound in rodents	Binding to brain tissue	Unbound NKCC1-inhibitory concentrations reached in brain parenchyma?	IC_{50} (μM) for NKCC1[a]	Selectivity for NKCC1?	Reference
5-sulfamoylbenzoic acid derivatives								
Bumetanide	–	~0.01–0.02 (lower in neonates)	–	83%	Only with high parenteral doses (≥2–10 mg/kg i.v. or i.p.)	0.16–0.28 μM (hNKCC1-transfected HEK293 cells)	No (also inhibits NKCC2 with similar potency)	Payne et al. (1995); Isenring et al., 1998a, b; Brandt et al. (2010); Cleary et al. (2013); Brandt et al. (2018); Hampel et al. (2021a)
ARN23746	?	–	~0.043	N/A	N/A	~20 μM (NKCC1-transfected HEK293 cells)	N/A (see section 3.4)	Savardi et al. (2020)
Bumetanide prodrugs								
DIMAEB (BUM5)	Yes	~0.03[b]	–	See bumetanide	Yes, with lower doses than bumetanide[b]	See bumetanide	See bumetanide	Töllner et al. (2014)
Non-acids with sulfamoyl group								
Azosemide	No	–	0.014–0.015	96%	Only with high doses (≥10 mg/kg i.v.)	0.25 μM (hNKCC1A in *Xenopus* oocytes)	No (also inhibits NKCC2)	Hampel et al. (2018); Hampel et al. (2021a)
Torasemide	No	–	0.012–0.015	88%	Only with high doses (>10 mg/kg i.v.)	6.2 μM (hNKCC1A in *Xenopus* oocytes)	No (also inhibits NKCC2)	Hampel et al. (2018); Hampel et al. (2021a)
Bumepamine (BUM13)	Little	–	~1.5	>99%	Does not inhibit NKCC1 directly	Does not inhibit NKCC1 directly	Does not inhibit NKCC1 directly	Brandt et al. (2018)
BUM66 (STS66)	Little	–	0.93	N/A	N/A	~40 μM, but no clear dose-dependency	N/A	Luo et al. (2020); and unpublished data (see Fig. 9)

[a] Varies largely with preparation (cf., Alvarez-Leefmans, 2012).
[b] Brain levels of bumetanide ~3-5-fold higher than after injection of equimolar doses of bumetanide.

Kaila, 2021).

Bumetanide is a relative strong carboxylic acid ($pK_a = 3.6$) with an accordingly high ionization rate (>99%) at physiological pH, which, together with its high plasma protein binding (97–98%), significantly limits its tissue distribution (Fig. 3, Tables 1 and 2). Consequently, bumetanide only poorly penetrates into most organs, and especially into the brain. In contrast, it accumulates into the kidney and liver, explaining its selective diuretic effect and fast metabolic inactivation, respectively (Löscher et al., 2013) (Fig. 3). The accumulation of bumetanide in these organs is mediated by active drug uptake via organic anion transporters (OATs; Burckhardt, 2012), whereas the low concentrations of bumetanide in other tissues suggest that penetration therein is mediated by passive diffusion and limited by the high ionization rate and plasma protein binding described above (see also Puskarjov et al., 2014). Notably, after bolus application, bumetanide levels in the brain parenchyma (and CSF) are even lower than in other tissues (Fig. 3), which is a consequence of the low permeability and presence of active efflux transport in the BBB (Donovan et al., 2015; Römermann et al., 2017). The free, unbound (i.e., pharmacologically active) levels of bumetanide in the brain are further reduced to only <20% of the total concentration in the tissue by unspecific binding to lipids and proteins within the parenchyma (Donovan et al., 2015, 2016; Brandt et al., 2018).

Bumetanide is both a substrate of monocarboxylate transporters (MCTs) and OATs, which may mediate the uptake and efflux, respectively, of this drug at the BBB (see section 6). The low brain levels of bumetanide suggest that active brain efflux exceeds brain uptake. Interestingly, a similar phenomenon has been reported for the antiseizure drug valproate, which also is a carboxylic acid and is transported into the brain by MCTs (Löscher, 2002; Vijay and Morris, 2014). Thus, following i.v. injection in rodents, bumetanide rapidly penetrates into the brain (Fig. 4A), indicating that its uptake may be mediated by active transport at the BBB (see above). Peak brain levels are already achieved 2 min after i.v. injection, followed by a rapid decline over 15–30 min (Fig. 4A). Brain:plasma ratios of bumetanide in this period are very low (Fig. 4B). Thereafter, a much slower decrease of bumetanide brain levels is observed, indicating slower elimination from the brain than the plasma (Hampel et al., 2021a), which has also been observed in rats (Cleary et al., 2013; Wang et al., 2015). As a consequence, brain:plasma ratios increase (Fig. 4B).

As shown in Fig. 4C, bumetanide brain levels in the minimal NKCC1 inhibitory concentration range (0.1–0.3 μM; cf., Puskarjov et al., 2014) are only reached at doses of ≥2 mg/kg. However, when unspecific brain binding is taken into account, even such doses may not be sufficient in this regard (Fig. 4D). For the corrected data shown in Fig. 4D, unspecific brain binding was taken from in vitro studies using brain homogenates from rats or mice (Donovan et al., 2016; Brandt et al., 2018). However, unspecific binding may be much higher in vivo. This is suggested by a study from Donovan et al. (2015), in which bumetanide concentrations were determined by microdialysis in the extracellular fluid of the hippocampus following a bumetanide bolus and continuous i.v. infusion of 10 mg/kg and 6 mg/kg/h in rats (see Table 1). Following 5 h of infusion, bumetanide was determined also in tissue homogenates of the hippocampus. Compared to whole tissue levels, only 9.6% of the bumetanide brain concentration appeared in the dialysates, which were corrected for bumetanide recovery (Donovan et al., 2015). At the high plasma levels of bumetanide (~20 μg/ml) obtained at steady-state during prolonged i.v. infusion, free functionally relevant bumetanide levels in the hippocampal dialysates (~0.3 μM) were in the minimal NKCC1 inhibitory concentration range (Table 1; Donovan et al., 2015).

The above observations readily explain the fact that, at the low oral or parenteral doses (0.01–0.3 mg/kg in pediatric patients, 0.5–2 mg/day in adult patients) of bumetanide used clinically for its diuretic effect, the drug does not reach NKCC1-inhibitory drug levels in the adult brain parenchyma (Brandt et al., 2018) (Table 1). This is similar in the neonatal brain (Fig. 3; Li et al., 2011; Cleary et al., 2013; Johne et al.,

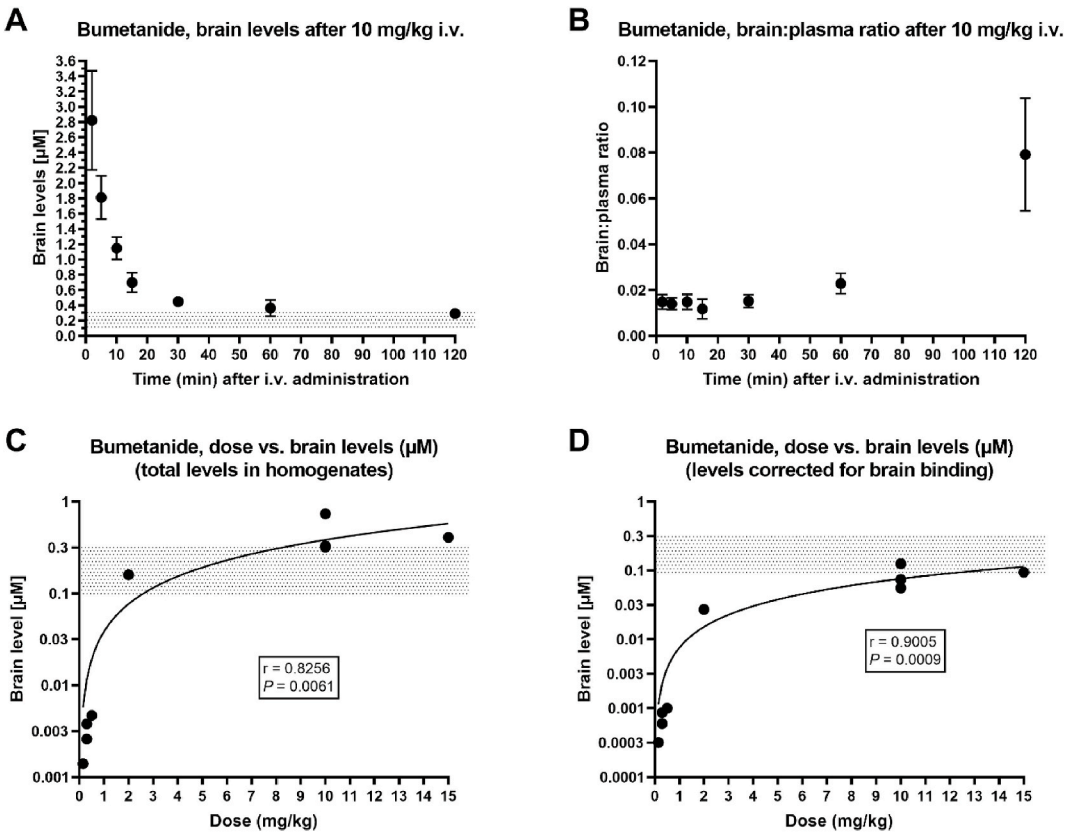

Fig. 4. Brain levels of bumetanide after systemic (parenteral) administration in rodents (mice or rats). Data in A and B are from Hampel et al. (2021a), whereas data in C and D were taken from Table 1. Note the logarithmic scale of the y-axis in C and D. Correlation for the data in C and D were calculated by the method of Pearson. (A) Brain levels (in µM) following i.v. injection of 10 mg/kg bumetanide in adult mice. Data are shown as means ± SEM of 6–7 mice per time point. Note the initial steep decline in brain levels (within the first 15 min) after injection, which is followed by a much slower elimination phase. The stippled area in this panel and panels C and D indicates the minimal NKCC1 inhibitory concentration range (0.1–0.3 µM) as calculated from in vitro experiments (Puskarjov et al., 2014). Note that the brain levels shown were not corrected for unspecific binding to brain lipids and proteins, which is ~83% in the mouse brain (Hampel et al., 2021a). When correcting brain levels of this experiment for unspecific binding, minimal NKCC1 inhibitory concentrations would be reached only for the first ~20 min after drug administration (not illustrated; see text). (B) Brain:plasma ratio of bumetanide following i.v. injection of 10 mg/kg bumetanide in adult mice. Data are shown as means ± SEM of 6–7 mice per time point. Note that the brain:plasma ratio is about the same over the first 30 min after drug injection, which is due to the parallel rapid decline of plasma and brain levels. Thereafter, the brain:plasma ratio increases, which is due to the slower elimination of bumetanide from the brain than plasma (cf., Hampel et al., 2021a). A slower elimination of bumetanide in brain vs. plasma has also been reported by other groups for rats (Cleary et al., 2013; Wang et al., 2015). (C) Correlation between the systemic dose of bumetanide and the achieved average brain concentration. Nine dose groups are shown: 0.15 mg/kg, 0.3 mg/kg (two groups), 0.5 mg/kg, 2 mg/kg, 10 mg/kg (three groups), and 15 mg/kg. Except for 2 mg/kg, brain levels were determined 30 min after i.v. or i.p. administration, i.e., a time point that is often used in experiments on bumetanide. Note that the brain levels shown are not corrected for unspecific binding to brain lipids and proteins, which reduces the free levels of bumetanide by 77 and 83% in rat and mouse brain homogenates, respectively (see text). (D) After correction for unspecific binding NKCC1 inhibitory concentration of bumetanide were observed at 30 min in only one experiment using the 10 mg/kg dose. However, as shown in A, bumetanide rapidly penetrates into the brain after parenteral administration; so following doses of ≥2 mg/kg, free peak drug levels in the brain may reach or exceed the minimal NKCC1 inhibitory concentration range (see also Fig. 7).

2021b), which means that the numerous effects of bumetanide reported in CNS disorders (see below) cannot be related to inhibition of NKCC1 in neurons or in any cell type located in the brain parenchyma (see section 5; and Löscher and Kaila, 2021). Moreover, as mentioned already, the metabolism of bumetanide in rodents is extremely fast, which has been a problem even in studies of the drug's 'canonical' diuretic action. These pharmacokinetic topics are obviously among the major problems in current and past research of bumetanide actions, and they will be further discussed (see section 5). Importantly, seizures do not alter the BBB permeability of bumetanide in neonatal or adult rodents to any functionally significant extent (Cleary et al., 2013; Töllner et al., 2014; Johne et al., 2021a,b).

Bumetanide is rapidly metabolized in different species including humans by oxidation of the N-butyl side chain (Olsen, 1977; Schwartz, 1981). About 60% of bumetanide is eliminated unchanged in humans and dogs, while rats excrete less than 10% in the non-metabolized form (Schwartz, 1981). Six urinary metabolites have been identified, including N-desbutyl-bumetanide and the δ-, γ-, and β-hydroxybutyl-metabolites (Schwartz, 1981). As expected (see section 3.3), these metabolites are devoid of significant diuretic activity (Schwartz, 1981), which is in line with the fact that rats and mice, which metabolize bumetanide much more rapidly and extensively than humans or dogs, exhibit a much weaker and shorter diuretic effect (Olsen, 1977). Inhibition of drug metabolism with piperonyl butoxide (PBO) in rats increased the half-life and the diuretic activity of bumetanide twofold (Halladay et al., 1978). We confirmed these effects of PBO in mice and rats and additionally found that PBO increases brain levels of bumetanide. This was, however, not associated with antiseizure activity in two rodent models of TLE (Töpfer et al., 2014 [cf. Table S1]). Overall, these findings do not suggest that bumetanide metabolites are involved in the diuretic or antiseizure activity of the parent drug. However, all of the identified metabolites of bumetanide retain the sulfamoyl moiety (Schwartz, 1981), which may mediate effects on targets other than NKCCs (see section 6).

Standard analytical techniques for measuring plasma and brain levels of bumetanide (and its metabolites) include liquid chromatography/tandem mass spectrometry (Li et al., 2011; Cleary et al., 2013; Wang et al., 2015; Savardi et al., 2020) or high-performance liquid chromatography with ultraviolet (Brandt et al., 2010; Töllner et al., 2014) or fluorescence detection (Donovan et al., 2015, 2016, 2016). All these techniques are sensitive enough to measure the low brain levels of bumetanide, and despite differences in extraction and detection of bumetanide in brain tissue samples all laboratories involved in this kind of work (see references above) have reported low brain:plasma ratios of this drug (cf., Table 1).

3. Strategies to enhance the brain penetration of NKCC1 inhibitors and to increase their selectivity

The recognition of the poor brain penetration of bumetanide has launched a search for novel pharmacological approaches for inhibiting NKCC1 in the CNS. To the best of our knowledge, the Löscher lab was the first to describe the low brain levels obtained by systemic administration of bumetanide (Brandt et al., 2010). Prompted by these observations in rats and the earlier dog CSF study by Javaheri et al. (1993), the group started in 2007 to develop novel and more effective strategies for inhibiting brain NKCC1, in cooperation with the chemists Peter W. Feit and, later, Thomas Erker and Markus Kalesse, and the labs of Kai Kaila and Nanna MacAulay. The following five strategies were implemented: (1) Development and characterization of brain-permeant prodrugs of bumetanide with the aim of increasing bumetanide brain levels (Töllner et al., 2014); (2) characterization of bumetanide side-chain derivatives with the aim of obtaining brain-permeable, NKCC1-selective derivatives that are devoid of a potent diuretic action (Lykke et al., 2015, 2016; Brandt et al., 2018); (3) characterization of clinically available lipophilic non-acid loop diuretics (e.g., azosemide) with the aim of identifying compounds that are brain-permeable, highly potent to inhibit NKCC1, and possibly selective for one of the splice variants of NKCC1, which may also reduce ototoxicity (Hampel et al., 2018; Hampel et al., 2021a, b); (4) coadministration of a compound (PBO) that inhibits the rapid metabolism of bumetanide (Töpfer et al., 2014); (5) coadministration of a compound (e.g., probenecid) that inhibits active efflux of bumetanide from the brain (Töllner et al., 2015b; Römermann et al., 2017).

In the following, we will first summarize our recent data on clinically used loop diuretics with potential advantages as NKCC1 inhibitors vs. bumetanide. Then, we will review the pharmacological characteristics of new bumetanide prodrugs and side-chain derivatives and compare their in vitro and in vivo efficacies with those of novel NKCC1 inhibitors reported by other groups, including a compound (ARN23746) that was proposed to be selective for NKCC1 (Savardi et al., 2020).

3.1. Evaluation of clinically approved loop diuretics as NKCC1 inhibitors

Currently, bumetanide is the only drug that has been used in clinical studies with the aim to inhibit neuronal NKCC1 in neurological or psychiatric disorders. Other clinically used 5-sulfamoylbenzoic acid derivative loop diuretics include furosemide, piretanide, and benzmetanide, but, in contrast to bumetanide, the latter drugs are not selective for NKCCs but also block KCC2 at roughly similar concentrations (Russell, 2000; Alvarez-Leefmans, 2012). In addition to sulfamoylbenzoic acid derivatives, various other loop diuretics with different chemical structures are in clinical use (Fig. 5), including drugs with an azosemide group (i.e., non-acids with a sulfonamide moiety, such as azosemide, torasemide, tripamide, and tizolemide, which are expected to have a higher BBB permeability). There are also non-sulfonamides which include both carboxylic acids, like ethacrynic acid, ticrynafen (tienilic acid), indacrinone, and ozolinone; and non-acids, such as etozolin and muzolimine (Wargo and Banta, 2009; Roush et al., 2014; Oh and Han, 2015). All these compounds act by inhibiting NKCC2 in the ascending loop of Henle but differ in diuretic potency and efficacy, duration of the diuretic effect, pharmacokinetic properties, and safety profile. However, until recently, it was not known whether some or all of them inhibit NKCC1. We used ten compounds of the four structurally different groups shown in Fig. 5 to evaluate their structure-activity relationship on hNKCC1a vs. hNKCC1b (Hampel et al., 2018). Our experiments were prompted by the fact that, until recently, the pharmacological sensitivity of the two main NKCC1 splice variants to various inhibitors were unknown. Developing pharmacological tools selectively targeting each variant has a potential impact on elucidating the cellular and physiological functions of these variants, as well as on the possible therapeutic implications.

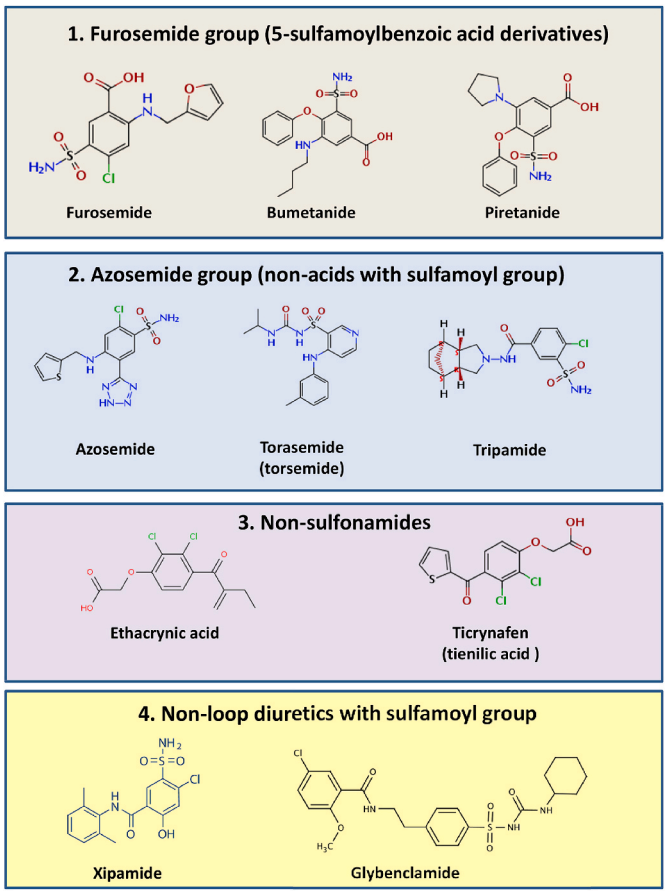

Fig. 5. Chemical structures of clinically approved loop diuretics and two related compounds. The former are assigned into three groups according to their structures and were tested for their potency to inhibit hNKCC1a vs. hNKCC1b (Hampel et al., 2018). Group 4 (non-loop diuretics with a sulfamoyl group) was included to test the overall specificity of NKCC1-mediated ion transport in the heterologous *Xenopus* oocyte expression assay. See text for details.

Furthermore, based on structure, physicochemical properties, and pharmacokinetics, several of the loop diuretics shown in Fig. 5, particularly those without an acid group may have advantages vs. bumetanide as CNS drugs. Two non-loop diuretics with a sulfamoyl group (xipamide, glybenclamide) were included for comparison; these compounds did not exert any effects on hNKCC1a and hNKCC1b (Hampel et al., 2018).

In the *Xenopus* oocyte heterologous expression system, azosemide was the most potent NKCC1 inhibitor (IC_{50} values 0.246 μM for hNKCC1a and 0.197 μM for NKCC1b), being about 4-times more potent than bumetanide. A carboxylic group as in bumetanide (R1 in Fig. 1C) was not a prerequisite for potent NKCC1 inhibition, whereas loop diuretics without a sulfamoyl group (R5 in Fig. 1C) were less potent. None of the drugs were selective for hNKCC1b vs. hNKCC1a. As shown in Fig. 6A, there is a highly significant correlation between the inhibitory

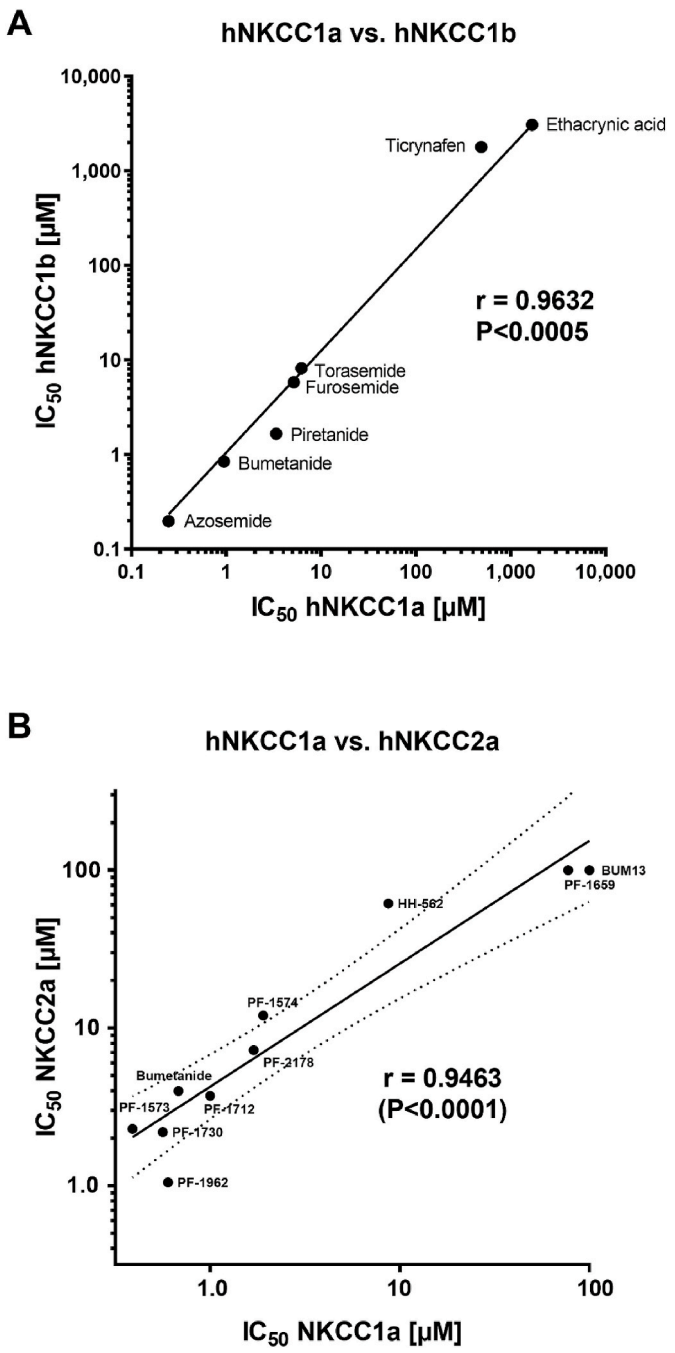

Fig. 6. (A) Correlation between IC_{50} for inhibition of hNKCC1a vs. hNKCC1b of various loop diuretics in the *Xenopus* oocyte assay. Data are from Hampel et al. (2018). (B) Correlation between IC_{50} for inhibition of hNKCC1a vs. hNKCC2a for the 10 bumetanide derivatives illustrated in Fig. 10. The dotted lines indicate the 95% confidence limits. Data are from Lykke et al. (2016). Spearman's rank correlation coefficient was calculated in both A and B.

potency of these compounds on the two human NKCC1 splice variants. However, when compared to published data on NKCC2, azosemide was about 12-times more potent in inhibiting NKCC1 vs. NKCC2 (Hampel et al., 2018).

Because of the lack of an acidic group in azosemide and torasemide (Fig. 5), we expected that these drugs should penetrate into the brain more effectively than bumetanide. However, a pharmacokinetic study in mice showed that the brain:plasma ratio of azosemide and torasemide was as low as that of bumetanide (Fig. 7), which was attributable to the probenecid-sensitive efflux transport at the BBB (Hampel et al., 2021a). When correcting for unspecific binding to brain tissue, the peak free brain concentrations of bumetanide and azosemide (determined shortly after i.v. administration) were in the NKCC1-inhibitory concentration range, while levels of torasemide were below this range at near-equimolar systemic doses (10 mg/kg i.v.) (Fig. 7D).

In a subsequent study, we examined whether azosemide and torasemide exert anticonvulsant effects or potentiate the anticonvulsant activity of PB in epileptic mice (Hampel et al., 2021b). Both drugs were ineffective when administered alone, and they did not potentiate the anticonvulsant activity of PB on electrically determined seizure threshold in nonepileptic mice, but did so in chronically epileptic mice. These data suggest that azosemide and torasemide share the modes of action of bumetanide as adjuncts to PB, and point to NKCC1 as the primary target in the experiments (see Section 6).

3.2. *Development of brain-permeant prodrugs of bumetanide*

Based on our previous experience with other compounds with an acid moiety and poor brain accessibility (Frey et al., 1979; Frey and Löscher, 1980; Löscher et al., 1983; Löscher, 1985), we designed several lipophilic prodrugs of bumetanide (Fig. 8) and determined their brain penetration in rodents (Töllner et al., 2014). Based on achieved brain levels of bumetanide, the *N*,*N*-dimethylaminoethyl ester of bumetanide (DIMAEB; also termed BUM5 or STS5) was the most interesting compound and was further characterized in rodent models of epilepsy (Tables 1 and 2). As shown by Töllner et al. (2014), (1) DIMAEB rapidly enters the brain of mice and rats and is cleaved to bumetanide, yielding 3-5-fold higher brain levels of bumetanide than observed after systemic administration of an equimolar dose of the parent drug itself (see Fig. 9A); (2) DIMAEB blocks GDPs in neonatal hippocampal slices, most likely upon cleavage to bumetanide; (3) DIMAEB potentiates the anti-seizure effect of PB in amygdala-kindled rats and epileptic mice more markedly than bumetanide; (4) DIMAEB exerts disease-modifying effects (by counteracting the alteration in seizure threshold during the latent period) in the pilocarpine model in mice (not seen after injection of bumetanide); (5) DIMAEB is less diuretic than bumetanide. Based on these findings, we initially concluded (but see sections 4 and 5) that DIMAEB may resolve some of the insurmountable problems associated with using bumetanide as a CNS drug (Töllner et al., 2014; Erker et al., 2016).

Importantly, DIMAEB exerted no direct effects on NKCC1 but acted solely as a prodrug of bumetanide (Töllner et al., 2014). The unexpected finding that DIMAEB is less diuretic than bumetanide despite the higher ensuing bumetanide plasma levels compared to administration of the parent drug (Fig. 9A) can be explained by inhibition of active transport of bumetanide into the kidney by DIMAEB (unpublished findings). Indeed, in Chinese hamster ovary (CHO) cells expressing mouse Oat3, which is mainly responsible for renal uptake of bumetanide (see section 6), DIMAEB inhibited the uptake of bumetanide (Römermann et al., 2017).

Töllner et al. (2014) also tested various other ester and amide prodrugs of bumetanide (Figs. 7 and 8), but DIMAEB turned out to be the most promising compound because it led to higher brain bumetanide levels than most other prodrugs and was less diuretic. In subsequent experiments, DIMAEB was reported to decrease infarct volume in a mouse stroke model (Huang et al., 2019b).

The idea to synthesize DIMAEB was based on the previous use of *N*,*N*-dimethyl (or diethyl) aminoethyl esters for increasing the bioavailability and tissue distribution of penicillins (Töllner et al., 2014). In both CNS drug discovery and drug development, prodrug approaches have become an established tool, and designing ester-linked prodrugs is the most commonly employed approach for increasing lipophilicity of polar molecules with limited CNS penetration (Rautio et al., 2008). An important advantage of prodrugs of clinically approved compounds such as bumetanide is that the drug development pipeline to first use in humans is much shorter compared to novel chemical entities (Rautio

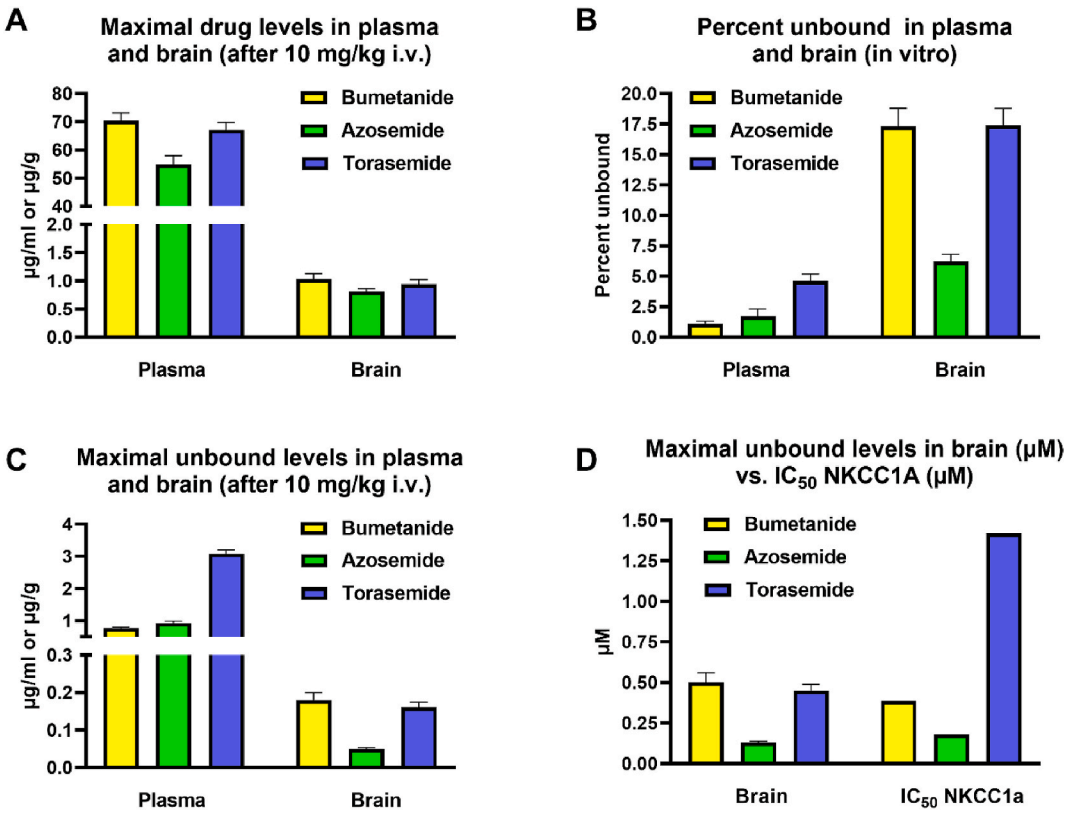

Fig. 7. Pharmacokinetic-pharmacodynamic basis of NKCC1 inhibition by bumetanide, azosemide, and torasemide in mouse brain. Data are shown as means ± SEM; sample size was 6–9. (A) Maximal drug levels in plasma and brain of mice 2 min after i.v. administration of 10 mg/kg i.v. (B) Free (unbound) drug levels (shown in percent of total level) in mouse plasma and brain determined by equilibrium dialysis in vitro. (C) Maximal free (unbound) drug levels in plasma and brain of mice 2 min after i.v. administration of 10 mg/kg i.v. Free plasma and brain concentrations were calculated from total concentrations (shown in A) based on estimates of fractional binding (shown in B). (D) For pharmacokinetic-pharmacodynamic modeling, the free maximal brain concentrations in mice (in µM) are compared with the lower range of IC_{50} values of bumetanide for inhibition of hNKCC1a. Note that free brain levels of bumetanide and azosemide (after i.v. injection of 10 mg/kg) are in the range of IC_{50} levels of these drugs, whereas torasemide does not reach IC_{50} levels. Data are from Hampel et al. (2018) and Hampel et al. (2020a).

et al., 2008, 2017).

In a preliminary report on nonhuman primates, only available as an abstract, Hochman and Haglund (2009) reported that some ester prodrugs of bumetanide elicited little or no diuresis, while being as efficacious as systemic administration of bumetanide (2 mg/kg i.v.) to suppress electrographic seizures evoked by intracortical administration of bicuculline, 4-aminopyridine, or electrical stimulation. However, the chemical structure of the prodrugs was not reported. Furthermore, 2 mg/kg i.v. bumetanide is a huge dose for primates, which will induce massive diuresis that, by its consequences, could suppress seizures without any involvement of NKCC1 (see section 5).

Several bumetanide prodrugs have been patented, including *N*-morpholinylamide (NTP-2024) and *N*-morpholinylthioamide (NTP-2006) derivatives of bumetanide (Hochman and Partridge, 2006, 2007; Wanaski et al., 2010, 2012; Pardridge and Hochman, 2017). However, to our knowledge, information on the pharmacokinetics of these compounds is not available in the public domain. The only published data on NTP-2024 and NTP-2006 are anticonvulsant effects following systemic administration in the intrahippocampal kainate model of TLE (Stamboulian-Platel et al., 2016). In the latter study, both compounds decreased the number and cumulative duration of spontaneous recurrent hippocampal paroxysmal discharges (HPDs) by ~40–60% when administered at doses of 200 (NTP-2024) or 150 (NTP-2006) mg/kg i.p.; however, brain bumetanide levels were not determined. We did not observe any significant effect of systemic (i.v.) administration of bumetanide (10 mg/kg; combined with PBO) on HPDs in this model (Töpfer et al., 2014).

More recently, using a non-invasive rat model of birth asphyxia (Ala-Kurikka et al., 2021), we found that DIMAEB significantly potentiates the anticonvulsant effect of PB on neonatal seizures, while bumetanide, even at a high dose (10 mg/kg), was ineffective with and without PB (Johne et al., 2021a,b). The lack of efficacy of bumetanide is in line with the first clinical trial on bumetanide as an add-on treatment of neonatal seizures in newborns with hypoxic-ischemic encephalopathy, which was stopped early because of serious adverse reactions (ototoxicity) and no evidence for additional seizure reduction compared to PB alone (Pressler et al., 2015).

However, in contrast to clinical trials on bumetanide (Pressler et al., 2015; Soul et al., 2021), DIMAEB and PB were administered *before* induction of asphyxia in rats, which may reduce the translational relevance of the preclinical findings. In this respect, it is important to note that in several preclinical studies with positive findings on bumetanide the animals were treated before the induction of seizures (Dzhala et al., 2005; Cleary et al., 2013). Another research group has shown that bumetanide given *after* repetitive ischemic or pentylenetetrazole induced seizures was inefficacious (Kang et al., 2015; Kharod et al., 2018). In line with the latter observations, we found that administration of PB plus bumetanide *after* asphyxia is ineffectrive to block neonatal seizures (Johne et al., 2021a). These publications demonstrate the importance of testing bumetanide and/or novel NKCC1 inhibitors in models of refractory neonatal seizures using translationally relevant protocols.

It will be of interest to see if DIMAEB is able to successfully suppress spontaneous recurrent seizures when added on with PB in models where PB alone is refractory as a post-treatment rather than using pretreatment protocols. In this respect, it is interesting to note that even

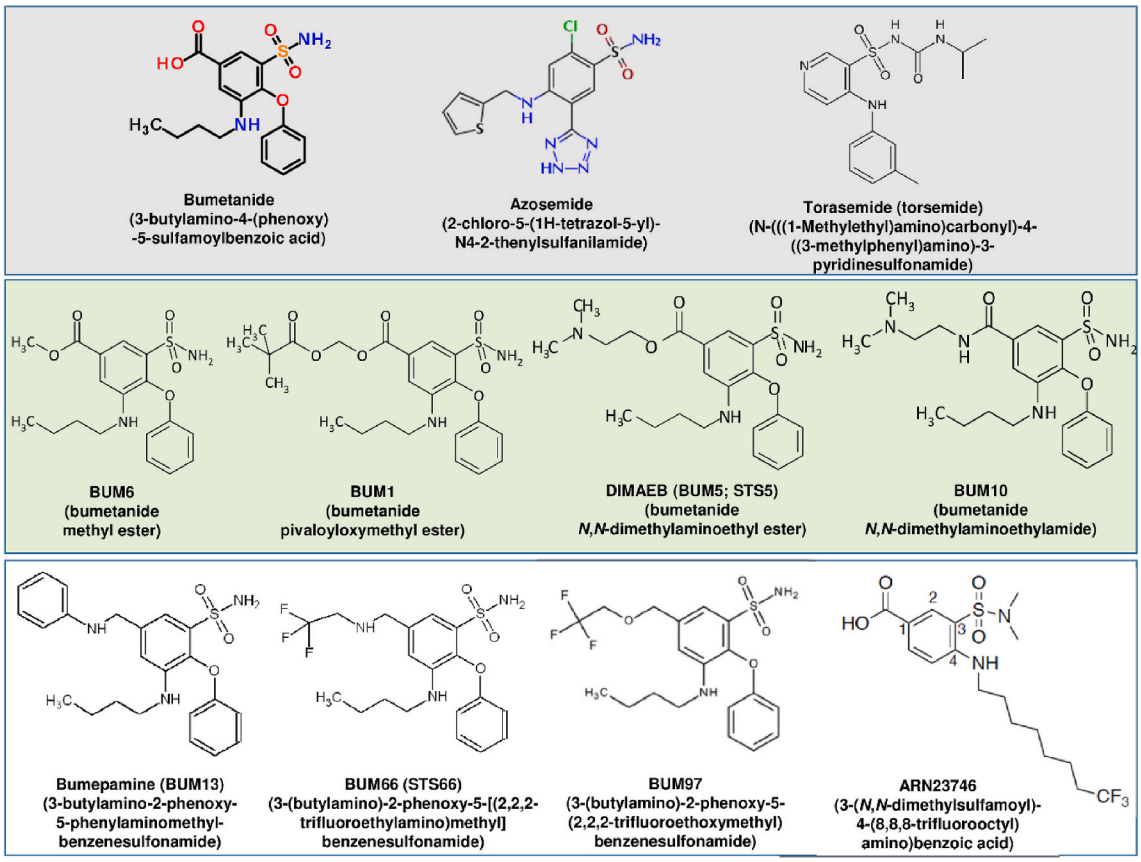

Fig. 8. Chemical structures of bumetanide, other loop diuretics, prodrugs of bumetanide, and bumetanide side-chain derivatives. First row: Clinically used loop diuretics that inhibit NKCC1. Note the lack of a carboxylic group in azosemide and torasemide. Second row: Ester and amide prodrugs of bumetanide. Third row: bumetanide side-chain derivatives. Note the lack of an acidic group in bumepamine, BUM66, and BUM97. See text for details.

high doses of bumetanide administered *after* onset of epilepsy were not capable of reducing the frequency of spontaneous recurrent seizures or potentiating the antiseizure effect of PB in an adult mouse model of TLE (Töpfer et al., 2014).

The rationale of using an ester prodrug such as DIMAEB is that the brain blood flow per unit amount of tissue is higher than in most other organs and tissues, which enables small, lipophilic prodrugs to penetrate into the brain parenchyma rapidly, where they are metabolized by esterases to the parent drug. Using neonatal serum and brain tissue homogenate, we observed rapid hydrolytic biotransformation of DIMAEB to bumetanide (Theilmann et al., 2020). These data provide a prerequisite for further evaluation of the potential of bumetanide prodrugs as add-on therapy to PB (and to other standard antiseizure drugs).

3.3. Development of brain-permeant bumetanide side-chain derivatives

Bumetanide has been reported to block NKCC1 and NKCC2 at similar concentrations (Alvarez-Leefmans, 2012). To our knowledge, we were the first to compare the effect of bumetanide on human NKCC1 and NKCC2 (hNKCC1 and hNKCC2) in the same assay (Lykke et al., 2016). In the search for brain-permeant NKCC1-selective bumetanide derivatives, we chose structurally different bumetanide derivatives from ~5000 3-amino-5-sulfamoylbenzoic acid derivatives that were synthesized in the 1960s and 1970s by Peter W. Feit and colleagues for the screening of compounds (see section 2.3) with high diuretic efficacy in dogs (Lykke et al., 2016). These included compounds that lack a carboxyl group at the key position R1. The bumetanide derivatives chosen are shown in Fig. 10, and they are grouped according to the positions of the modified bumetanide side-chains (R1, R3, R4, R5) which interact with NKCC1/2 (see Fig. 1C). The heterologous *Xenopus* oocyte expression system was used to compare bumetanide's effects on hNKCC1a and hNKCC2a (Lykke et al., 2016).

In our structure-activity studies on hNKCC1a, bumetanide had an IC_{50} of 0.68 μM (Fig. 11A). Replacement of the carboxylic acid residue of bumetanide in the R1 position with sulfonic acid (PF-2178; Fig. 10) yielded an inhibitor with lower potency (relative potency vs. bumetanide 0.4). Notably, the substitution of the carboxylic acid residue with an anilinomethyl group (bumepamine; see section 3.6) abolished the inhibitory effect, at least in concentrations of up to 100 μM. Replacement of the 3-butylamino group at position R3 of bumetanide with a butylthio side-chain (PF-1962) had no significant effect on potency (Fig. 10). Prolongation of the side-chain at R3 to a pentylamino group (PF-1712) only moderately decreased, while replacement with a 1,3-benzodioxol-5-ylmethylamino group (PF-1659) markedly reduced the inhibitory potency (Fig. 10). Concerning position R3 and R4, the three derivatives in this group (HH-562, PF-1574, PF-1573) contained a benzylamino residue instead of the butylamino side-chain at position 3 (Fig. 10). Additional replacement of the phenoxy substituent at position R4 with Cl^- (HH-562) significantly decreased, whereas exchange with a 4-chloroanilino group (PF-1573) almost doubled the inhibitory potency towards hNKCC1a (IC_{50} 0.39 μM) relative to bumetanide. Exchange to a 2,4-dimethylanilino group (PF-1574) reduced potency (Fig. 10). For R3/5 analogs, the butylamino group in position 3 was replaced by a benzylamino residue, but an additional exchange of the sulfamoyl group in R5 (not required for loop diuretic activity of bumetanide [Nielsen and Feit, 1978]) with a methylsulfonyl group resulted in the compound PF-1730 (Fig. 10) which inhibited hNKCC1a as potently as bumetanide.

The above structure-activity studies allowed defining the minimal structural requirements of bumetanide derivatives for hNKCC1a inhibition. *The presence of an anionic group at position R1 appears to be*

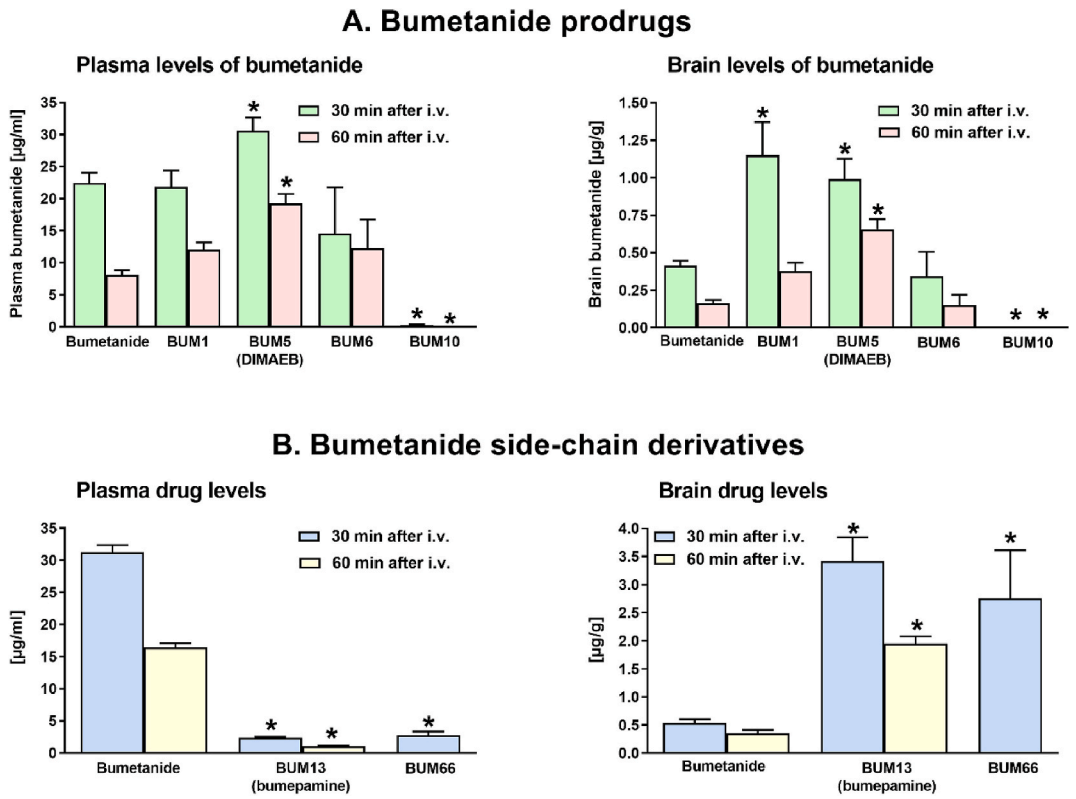

Fig. 9. Plasma and brain levels of bumetanide prodrugs (A) and side-chain derivatives (B) in mice. All drugs were i.v. administered at equimolar doses, using 10 mg/kg for bumetanide. Blood and brain were sampled at 30 and 60 min after administration except for BUM66 (30 min time point only). Data are shown as means ± SEM; significant differences to bumetanide are indicated by asterisks (*$P < 0.05$). Negligible brain levels of bumetanide were determined after administration of BUM13 (bumepamine) or BUM66. Data are from Töllner et al. (2014), Brandt et al. (2018), and unpublished experiments by Claudia Brandt and Wolfgang Löscher.

essential: carboxylic acid and sulfonic acid derivatives (at R1) are highly ionized at physiological pH and exert an inhibitory action on both hNKCC1a and hNKCC2a. With an uncharged anilinomethyl group at R1, as in bumepamine, the inhibitory activity against both transporters was lost. Thus, the relatively potent diuretic effect observed with bumepamine in vivo (Lykke et al., 2015) is most likely a consequence of the metabolism of this drug to bumetanide, as shown in mice. However, bumetanide (generated as a metabolite) played no role in the central effects of bumepamine (Brandt et al., 2018). Thus, the overall conclusion from the above work is that *it is most likely not possible to develop brain-permeant (non-acid) bumetanide side-chain derivatives that retain inhibitory effects on NKCC1*.

To determine whether and how the inhibitory effects of bumetanide and the nine tested derivatives on hNKCC1a and hNKCC2a are correlated, their IC_{50} values were compared (Lykke et al., 2016). Bumetanide was almost 6 times more potent in inhibiting hNKCC1a than hNKCC2a (Fig. 11A). The R3/R4 analogs (HH-562, PF-1574, PF-1573) also have this preferential action on hNKCC1a, with NKCC2 vs. NKCC1 potency ratios ranging from 5.9 to 7.1. All other derivatives had smaller potency ratios (ranging from 1.3 to 4.3), but still were more potent in inhibiting hNKCC1a than hNKCC2a. Only BUM13 (bumepamine) was not active on either transporter, but the very low solubility of this compound precluded testing at concentrations >100 µM. The drugs' hNKCC1a vs. hNKCC2a IC_{50} values yielded a highly significant correlation coefficient ($r = 0.9463$, $P < 0.0001$; Fig. 6B) between their inhibitory potency on the two human NKCC isoforms (Lykke et al., 2016). This substantiates the proposal of Hannaert et al. (2002) that the two cotransporter splice isoforms have a similar protein conformation that binds the R1, R3, R4, and R5 drug residues (Fig. 1C). Thus, it will be difficult, if not impossible, to develop bumetanide derivatives with higher selectivity for NKCC1 vs. NKCC2, a conclusion which will be further discussed below.

The diuretic potency of the derivatives chosen for our structure-activity experiments on dogs showed wide variation; some compounds (PF-2178, PF-1962) had the same potency as bumetanide, while others (BUM13, PF-1659, PF-1574) had 10–40 times lower one (Lykke et al., 2015). A significant correlation was found between the diuretic potency of these compounds in dogs and IC_{50} values with regard to hNKCC2a ($r = 0.778$; $P = 0.0081$). This indicates that the in vitro approach of determining inhibitory potencies of the bumetanide derivatives provides functionally meaningful data for in vivo studies.

In conclusion, an acidic group at the position R1 in the various bumetanide side-chain derivatives shown in Fig. 10 is a requirement for inhibition of both NKCC1 and NKCC2. Modifications at the R3 or R5 position can increase the inhibitory potency of the derivatives, which is associated with a high-ceiling diuretic activity. However, we did not succeed in identifying compounds that preferentially inhibit NKCC1a vs. NKCC2a. The 6-fold higher potency of bumetanide action on hNKCC1a vs. hNKCC2a is too small to justify any arguments on isoform specificity (see also section 3.4).

In a recent search for NKCC1-selective inhibitors, Laura Cancedda and colleagues tested 15 novel bumetanide analogs with diverse substituents in positions R1, R3, and R5 in bumetanide's core structure (Savardi et al., 2020). Using a Cl^- influx assay in human embryonic kidney (HEK293) cells transfected with NKCC1 or NKCC2, they found that the carboxylic acid group in position R1, although suboptimal concerning pharmacokinetic properties required from a CNS drug, was essential for blocking NKCC1. This confirms our previous findings, although in our experiments, bumetanide derivatives with other acidic groups in position R1 were also potent NKCC inhibitors (Lykke et al., 2016). Small modifications of the linear (six to eight carbon atoms) alkyl chain in position R3 and dimethylation of the sulfonamide in R5 decreased activity against NKCC2, while retaining significant activity against NKCC1 (Savardi et al., 2020). However, all modifications that reduced NKCC2 inhibition also led to a significant loss of potency

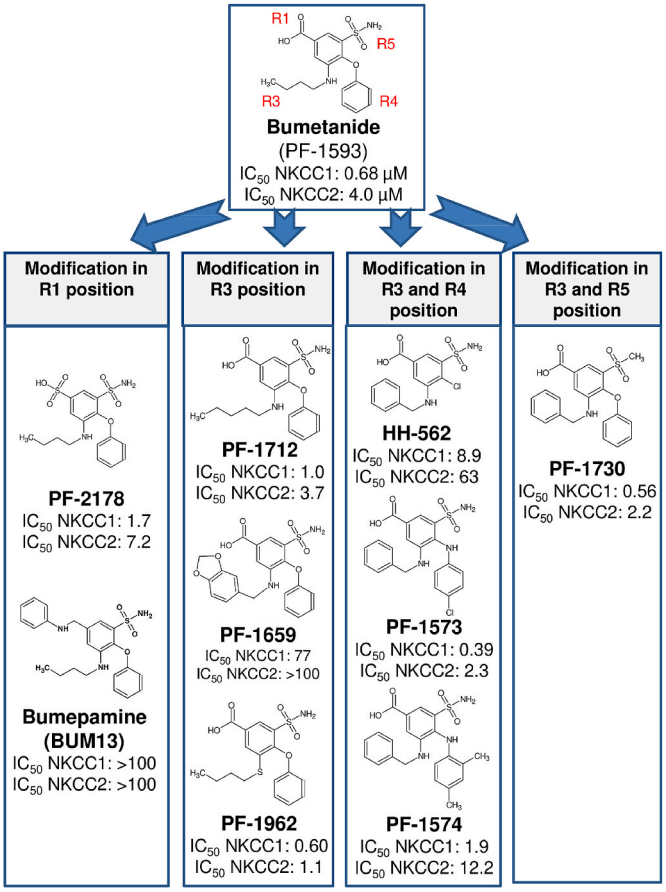

Fig. 10. Structures of bumetanide side-chain derivatives with their code numbers and, for comparison, bumetanide (PF-1593). For each, the IC_{50} (in µM) for hNKCC1a and hNKCC2a determined by $^{86}Rb^+$ uptake in transfected *Xenopus* oocytes is shown (data from Lykke et al., 2016). All derivatives were synthesized by Peter W. Feit ("PF"), including bumepamine (Nielsen and Feit, 1978), which was resynthesized by Thomas Erker and, later, Markus Kalesse (Brandt et al., 2018). The derivatives were chosen based on their diuretic activity in dogs, covering a wide range of diuretic potencies and structural modifications (Lykke et al., 2015, 2016).

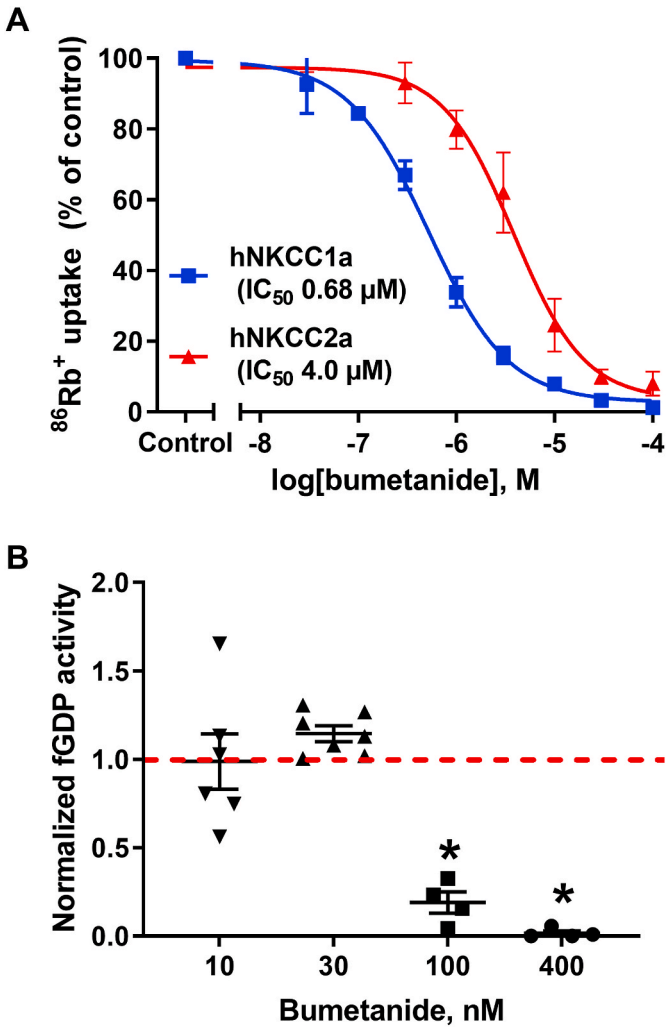

Fig. 11. In vitro concentration-effect experiments with bumetanide. (A) Effect of bumetanide on hNKCC1a- and hNKCC2a-mediated $^{86}Rb^+$ uptake in *Xenopus* oocytes. The figure illustrates dose-inhibition curves of bumetanide (corrected for endogenous NKCC contribution in uninjected oocytes) and averaged across six experiments per NKCC isoform. Data from Lykke et al. (2015, 2016). (B) Quantification of the effect of different bumetanide concentrations on mean normalized field giant depolarizing potential (fGDP) activity in hippocampal slices from P3–P4 rats (see Fig. 13 for original recordings). Individual data (and mean ± SEM) are shown. Significant suppression of fGDPS is indicated by asterisks ($P < 0.001$). Note that low concentrations of bumetanide (<100 µM) do not affect fGDPs, which is in line with the minimal NKCC1 inhibitory concentration range of bumetanide (100–300 nM) discussed in the text and Puskarjov et al. (2014). Data are from Brandt et al. (2018).

against NKCC1, supporting the conclusion (see above) that it is difficult if not impossible to develop new and potent bumetanide derivatives with significant selectivity for NKCC1 over NKCC2 (Lykke et al., 2016). Savardi et al. (2020) therefore sought new molecular entities, structurally unrelated to bumetanide, as selective NKCC1 inhibitors.

3.4. An integrated in silico and in vitro screening approach for developing brain-permeant NKCC1-selective inhibitors

Cancedda and coworkers (Savardi et al., 2020) applied a ligand-based computational strategy to build a pharmacophore model based on bumetanide and other known NKCC1 inhibitors. The main aspects in the optimization of target specificity included (i) the crucial importance of the carboxylic group and (ii) the contribution to the selectivity of a linear alkyl chain attached to an aromatic core. They used an iterative approach involving in silico and in vitro screening, followed by structural and functional optimization of candidate small-molecule inhibitors, to achieve enhanced efficacy. A total of 135,000 compounds were screened in silico, followed by in vitro testing of 255 compounds in a functional NKCC transporter (HEK293 Cl^- influx) assay. Using this integrated drug discovery strategy, the authors identified two novel candidate drugs, ARN22642 and ARN22430, that showed potent NKCC1 inhibition, but had low solubility and metabolic stability. The addition of a trifluoromethyl group to ARN22430 improved its drug-like (physico-chemical and metabolic) properties, and the resulting analog, ARN23746 (Fig. 8), showed increased potency and apparent selectivity for NKCC1 inhibition in multiple assays with an IC_{50} of about 20 µM. Notably, however, an IC_{50} of 20 µM indicates a potency that is much lower (by a factor of >20) than that of bumetanide, which is typically <1 µM as already stated above (see also Koumangoye et al., 2021). At 10 µM, ARN23746 did not significantly inhibit NKCC2 or KCC2 and did not exert significant off-target activity as an agonist or antagonist for a panel screen of 47 standard pharmacological targets. However, given the NKCC1 IC_{50} of about 20 µM, the selectivity of ARN23746 for NKCC1 vs. NKCC2, which was reported by Savardi et al. (2020) only at a concentration of 10 µM, is not meaningful. For obvious reasons, target selectivities of drugs are examined and compared at concentrations higher than their IC_{50} values. For instance, in our experiments with bumetanide

and side-chain derivatives on hNKCC1a vs. hNKCC2a, bumetanide and several of its derivatives were on average 6–7 times more potent in inhibiting hNKCC1a than hNKCC2a, yet this does not characterize these compounds as NKCC1-selective (see section 3.3) (Lykke et al., 2016). In pharmacology, target specificity of a drug is typically defined by much higher differences (by several orders of magnitude) between drug concentrations affecting the target vs. effects on a related target or off-target effects (Huggins et al., 2012).

In vivo, a low dose of ARN23746 (0.2 mg/kg i.p.) exerted no diuretic effect in mice but, surprisingly, no data on higher doses were provided (Savardi et al., 2020). Again, it is worthwhile to point out here that the much more potent NKCC1/NKCC2 inhibitor, bumetanide, would not, either, induce diuresis in mice at such a low dose (Olsen, 1977). This means that the alleged NKCC1 selectivity and the lack of diuretic action of ARN23746 are simply based on the low concentrations and doses used, and not on the drug's genuine pharmacodynamic characteristics.

In pharmacokinetic analyses by Savardi et al. (2020), bumetanide and ARN23746 were administered at 2 mg/kg i.v., and plasma and brain levels were determined at different times after administration. At the time of peak drug levels, ARN23746 achieved about twice as high brain levels as bumetanide; brain:plasma ratio was ~0.005 for bumetanide vs. ~0.043 for ARN23746 (Table 2). Thus, despite this higher brain:plasma ratio, the carboxylic group in ARN23746 and the resulting high ionization rate still hampered its brain penetration compared to compounds without an acid group (Tables 1 and 2). Also, it should be re-emphasized that ARN23746 exhibits some of the structural characteristics of bumetanide (Fig. 8), indicating that both phenotypic screening as used by Feit in the 1960s and the integrated in silico/in vitro drug discovery strategy used by Savardi et al. (2020) resulted in compounds with structural similarities.

Savardi et al. (2020) also tested ARN23746 in a model of Down syndrome (DS; Ts65Dn mice) that was reported to have elevated neuronal $[Cl^-]_i$ in experiments in vitro, resulting from NKCC1 upregulation (Deidda et al., 2015). Similar to bumetanide, ARN23746 (at 10 μM) was reported to induce a decrease in $[Cl^-]_i$ to physiological levels in DS neurons in vitro, without significantly affecting $[Cl^-]_i$ in wild-type neurons. While numerous beneficial effects of the drug on neuronal functions and behavior of the DS and the autism spectrum disorder (ASD) mouse models were reported by Savardi et al. (2020), it is not possible to reconcile these effects with the actual in vivo doses that were used.

The peak brain levels of ARN23746 following i.v. administration of 2 mg/kg were only ~120 ng/g, which corresponds to ~0.33 μM. Notably, this is a concentration that is roughly *two orders of magnitude below the unimpressively high IC_{50}* of ARN23746 (~20 μM). Moreover, in the experiments in DS and ASD mouse models, ARN23746 was administered at a dose of 0.2 mg/kg i.p., i.e., *one-tenth of the dose used in the experiments on pharmacokinetics*. No brain levels were determined with the lower dose, but assuming linear kinetics, maximal brain levels of ARN23746 would be in the range of 0.03 μM, i.e., *three orders of magnitude* below the drug's IC_{50}. Finally, Savardi et al. (2020) reported that ARN23746 restores $[Cl^-]_i$ in DS neurons; however, this was examined in vitro with a concentration of 10 μM, which is *~300-times higher than the achieved peak brain level* of ARN23746 in the in vivo experiments in DS mice. We are unable to explain these striking discrepancies.

Although the drug-design approach of Savardi et al. (2020) is valid in itself (Raveendran et al., 2020), this does not mean that a useful new drug is bound to be discovered, as is evident from the present evaluation of their data.

More recently, Cancedda and colleagues reported another derivative (ARN24092) as a backup/follow-up compound for ARN23746 (Borgogno et al., 2021). ARN24092 differs from ARN23746 only by substitution of a hydroxyl group in R2 (see Fig. 8). In the Cl^- influx assay in NKCC1-transfected HEK293 cells, percentage inhibition of Cl^- influx at 10 and 100 μM was 13.9% and 51.9% for ARN24092; 45.7% and 92.8% for ARN23746; and 58.8% and 71.7% for bumetanide, respectively. IC_{50} values were not reported. As was the case with ARN23746 (Savardi et al., 2020), selectivity for NKCC1 vs. NKCC2 was only tested at 10 μM, at which concentration ARN24092 has hardly any effect on either of the two NKCC isoforms, but Borgogno et al. (2021) claimed that ARN24092 is selective for NKCC1. Again, there's a major flaw underlying this conclusion, which is identical to the one on the alleged selectivity of ARN23746.

3.5. Discovery of novel NKCC1 inhibitors by high-throughput screening

Scientists from Aurora Biomed Inc. (Vancouver, Canada) and Hoffmann-La Roche (Basle, Switzerland) developed a high-throughput screening (HTS) assay for NKCC1 (Gill et al., 2017). This nonradioactive rubidium (Rb^+) flux assay coupled with ion channel reader series provided a working screen for NKCC1 expressed in a HEK cell line and also allowed to compare drug effects in HEK cells in which NKCC1 expression was controlled by doxycycline. In a first step, the Rb^+ influx assay was optimized into 384-well format and used to screen a focused library of 1450 compounds in three independent runs, which produced robust data across the three runs and a hit rate of 0.7% (Gill et al., 2017). Then, a full HTS of 1.2 million compounds was performed. Chemical classes of specific hits were generated with dose-response confirmation from the Rb^+ influx assay. A counter screen Rb^+ influx assay on the wild-type cells was also carried out for comparison with Rb^+ entry routes through other endogenous ion channels and cotransporters. IC_{50} values of several novel compounds were presented, including one compound (#4636277) that was 5 times more potent than bumetanide (Gill et al., 2017). However, to our knowledge, detailed data on these novel compounds, including their chemical structure and pharmacological properties, are not in the public domain.

3.6. In silico identification of potential NKCC1 inhibitors

Recently, Roy et al. (2021) used the predicted crystal structure of human NKCC1 for virtual compound screening and molecular docking to identify novel NKCC1-selective inhibitors. For this purpose, an SDF (simulation description format) library of 1930 brain-permeant compounds was used, resulting in the identification of four compounds, which along with control (bumetanide) underwent molecular dynamics simulations to validate the docking interactions. The in silico evaluation suggested that all four compounds are potent inhibitors of NKCC1, which, however, was not verified in vitro. Interestingly, the chemical structures of the four identified compounds markedly differed from bumetanide and other loop diuretics (Fig. 12). As also concluded by Roy et al. (2021), in vitro and in vivo experiments are required to confirm that these compounds indeed inhibit NKCC1 with the potency and selectivity suggested by the in silico study and that they reach NKCC1-inhibitory brain concentrations at tolerable systemic doses.

3.7. Effects of novel bumetanide derivatives that do not directly inhibit NKCC1

As described in section 3.3, the substitution of the carboxylic residue of bumetanide in the R1 position with an anilinomethyl group (bumepamine; Fig. 10) abolished the inhibitory effect on NKCC1 and NKCC2. However, the non-acid derivative, bumepamine, exerted potent diuretic activity in dogs, which, at least in part, could be related to metabolism to bumetanide in the periphery (Lykke et al., 2015, 2016). However, in mice, plasma and brain levels of bumetanide after administration of bumepamine were very low, indicating that metabolism to bumetanide is not important for the pharmacodynamic effects of bumepamine (Brandt et al., 2018). Based on the preliminary pharmacokinetic and pharmacodynamic experiments, we decided to characterize the brain-permeant bumepamine in more detail. The rationale was that this compound offers the possibility to study whether some of the

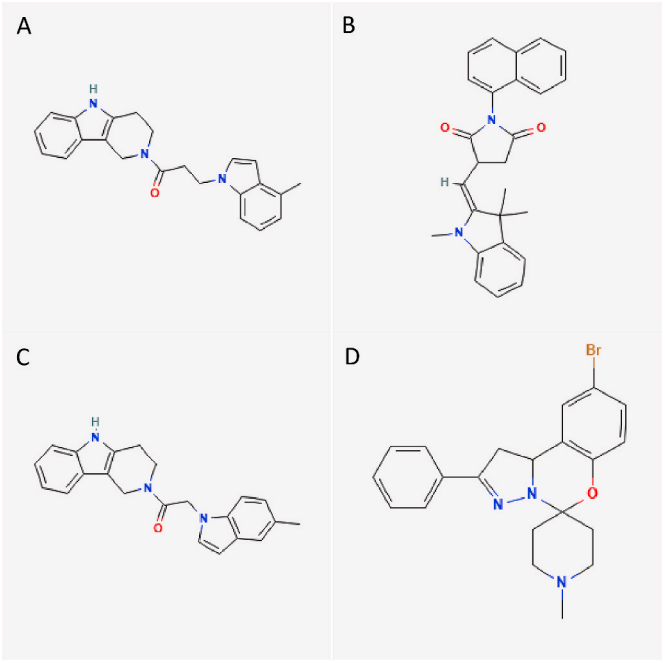

Fig. 12. Structures of the four novel NKCC1 inhibitors identified by an in silico strategy by Roy et al. (2021). (A) 3-(4-Methyl-1H-indol-1-yl)-1-(1,3,4,5-tetrahydro-2H-pyrido [4,3-b]indol-2-yl)-1-propanone (Pubchem CID: 71753382); (B) (E)-1-(Naphthalen-1-yl)-3-((1,3,3-trimethylindolin-2-ylidene)methyl)pyrrolidine-2,5-dione (CID: 5740383); (C) 2-(5-Methyl-1H-indol-1-yl)-1-(1,3,4,5-tetrahydro-2H-pyrido [4,3-b]indol-2-yl)ethanone (CID:71692222); (D) 9′-Bromo-1-methyl-2′-phenyl-1′,10′bdihydrospiro(piperidine-4,5′-pyrazolo[1,5-c][1,3]benzoxazine)(CID: 3442850). Note the differences to the structure of bumetanide. It remains to be demonstrated that these compounds inhibit NKCC1 in vitro and in vivo.

CNS effects of bumetanide which are thought to be mediated by NKCC1 inhibition can also be achieved by a close derivative that apparently does not share this molecular mode of action.

As shown in Fig. 9B, bumepamine reaches ~7-fold higher brain levels than bumetanide after systemic administration of equimolar doses. Plasma levels are lower than those of bumetanide, indicating rapid tissue distribution (Brandt et al., 2018). Bumepamine is significantly more efficient than the parent drug in potentiating PB's anticonvulsant effect in two rodent models of chronic, drug-resistant epilepsy: amygdala kindling in rats and the pilocarpine model in mice. As expected from its lack of direct inhibitory action on NKCC1, bumepamine suppressed NKCC1-dependent GDPs in neonatal rat hippocampal slices much less effectively than bumetanide (Fig. 13) and did not inhibit Ca^{2+} transients induced by depolarizing $GABA_A$-receptor currents in the slices (Brandt et al., 2018). As is the case with bumetanide, bumepamine exerts high unspecific brain tissue binding (Table 2). In a rat model of birth asphyxia, bumepamine was much more effective than bumetanide (and DIMAEB) in potentiating the effect of PB on neonatal seizures (Johne et al., 2021a,b). Thus, bumepamine may be useful in sorting out the so-far unknown mechanisms whereby systemic bumetanide might act when administered at doses that do not lead to brain concentrations that inhibit NKCC1.

Because of the structural similarity of bumepamine to a 4-aminopyridine derivative of bumetanide (AqB013) that has previously been reported to inhibit aquaporin (AQP) 1 and AQP4 (Migliati et al., 2009), we hypothesized that inhibition of AQP4 may constitute a mechanism of action of bumepamine (and possibly also bumetanide). The glial water channel AQP4 is expressed strongly throughout the brain and has been implicated in epilepsy and in the effects of some ASDs (Hubbard et al., 2018; Vandebroek and Yasui, 2020). However, neither bumetanide nor bumepamine exerted any significant effect on AQP4-mediated osmotic water permeability in our experiments (Brandt et al., 2018).

More recently, Thomas Erker synthesized a benzylamine compound (BUM66, STS66) with a similar structure as bumepamine except that the phenyl group was replaced by a trifluoroethyl group that further increases lipophilicity (Fig. 8). As shown in Fig. 9B, brain levels of bumepamine and STS66 are similar, both exceeding the levels obtained with an equimolar dose of bumetanide.

STS66 reduced brain damage after ischemic stroke in mice, and was more effective than bumetanide or its prodrug DIMAEB (Huang et al., 2019b). Interestingly, STS66 treatment completely blocked the ischemia-induced elevation of phospho-NKCC1 $pThr^{206}$, indicating an inhibitory effect on the brain WNK-SPAK/OSR1 upstream regulatory pathway of NKCC1 (Huang et al., 2019b). It will be interesting to examine whether bumepamine might also inhibit this pathway. However, we do not include other drugs that act on (de)phosphorylation cascades targeting NKCC1 in the present review, and the interested reader is referred to specific papers in this field (Huang et al., 2019a; Zhang et al., 2020a,b). In addition to its beneficial effect in a stroke model, STS66 was reported to reduce glioma cell growth in part by inhibiting NKCC1 in cultured glioma cells with an IC_{50} of ~40 μM (Luo et al., 2020).

In the hippocampal CA3 region of acute neonatal rat brain slices, the effects of STS66 on GDPs (see section 2.1) were compared with those of bumepamine and bumetanide. All three compounds suppressed these NKCC1-dependent network events (Fig. 13). The efficacy of STS66 aka BUM66 was similar to bumetanide, whereas bumepamine was about 5 times less potent. STS66 and especially bumepamine inhibited GDPs more slowly than bumetanide, possibly indicating an indirect effect on NKCC1 or off-target effects.

Another recent compound synthesized by Thomas Erker is BUM97, a trifluoroethyoxy derivative of bumetanide (Fig. 8). This compound was reported to suppress spontaneous electrographic seizures in the intrahippocampal kainate mouse model of TLE without inducing diuresis (Auer et al., 2020b). Among three bumetanide derivatives examined (BUM97, BUM532, BUM690), BUM97 showed remarkable pharmacological properties with a strong and long-lasting reduction of spontaneous recurrent seizures by itself, but particularly in combination with PB. However, bumetanide (10 mg/kg) alone also suppressed electrographic seizures in this study (Auer et al., 2020b). In contrast, we have never observed any robust anticonvulsant effect of bumetanide when administered alone in different rodent models of seizures or epilepsy. We are not aware of studies on possible direct actions of BUM97 on NKCC1.

4. The complexity of NKCC1 as a drug target within the brain

There is an abundance of knowledge regarding the modes of actions of NKCC1 blockers such as bumetanide on neurons (see Section 2.1). Bumetanide has been widely used to examine the role of NKCC1 in GABAergic signaling, and we do know that this transporter is involved in the changes in chloride regulation that take place during neuronal development and disease (Kaila et al., 2014a,b; Virtanen et al., 2021; see Fig. 2). NKCC1 is also located in presynaptic terminals of certain neurons, where it modifies transmitter release in a $GABA_A$ receptor-dependent manner (Blaesse et al., 2009). Bumetanide has also been useful in studying the role of depolarizing actions of GABA in network events such as GDPs (see section 3.7, Figs. 11B and 13) as well as in interictal-like activity in chronically-epileptic tissue (Huberfeld et al., 2007; for review see Kaila et al., 2022). With respect to inhibition of GDP activity, it is interesting to note that low concentrations of bumetanide (<100 μM) do not affect GDPs (Fig. 11B), which is in line with the minimal NKCC1 inhibitory concentration range of bumetanide (100–300 nM) used repeatedly in this review. However, all this work has been done under well-defined experimental conditions in vitro, which formed the basis for preclinical and clinical in vivo studies.

The modes of action of NKCC1 blockers are very difficult to study in

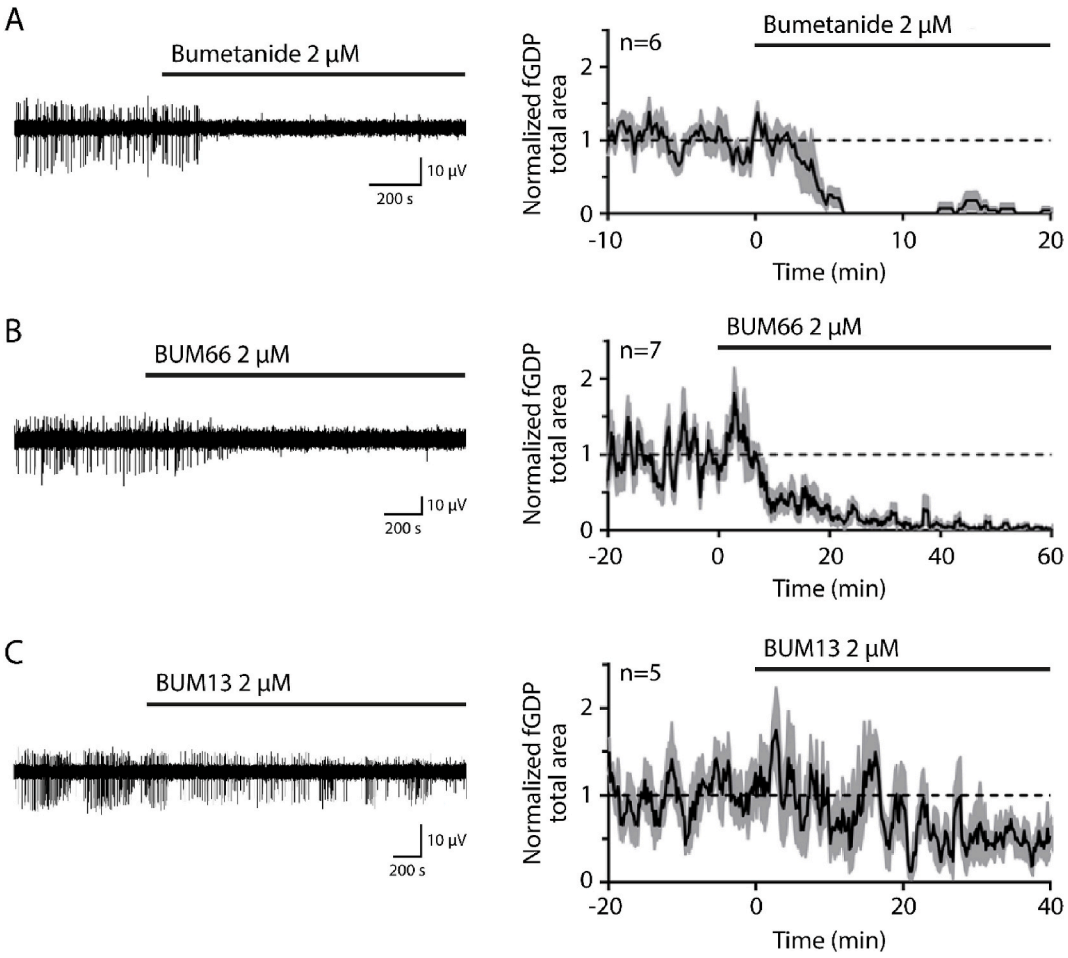

Fig. 13. Effect of bumetanide and side-chain derivatives on field giant depolarizing potentials (fGDPs). Low concentrations of bumetanide and BUM66 (STS66) caused a fast suppression of fGDPs, while the effect bumepamine (BUM13) was much slower and incomplete. Left panel: representative local field potential (LFP) recording traces from P4, P3, and P3 rat hippocampal slices (A, B and C, respectively) in the CA3 region (filtered 1–10 Hz). Right panel: Moving average plots of normalized fGDP total areas (mean ± SEM, 60 s window, 10 s steps). For methods, see Spoljaric et al. (2017). Exogenous application of 2 µM bumetanide and 2 µM BUM66 caused robust suppression of fGDPs (A and B, respectively), while 2 µM BUM13 had a much weaker and slower effect (C). BUM13 and BUM66 were kindly provided by Thomas Erker. Unpublished data by Pauliina Paavilainen and Kai Kaila.

vivo for various reasons. In addition to the low CNS accessibility of bumetanide and related compounds (see above), a major difficulty stems from the fact that NKCC1 is expressed by practically all cells in the brain, both within the parenchyma (e.g. oligodendrocytes, astrocytes, microglia, and neurons) as well as in structures outside it (e.g.choroid plexus epithelium, brain capillary endothelial cells of the BBB) (Markadieu and Delpire, 2014; Virtanen et al., 2020). This information has been available for several years by the time of writing this review, and it is surprising to find that even nowadays some studies targeting NKCC1 by systemically or intracranially applied bumetanide (and by means of non-specific RNA interference techniques) are based on the false idea that NKCC1 is only or mainly expressed in neurons (see section 5). In fact, the opposite is true, as will be shortly described. This also implies that parameters such as NKCC1/KCC2 ratios, when referring to amounts of RNA or protein in brain tissue samples, have absolutely no meaningful counterpart in neuronal functions or structure.

As shown in Fig. 14, *the neuronal expression of NKCC1 mRNA in the brain is a very small fraction, several orders of magnitude lower than the overall expression of this transporter*, and with an extremely low number (around 10 in 100.000) of transcripts for instance in hippocampal single-cell RNAseq data (http://mousebrain.org/genesearch.html; Zeisel et al., 2018). Consequently, the effects of global inhibition of NKCC1 in the brain under various conditions cannot be attributed to changes in neuronal functions. This makes the effects of NKCC1 blockers highly unpredictable, and they may include detrimental and/or beneficial ones, depending for instance on age- and disease-related alterations in the cellular NKCC1 expression patterns and functionality. For instance, both oligodendrocytes and astrocytes are able to modulate neuronal plasticity via NKCC1 functions (Henneberger et al., 2020; Yamazaki et al., 2021). Whether these mechanisms are also involved in shaping seizure activity is an interesting question for future work, but achieving sufficient celltype specificity for pharmacological block of NKCC1 remains, again, a problem.

Direct application of bumetanide into brain tissue has, indeed, been shown to exert both beneficial and adverse effects. For instance, in a rat model of posthemorrhagic hydrocephalus, intraventricular hemorrhage causes an inflammation-dependent hypersecretion of CSF, which is suppressed by intracerebroventricular but not systemic (i.v.) infusion of bumetanide (Karimy et al., 2017). In a study in which osmotic minipumps were used to infuse bumetanide (86 ng/24 h) intracerebrally between 2 and 5 days after pilocarpine-induced status epilepticus (SE) in rats, bumetanide was reported to partially block the SE-induced NKCC1 upregulation and fully restore KCC2 expression and function, normalize chloride homeostasis, and significantly reduce mossy fiber sprouting within the dentate gyrus (Kourdougli et al., 2017). Furthermore, Kourdougli et al. (2017) found that early transient bumetanide treatment after SE reduced spontaneous seizures recorded two months after SE, indicating an antiepileptogenic effect of the drug. Sivakumaran and Maguire (2016) examined the acute effect of intrahippocampal

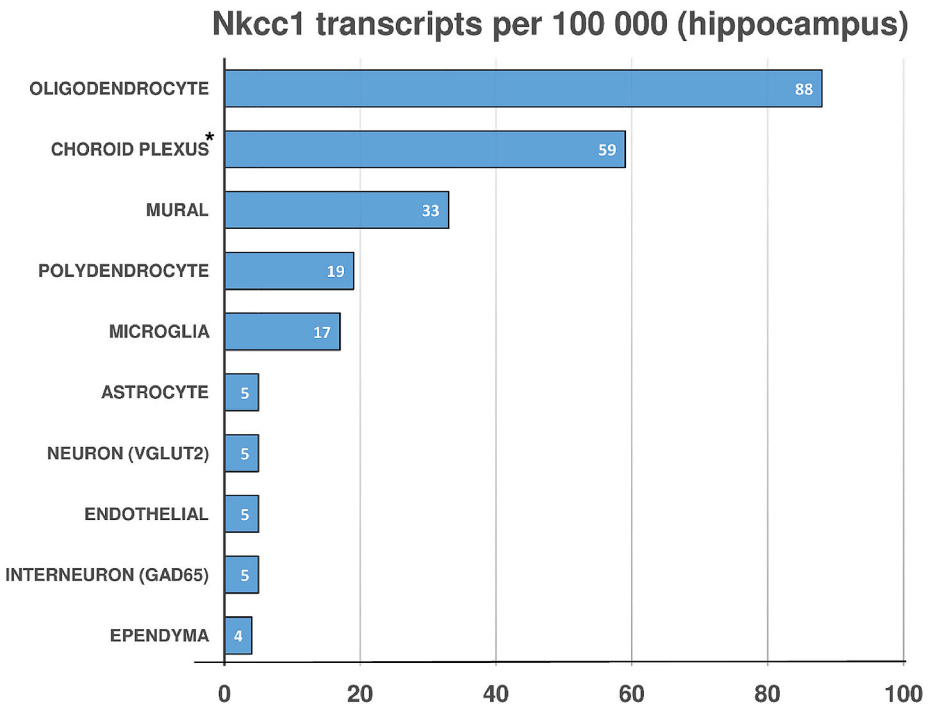

Fig. 14. Expression of NKCC1mRNA by different cell types in the mouse hippocampus and, for comparison, the choroid plexus (*). Data are from single-cell RNAseq datasets of P30 mice published by Zeisel et al. (2018) and were compiled using the Mouse brain.org database (http://mousebrain.org/genesearch.html). Note the very low expression of NKCC1 mRNA by neurons in comparison to other cell types in the brain parenchyma. See also Mahadevan and Woodin (2020) for discussion on cell type-specific expression of different cation chloride cotransporters in cortex and hippocampus of the adult mouse.

administration (54.8 μM, 500 nl) of bumetanide on seizures induced by intrahippocampal injection of kainate in mice. When injected 30 min before kainate, intrahippocampal bumetanide resulted in a significant increase in the latency to the onset of epileptiform activity and reduced epileptiform activity compared to vehicle-treated mice. Whether a decrease in cellular volume, leading to an increase in ECS, might play a role here (see e.g. Jefferys, 1995) remains an open question in these as well as in other experiments with intracranial application of bumetanide. However, in a study in which the effects of i.v. (10 mg/kg) and intracerebroventricular (i.c.v.; 14.6, 36.4, 58.3, or 583 ng) administration of bumetanide were compared in amygdala kindled rats, no robust anticonvulsant effect on seizure threshold or the severity and duration of seizures was observed, but the highest i.c.v. dose induced a pro-convulsant effect (Töpfer et al., 2014). In the hippocampus, roughly similar bumetanide levels were measured 30 min following i.v. injection of 10 mg/kg (0.26 μM) or i.c.v. injection of 583 ng bumetanide (0.22 μM). Further evidence that bumetanide can act in a pro-rather than anticonvulsant manner was provided by the finding that high (>100 μg) i.c.v. doses of the drug induces tonic–clonic seizures in adult mice (Inoue et al., 1989). More recently, it was reported that i.c.v. infusion of 0.4 mg/kg/day bumetanide over 28 days negatively alters the morphology of newly formed neurons in the rat dentate gyrus (Gómez-Correa and Zepeda, 2020). It should be noted that both beneficial and deleterious effects of bumetanide at high intracerebral doses could be due to off-target activities of bumetanide at the molecular and cellular level (see section 6).

There are several studies in the literature with a major confusion regarding data obtained with in vitro application of bumetanide on brain slice preparations and neuronal cultures; which is then employed for building hypotheses of the mechanistic bases of behavioral/cognitive rescue via systemic (e.g., i.p. or i.v.) drug application in vivo. While each piece of data may be valid in itself, the behavioral/cognitive effects cannot occur via block of NKCC1 in diseased neurons if the systemic drug concentrations are not even close to levels needed for achieving pharmacologically relevant concentrations in the brain parenchyma. This problem has been overlooked in most of the older studies on bumetanide actions in (neonatal) seizures (see Löscher et al. (2013); Puskarjov et al. (2014); and sections 2.1 and 2.5), and a more recent example of this kind of fallacy is provided by the studies by Cancedda and coworkers (e.g. Deidda et al., 2015; Savardi et al. (2020), see section 3.4). Another relevant example is the study by Dargaei et al. (2018), in which the authors demonstrate that hippocampal NKCC1 protein levels (which, notably, do not reflect neuronal levels as explained above) are upregulated and E_{GABA} has a more positive value in a Huntington's disease mouse model when compared to WT mice. The authors demonstrate that bumetanide application in slice preparations appears to re-set the E_{GABA} of the diseased animals, and two-week-long bumetanide i.p. injections rescue some cognitive behaviors in the model. But in the absence of continual bumetanide, and shortly after completing behavioral testing, the authors demonstrate that the depolarized E_{GABA} phenotype does not appear to be rescued, thus highlighting a lack of neuronal NKCC1-blockade in animals treated with bumetanide whereas still observing behavioral rescue. Below (sections 5 and 6), we make some suggestions on how paradoxical observations of the above kind might be explained.

While the effects of constitutive knockout (KO) of a given molecule in mice often leads to powerful compensatory effects during development (Brickley et al., 2001; Marder and Goaillard, 2006; Sipilä et al., 2009), it is still of interest that global KO of NKCC1 in mice results in *more severe* epilepsy in the intrahippocampal kainate mouse model of TLE compared to wildtype (WT) littermates (Hampel et al., 2021c). In a novel transgenic mouse line with inducible microglial NKCC1 deletion, the microglial NKCC1 KO animals exposed to experimental stroke showed significantly *increased* brain injury, inflammation, cerebral edema, and worse neurological outcome compared to WT controls (Tóth et al., 2021). Notably, cell-specific KO is not without compensatory and adaptive consequences, either, as shown for instance in the above study where major changes in microglial gene expression were observed during a standard period of post-KO induction time.

5. Clinical and preclinical studies on systemically-applied NKCC1 inhibitors: drug actions within or outside the CNS?

As described in section 1, increased expression and/or activity of NKCC1 in the CNS has been associated with a wide variety of brain disorders including developmental disorders, epilepsy, schizophrenia,

and stroke (Ben-Ari, 2017; Schulte et al., 2018). This has motivated the use of bumetanide in several clinical studies in neonates, children, adolescents, and adults, which, however, have had largely negative or inconclusive outcomes (for review cf. Schulte et al., 2018; Kharod et al., 2019). In the two trials in newborns with neonatal seizures, in which bumetanide was used as an adjunct to PB, bumetanide showed no efficacy (Pressler et al., 2015) or no convincing efficacy (Soul et al., 2021), but in both trials, ototoxicity occurred (Table 3). Surprisingly, the more recent one (Soul et al., 2021) was still based on the outdated idea that systemic bumetanide applied at clinically relevant concentrations targets mainly neuronal NKCC1 and, even more specifically, postsynaptic E_{GABA} in vivo, which is simply not possible (see section 4).

A series of clinical trials were conducted by Ben-Ari et al. in patients with ASD. Following a pilot study (Lemonnier and Ben-Ari, 2010), two consecutive placebo-controlled randomized phase 2 trials were carried out (Lemonnier et al., 2012, 2017) testing bumetanide (1 mg/day for three months) in 60 and 90 patients, ranging from infancy to adulthood respectively. Both pilot trials suggested that treatment with bumetanide significantly improved Childhood Autistic Rating Scale (CARS) scores and attenuated the severity of the disorder overall, with no major side effects other than diuresis (Lemonnier et al., 2012, 2017). However, in a more recent double-blind, placebo-controlled phase 2 trial, in which the efficacy of bumetanide on core symptom domains of ASD was tested, the trial outcome was negative (Sprengers et al., 2021). The authors concluded that "random off-label prescription of bumetanide for children with ASD is not recommended by our findings." A recent meta-analysis of double-blind, randomized, placebo-controlled trials, which examined the efficacy of pharmacological agents in the treatment of ASD, concluded that currently available drugs, including bumetanide, have at best only a modest benefit for the treatment of ASD, with most of the evidence supporting antipsychotic medications (Zhou et al., 2021). Finally, the results of two large phase 3 trials assessing bumetanide in the treatment of several hundred children and adolescents with moderate-to-severe ASD were reported; no effectiveness was observed, leading to early termination of the trials (https://servier.com/en/communique/servier-and-neurochlore-announce-the-main-results-of-the-two-phase-3-clinical-studies-assessing-bumetanide-in-the-treatment-of-autism-spectrum-disorders-in-children-and-adolescents/). Again, we would like to point out that the clinical studies on bumetanide in autism were (like those on neonatal seizures) based on the false assumption of the systemically-applied drug's specific and effective action on central GABAergic signaling in vivo. No clinical data are available for any of the novel NKCC1 inhibitors described in this review.

Based on off-label use of bumetanide in patients with tuberous sclerosis complex (TSC), which is strongly associated with broad neurodevelopmental disorders, including ASD symptomatology, van Andel et al. (2020) performed an open-label pilot study with bumetanide in a small group of TSC patients. Bumetanide did not affect seizure frequency while having significant effects on irritable behavior, social behavior, and hyperactive behavior. However, important limitations of this study are the single-arm open-label design and the absence of a placebo group. Similarly, the clinical evidence for effects of bumetanide in other seizure disorders is anecdotal, at best (see Kharod et al., 2019).

What about the numerous preclinical data indicating promising effects of systemically-applied (i.p or i.v.) bumetanide and its derivatives in animal models of CNS disorders (cf., Kahle et al., 2008; Ben-Ari, 2017; Schulte et al., 2018; Kharod et al., 2019)? In some animal studies, bumetanide has been used at doses (2–10 mg/kg or higher) that can be considered sufficient to obtain transient NKCC1-inhibitory drug levels in the brain parenchyma. For instance, systemic application of a rather high dose of 10 mg/kg in mice leads to a maximum free concentration in the brain of 0.48 μM, which falls to 0.12 μM within 15 min and 0.08 μM within 30 min, i.e., levels below the minimal NKCC1 inhibitory bumetanide levels of ~0.1–0.3 μM (Tables 1 and 2; Fig. 4A). From these data one may derive that bumetanide doses ≥2 mg/kg are sufficient to reach such minimal NKCC1 inhibitory drug levels at least shortly after administration. This is substantiated by the observation that 2 mg/kg bumetanide applied i.p. transiently blocked hippocampal sharp waves in freely-moving P7-9 neonatal rats in vivo within minutes after injection (Sipilä et al., 2006). These hippocampal network events in vivo share many characteristics with GDPs in slice preparations (cf. Sipilä et al., 2005), which can be blocked by NKCC1 inhibitors (Figs. 11B and 13; section 2.1.).

However, for instance in models of neonatal seizures, significant effects have been reported when bumetanide was administered at clinically relevant doses (0.1–0.3 mg/kg) (cf. e.g., Cleary et al., 2013), which do not lead to NKCC1-inhibitory drug levels in the brain as extensively discussed in previous sections (see also Wang et al., 2015; and Löscher and Kaila, 2021). Similarly, Marguet et al. (2015) reported a very interesting, protracted antiepileptogenic effect of bumetanide in a genetic mouse model of epilepsy. Bumetanide (at a low dose of 0.2 mg/kg applied twice a day during postnatal days 0–14) prevented the developmental establishment of seizures with obviously no direct CNS actions. As discussed in section 3, interesting preclinical data were also reported for several of the novel bumetanide prodrugs and side-chain derivatives as well as other NKCC1 inhibiting loop diuretics, such as azosemide. However, as with bumetanide, the effects of systemic administration of these compounds were often not associated with brain levels that would inhibit NKCC1 in the brain parenchyma. Thus, the mechanisms underlying indirect CNS effects by bumetanide and its derivatives, mediated by NKCC1 expressed outside of the brain parenchyma need consideration (Puskarjov et al., 2014; Kharod et al., 2019). Possible off-target effects at the molecular level are described in section 6.

NKCC1 is highly expressed on the luminal membrane of the cerebral vascular endothelium, so the transporter is directly exposed to blood levels of systemically administered bumetanide or other NKCC1 inhibitors. NKCC1 in brain endothelial cells contributes to the ionic composition and volume of brain interstitial fluid and seems to be critically involved in ionic edema and swelling of the parenchyma following brain insults, including SE (Kahle et al., 2009; Simard et al., 2010; Wallace et al., 2011; Mokgokong et al., 2014). Brain edema is thought to be one of the major factors leading to mortality and early (insult-associated) seizures and may also be involved in the development of acquired epilepsy (Donkin and Vink, 2010; Iffland et al., 2014; Glykys et al., 2017). Thus, it has been proposed that a reduction of the intracerebral volume (and pressure) via NKCC1 inhibition at the BBB might contribute to the seizure-reducing effect of bumetanide (Puskarjov et al., 2014; Auer et al., 2020a). Furthermore, NKCC1 inhibition at the BBB and/or at the choroid plexus (Lu et al., 2006; Karimy et al., 2017) would explain the effects of bumetanide in models of ischemic stroke, because NKCC1 is phosphorylated and functionally stimulated under ischemic conditions, thereby facilitating ionic edema in the early stages of brain ischemia (Kahle et al., 2009). In the NKCC1 pharmacology of the choroid plexus, it should be noted that NKCC1 is typically expressed in

Table 3
Ototoxicity associated with oral administration of bumetanide as an add-on to phenobarbital for treatment of seizures in two clinical trials in neonates. Except one neonate ([a]), all babies with hearing loss received an aminoglycoside antibiotic, which is known to potentiate the ototoxic activity of bumetanide (Ding et al., 2016). Note that the incidence of ototoxicity in the two trials was not significantly different (P = 0.1926; Barnard's test). In the Soul et al. (2021) study, no ototoxicity was observed in the placebo arm (n = 16).

Reference	Dose of bumetanide (mg/kg)				
	0.05	0.01	0.02	0.03	All
	Incidence of hearing loss				
Pressler et al. (2015)	1/3	0/3	1[a]/6	1/1	3/13 (23.08%)
Soul et al., 2021	–	0/7	1/15	1/5	2/27 (7.4%)
Combined	1/3	0/10	2/21	2/6	5/40 (12.5%)

[a] No aminoglycoside.

the apical membrane and thus less accessible to blood-borne drugs than for instance the endothelial cells of the BBB (Delpire and Gagnon, 2019).

Notably, the BBB is not uniform throughout the brain (Wilhelm et al., 2016; Löscher and Friedman, 2020). For example, at the level of circumventricular organs (such as the area postrema, posterior pituitary, intermediate lobe of the pituitary gland, median eminence, subcommissural organ, pineal gland, subfornical organ, and the organum vasculosum laminae terminalis) capillaries are more permeable, containing fenestrations and discontinuous tight junctions. However, to our knowledge, there are no data in the public domain showing that, following systemic administration, higher levels of bumetanide are obtained in such brain regions. We recently examined the regional brain distribution of bumetanide in rats and found no significant differences across 14 brain regions (Fig. 15). Despite the high dose (10 mg/kg i.v.) of bumetanide and pretreatment with PBO (which inhibits the oxidative metabolism of bumetanide), brain levels were clearly below the IC_{50} of bumetanide for inhibition of rat NKCC1 (2.4 μM [Dehaye et al., 2003]; corresponding to a bumetanide brain concentration of 0.87 μg/g).

Stress is a well-known trigger of seizures and, thus, one of the mechanisms whereby bumetanide might exert an anxiolytic action (Ko et al., 2018) and suppress seizures is by blocking NKCC1 in the neurosecretory terminals of corticotrophin-releasing neurons in the paraventricular nucleus, thus limiting activation of the hypothalamic-pituitary-adrenal (HPA) axis (Maguire and Salpekar, 2013; Hooper et al., 2018). Here, it is also interesting to note that NKCC1 is robustly expressed in the adrenal gland (Hübner et al., 2001b). In line with the endocrine effects of bumetanide, a low dose of the drug (0.2 mg/kg i.p.) was demonstrated to block seizure-induced activation of the HPA axis and decrease susceptibility to seizures in adult mice (O'Toole et al., 2014). Moreover, seizure-induced activation of the HPA axis has been shown to enhance seizure frequency and comorbid depression-like behaviors (Hooper et al., 2018). Interestingly, autism is associated with enhanced stress reactivity of the HPA axis (Spratt et al., 2012; Hollocks et al., 2014). Thus, effects on the HPA axis may well be involved also in the effects of bumetanide in other models of CNS disorders.

NKCC1 is also expressed in numerous cells involved in chronic inflammation and the immune system (Panet et al., 2002; Norlander et al., 2017; Hung et al., 2018; Perry et al., 2019) which, in turn, are known to be in tight bidirectional communication with the central and peripheral nervous systems (Tracey, 2002; Miller et al., 2017; Chavan et al., 2017; Pavlov et al., 2018) Notably, these interactions have been shown to contribute to numerous clinical manifestations that were previously considered to be of neuronal origin, including ASD (Brown et al., 2004; Vargas et al., 2005; Hodes et al., 2015; Dawidowski et al., 2021). Thus, it is entirely possible that systemically applied bumetanide might have disease-modifying actions mediated by the above pathways. Here, it might be of interest that the constitutive NKCC1 KO mouse is protected against sepsis and bacteremia in response to *Klebsiella pneumoniae* infection in the lung. In addition, the increase in vascular permeability associated with the inflammation was attenuated in these animals (Nguyen et al., 2007).

Clinically relevant doses of the loop diuretic bumetanide (0.05–0.3 mg/kg in neonates and children, 0.5–2 mg/kg in adults) induce marked diuresis in humans. This results in volume depletion, including reduction of the ECS, electrolyte depletion, and hypokalemia. Antiseizure effects of various kinds of diuretics have been reported, including i.v.-applied mannitol, which do not inhibit NKCC1 (Löscher et al., 2013; Kharod et al., 2019). Notably, drugs that modulate the size and osmolarity of the ECS block epileptiform activity in adult brain tissue (Jefferys, 1995; Schwartzkroin et al., 1998; Hochman, 2012). Indeed, such drugs block epileptiform activity in a variety of adult rodent models, regardless of the underlying synaptic and physiological mechanisms. Furthermore, i.v. mannitol exerted antiseizure effects in patients with epilepsy (Haglund and Hochman, 2005). Thus, the diuretic effect of bumetanide alone might contribute to its antiseizure effects (cf.,

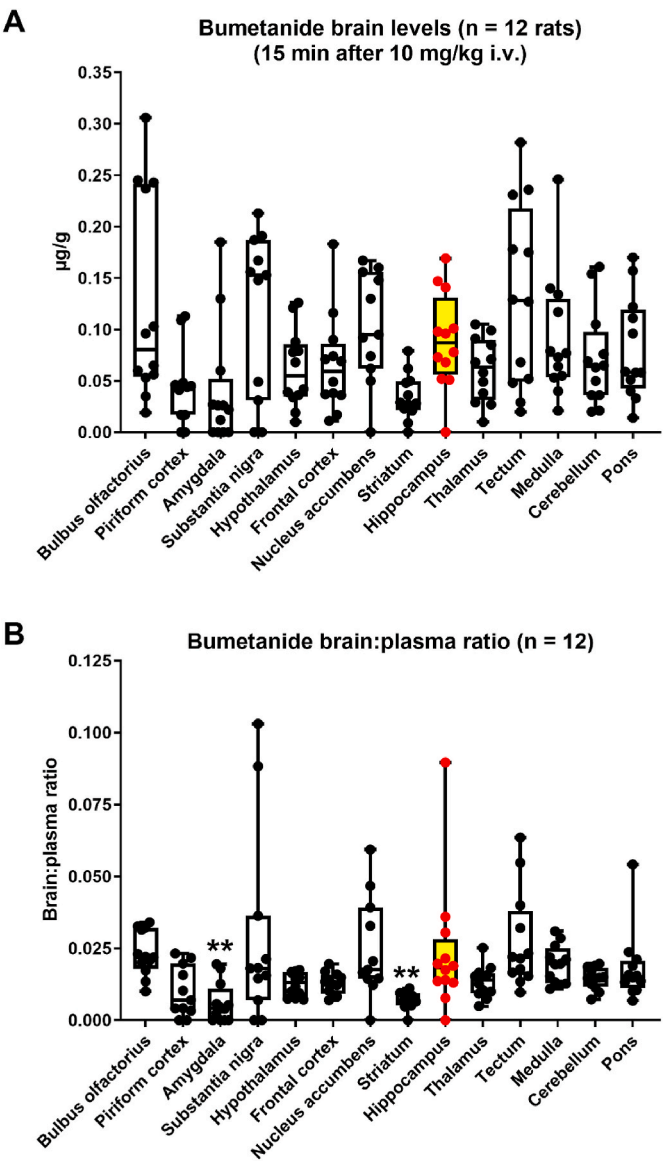

Fig. 15. Regional brain distribution of bumetanide in rats following i.v. administration of 10 mg/kg (unpublished data from Kerstin Römermann, Martina Gramer and Wolfgang Löscher). For inhibition of bumetanide metabolism, rats were pretreated with piperonyl butoxide (PBO) given i.p. in two doses (150 mg/kg at 30 and 10 min prior to bumetanide) as described previously (Töpfer et al., 2014). Based on previous data on peak brain bumetanide levels in rats pretreated with PBO (Töpfer et al., 2014), plasma and brain regions were sampled 15 min after administration. The plasma level was 5.35 ± 1.04 μg/ml (mean and SEM of 12 rats). Brain levels were determined in 14 individual brain regions; note that tissue levels were not corrected for unspecific binding to brain proteins or lipids. Brain levels (A) and the brain: plasma ratio (B) are shown as boxplots with individual data points (n = 12) and whiskers from minimum to maximal values; the horizontal line represents the median value. Bumetanide levels in the hippocampus are highlighted in red color. None of the brain regions differed significantly from the hippocampus (data in A were analyzed by the Kruskal-Wallis test, followed by Dunn's multiple comparisons test). When data in B were analyzed by the Kruskal-Wallis test, followed by Dunn's multiple comparisons test, the brain:plasma ratio in the amygdala ($P = 0.0085$) and striatum ($P = 0.0049$) differed significantly from the ratio determined for the hippocampus (indicated by asterisks). It should be noted that the brain levels of bumetanide shown in A are markedly lower than the IC_{50} of bumetanide for inhibition of rat NKCC1 expressed in HEK-293 cells, which was reported as 2.4 μM (corresponding to a bumetanide brain level of 0.87 μg/g)(Dehaye et al., 2003).

Hesdorffer et al., 2001), and could also be involved in the amelioration of symptoms in other CNS disorders.

6. Off-target effects of bumetanide and other NKCC1 inhibitors

In addition to effects on NKCC1 within or outside the CNS, bumetanide and other NKCC1 inhibitors may exert their CNS effects by acting on *molecular targets* other than cation-chloride cotransporters. With rare exceptions, all experimental as well as clinically used drugs are associated with such off-target effects. Therefore, secondary pharmacological in vitro profiling against a large number of potential targets has to be provided by pharmaceutical companies for regulatory review before starting the first clinical trials (Jenkinson et al., 2020). For this purpose, pharmaceutical companies profile compounds using a predefined (restricted) non-overlapping target panel consisting of a limited set of targets (typically ~100), including G protein-coupled receptors, enzymes, kinases, nuclear hormone receptors, ion channels, and transporters (Rao et al., 2019; Jenkinson et al., 2020). As a consequence, the number of off-targets for a small molecule is probably always significantly higher than what is being reported at the time of approval. More advanced in vitro or in silico drug screening and profiling panels include thousands of receptors, ion channels, enzymes, and other potential targets, and such panels are now increasingly being used during the preclinical characterization of novel drug candidates and their metabolites (Jenkinson et al., 2020). Small-molecule drugs in medical use have been shown to bind on average to a minimum of 6–11 distinct targets excluding their intended pharmacological target (Metz and Hajduk, 2010; Peón et al., 2017) and these additional targets are typically referred to as off-targets. To be relevant for a drug's therapeutic action (which is probably often the case), such off-target effects should occur at concentrations similar to those that act at the primary target; off-target effects occurring at higher drug levels are often relevant for toxicity mechanisms (Van Vleet et al., 2019). PB is a good example of a drug that, in addition to acting on $GABA_A$ receptors, has multiple additional targets that contribute to its pharmacological effects (Löscher and Rogawski, 2012).

At the time when bumetanide and other loop diuretics were developed (Feit, 1981), approaches of the above kind were not available. To our knowledge, such data on bumetanide are not even at the moment in the public domain, so it cannot be excluded that much of the reported preclinical and clinical CNS effects of bumetanide are related to off-target effects, as recently suggested for the beneficial actions of this drug in APOE4-related Alzheimer's disease (Taubes et al., 2021).

As most loop diuretics (Fig. 5), bumetanide (and all of its derivatives discussed here) contains a sulfamoyl group, which acts as a zinc-binding group in the metalloenzyme carbonic anhydrase (CA, EC 4.2.1.1) (Carta and Supuran, 2013). Indeed, soon after its discovery, the diuretic effect of bumetanide was suggested to be mediated in part by inhibition of CA in the kidney because of the increase in HCO_3^- excretion observed in preclinical experiments (cf., Olsen, 1977). However, much higher concentrations of bumetanide are needed to inhibit the renal CA isoform (CA II) than NKCC2, which is in line with its diuretic activity that is strikingly higher than that of classical CA inhibitors such as acetazolamide (Carta and Supuran, 2013).

More recently, it was found that bumetanide might exert a much more potent inhibitory effect on other CA isoforms, including CA VII (K_i 62 nM), CA IX (26 nM), and CA XII (21 nM) (Temperini et al., 2008; Carta and Supuran, 2013). However, the above estimates have been obtained in experiments on the purified protein, and higher concentrations would have to be tested for an inhibitory action in cells and tissues. As a whole, a total of 13 catalytically active CA isoforms are expressed in the human body, with a number of them in both neurons and glia. The brain parenchyma has CA isoforms with either a cytosolic (CAs II and VII) or extracellular (CAs IV and XIV) catalytic site (Chesler, 2003; Frost and McKenna, 2014; Bertling et al., 2021).

Because the structural requirements for inhibition of NKCCs (Fig. 1C) are different from the structural requirements of CA inhibition (Alterio et al., 2018), metabolites of bumetanide that do not contribute to bumetanide's diuretic activity (see section 2.5) are likely to exert inhibitory effects on CA isoforms, as long as the metabolites carry the sulfamoyl moiety. The same would apply to bumetanide derivatives and other loop diuretics with this moiety (Figs. 5, 8 and 10). This is highly relevant for the CNS effects of such compounds because global and local (microdomain) changes in brain pH have pronounced effects on neuronal excitability, as has been shown in experiments on brain CA isoforms such as the extracellular isoforms CA IV and CA XIV and the cytosolic isoforms CA II and CA VII (Ruusuvuori and Kaila, 2014). As a rule of thumb, an acid shift within and outside neurons leads to a suppression of excitability, and such an effect is achieved by applying CA inhibitors. In experiments in vivo, systemic application of CA inhibitors leads to an initial accumulation of CO2 (respiratory acidosis), and therefore even those CA blockers which do not readily cross the BBB (such as acetazolamide, but especially benzolamide) can exert a fast and robust seizure-suppressing action (Pospelov et al., 2021). Whether bumetanide or its metabolites share such effects has (to our knowledge) thus far not been systematically examined. Nevertheless, the putative effects of bumetanide and its metabolites on various CA isoforms illustrate that such off-target effects have to be taken into account when studying the CNS pharmacology of NKCC1 inhibitors.

An off-target effect of bumetanide at the molecular level might be provided by AQP4, which is known to participate in ischemia-induced astrocyte swelling and has been reported to mediate the effects of high bumetanide doses in a stroke model (Migliati et al., 2010). Furthermore, bumetanide was found to reduce AQP4 mRNA and protein upregulation after traumatic brain injury both in vivo and in vitro (Rao et al., 2011; Zhang et al., 2016). However, as described in section 3.7, bumetanide did not exert any significant effect on AQP4-mediated osmotic water permeability in our experiments (Brandt et al., 2018). Apart from AQP4, numerous additional off-target effects may play a role. Indeed, Taubes et al. (2021) suggested that bumetanide's effects in CNS disorders may involve networks of interacting proteins. Below, we discuss some additional (verified and predicted) off-target effects of bumetanide.

GPR35 is a G protein-coupled receptor (GPCR) that is expressed in numerous cell types within and outside the CNS (Divorty et al., 2015; Quon et al., 2020). Bumetanide and furosemide are agonists of human GPR35, but not of its counterpart in rats and mice (Yang et al., 2012). In the brain, this GPCR inhibits synaptic transmission, and it is also involved in the peripheral antinociceptive and anti-inflammatory effects of acetyl salicylic acid (aspirin) (Mackenzie and Milligan, 2017). The wide expression patterns of GPR35, which comprise several types of immune cells including those in the gut (Kaya et al., 2020), have suggested potential therapeutic opportunities (Quon et al., 2020). However, there is thus far no evidence whether and to what extent the numerous actions of bumetanide (and structurally related drugs) in the human might be mediated by activation of GPR35 in cells that are readily accessible to the drug.

Furosemide is known to be a potent inhibitor of high-affinity extrasynaptic $GABA_A$Rs containing the α4 and α6 subunits, but this effect is not shared by bumetanide (Korpi et al., 1995). However, in silico analysis (see below and Fig. 16) includes the α3 subunit of $GABA_A$Rs as a possible target of bumetanide. Outside the CNS, α3-containing $GABA_A$Rs are expressed in cancer cells (see Gumireddy et al., 2016), but whether long-term use of bumetanide might act as an anti-oncogenic agent is not known.

Bumetanide has been reported to increase plasma renin activity in animals and humans, which can be inhibited by pretreatment with indomethacin (Ward and Heel, 1984). Altered renal hemodynamics is probably responsible for increased plasma renin activity but not for the diuretic effects of bumetanide (Ward and Heel, 1984). Nabel et al. (1999) reported that bumetanide attenuated the inhibitory effect of angiotensin II on renin secretion from isolated perfused rat kidneys, which is most likely related to the altered transmembrane chloride

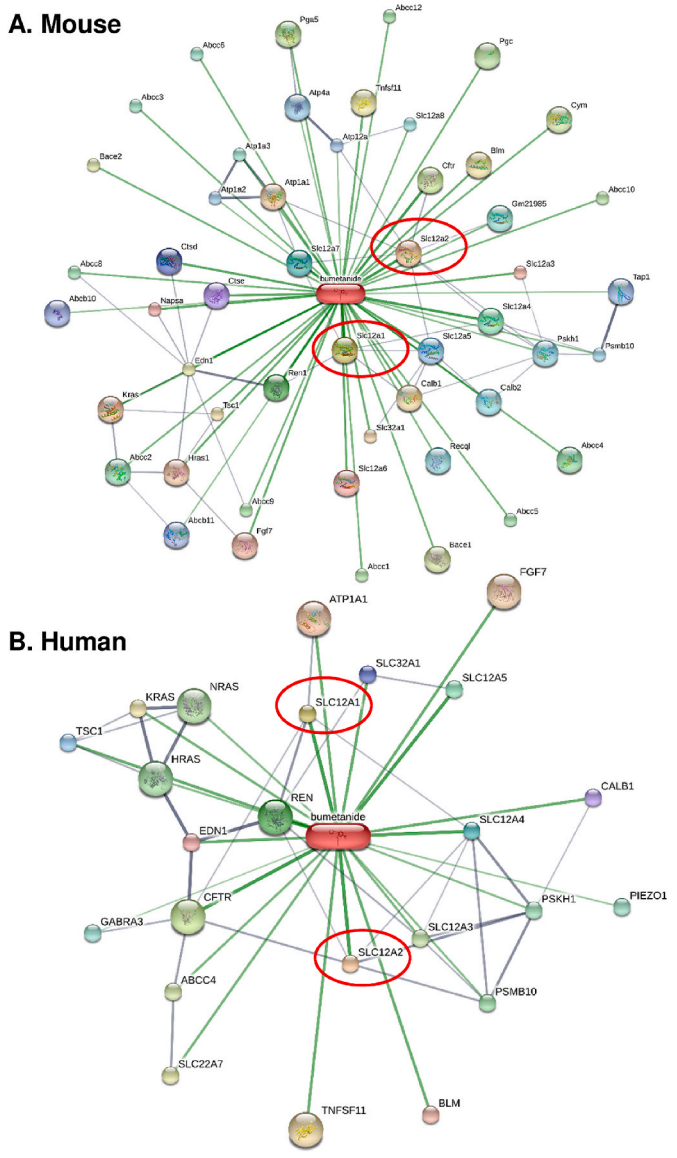

Fig. 16. Known and predicted drug-protein network interactions of bumetanide analyzed in silico by the STITCH database for the mouse (A) and human (B). Drug-protein and protein-protein networks are shown by the confidence view of the database, in which stronger associations are represented by thicker lines. The size of the nodes indicate whether the 3D structure of the protein is known or predicted. Networks were assembled using a medium confidence level of 0.400 (default) and a maximum number of 50 interactors. NKCC1 (Slc12a2) and NKCC2 (Slc12a1) are highlighted by the red circles. For details on predicted functional partners and their abbreviations see http://stitch.embl.de/cgi/network.pl?taskId=qmJHArIBoMQi for the mouse and http://stitch.embl.de/cgi/network.pl?taskId=thi1726VQdZz for the human. Note the species differences indicated by the analysis; e.g., GABRA3 (alpha3-subunit of the $GABA_A$ receptor) is indicated as an interactor for bumetanide in the human but not in the mouse.

gradient in renin-secreting cells.

As described in section 2.5, bumetanide is actively transported from the blood into renal tissue by OATs (*SLC22A*). This is mediated by hOAT1, hOAT3, and hOAT4, but not by hOAT2 (Hasannejad et al., 2004). In contrast, in mice, both Oat2 and Oat3 mediate the renal uptake of bumetanide (Kobayashi et al., 2005). The OAT substrate bumetanide also acts as a competitive inhibitor of these OATs, hOAT3 being the most sensitive transporter (IC_{50} 0.75 μM) (Hasannejad et al., 2004). OAT3/Oat3 is also expressed at the BBB and is involved in the brain-to-blood efflux of bumetanide (Donovan et al., 2015; Töllner et al., 2015b; Römermann et al., 2017). Furthermore, we found that a member of the organic anion-transporting polypeptide (OATP; *SLCO*) family, Oatp1a4 (previously termed Oatp2), may be involved in bumetanide efflux at the BBB (Römermann et al., 2017). In addition to OATs, bumetanide has been reported to be a substrate and competitive inhibitor of MCPs (*SLC16*), particularly hMCT6 (Murakami et al., 2005), which may play a role in the brain uptake of bumetanide (see section 2.5). Furthermore, bumetanide is a (weak) substrate of multidrug resistance protein (MRP) 4 (ABCC4) and breast cancer resistance protein (BCRP; ABCG2) (Hasegawa et al., 2007), which are both expressed at the BBB and may be involved in the active extrusion of bumetanide (Römermann et al., 2017). The STITCH database analysis (Fig. 16; see below) suggests that bumetanide may affect many more transporters than those described here.

The multiple transporters involved in uptake or efflux of bumetanide are obviously relevant for its pharmacodynamic effects, including its CNS pharmacology, because most of these transporters are known to be highly relevant in health and disease. For instance, MCTs mediate proton-dependent transport of L-lactate, pyruvate, short-chain fatty acids, and monocarboxylates in a wide variety of tissues, including the brain (Felmlee et al., 2020). Similarly, several members of the OAT and OATP families, including OAT3 and OATP1A4, which are involved in the transport of organic anions and cations, are expressed at the BBB, choroid plexus, and by cells in the brain parenchyma, including neurons and astrocytes (Kusuhara and Sugiyama, 2004, 2005; Löscher and Potschka, 2005; Furihata and Anzai, 2017; Saidijam et al., 2018; Schäfer et al., 2021). Thus, competitive inhibition of these transporters by bumetanide, particularly at the high systemic drug levels to which the BBB is directly exposed, will affect the physiological processes which are rate-limited by these transporters. Interestingly, significant effects on Oat3 were also observed with bumetanide derivatives such as DIMAEB and bumepamine (Römermann et al., 2017).

For identifying additional off-target effects of bumetanide, we performed an in silico protein-chemical interaction network analysis by using the STITCH (Search Tool for Interacting Chemicals) database, which aggregates high-throughput experimental data, manually curated datasets, and the results of several prediction methods into a single global network of protein-protein and protein–chemical interactions (Szklarczyk et al., 2016). As shown in Fig. 16, this analysis for the mouse and the human brain predicts several effects of bumetanide on protein networks, including targets such as TSC1, renin, and the alpha3-subunit of the $GABA_A$ receptor (see above). Overall, these data suggest that the pharmacology of NKCC inhibitors such as bumetanide may be much more complex than previously thought.

7. Conclusions

While neuronal cation-chloride cotransporters, such as NKCC1, are considered attractive CNS drug targets (Savardi et al., 2021), a large number of problems in drug design that are related to isoform specificity as well as pharmacokinetic and safety properties have to be overcome. It is often mistakenly stated that bumetanide is a specific NKCC1 blocker but, in fact, there are no drugs available that have been clearly demonstrated to discriminate between NKCC1 and NKCC2. Another major issue regarding CNS targeting is the poor BBB permeability of the currently available NKCC1 blockers. Furthermore, diuretic and potential ototoxic effects of such NKCC inhibitors limit their clinical use in CNS disorders.

Despite more than ~15 years of intensive research by different academic and industry groups, no brain-permeant NKCC1-selective compound is available in the public domain. Because of the structural basis of NKCC inhibitor actions illustrated in Fig. 1C, it may be very hard if not impossible to develop bumetanide derivatives that exhibit high brain permeability and high selectivity for NKCC1 vs. NKCC2. As evidenced by the non-acid loop diuretics azosemide and torasemide, there are

promising alternatives to bumetanide for inhibition of NKCC1 in CNS disorders (Hampel et al., 2018), particularly because of their lower diuretic activity, lower ototoxic potency, and longer duration of action (see section 3.1). However, these results are just a start in the direction of higher target specificity and, for CNS work, such pharmacodynamic properties should be combined with high BBB-permeability where pro-drug approaches may turn out to be the optimal design strategy.

For additional target selectivity at the cellular level, drugs that discriminate between the two splice variants, NKCC1a and NKCC1b, would be very valuable. However, the real advantages of this kind of high molecular specificity will become evident only after major advances in basic research on the cell-specific expression patterns of the splice isoforms within brain tissue (cf., Virtanen et al., 2020). Here, it is worthwhile pointing out that, given the steeply increasing amount of information of glial cells as *bona fide* elements in neuronal signaling (Allen and Barres, 2005; Dityatev and Rusakov, 2011; Yamazaki et al., 2021), it is by no means excluded that NKCC1 in glia, for instance in oligodendrocytes, might be a relevant drug target in CNS disorders (Chen et al., 2007; Song et al., 2020). Indeed, there is no reason to exclude a contribution from glial cells to the protective actions of bumetanide in experiments with direct delivery of the drug to the brain.

To sum up, the amount of solid information on NKCC1-targeting drugs in CNS disorders is in its infancy, and the same applies for basic research on the molecular biology and physiology of NKCC1 splice isoforms. However, we feel that admitting ignorance (rather than jumping into premature conclusions) in CNS drug research will catalyze, rather than hamper, future advances. These are likely to include further work on optimization of brain-permeant NKCC1 inhibitors, and on the detailed mechanisms whereby NKCC1 blockers exert beneficial and adverse effects within and outside the brain parenchyma. Ongoing and future work on molecular modeling on high-resolution, cryo-EM based structures of NKCC1 in various species (Chew et al., 2019; Yang et al., 2020) is likely to rapidly transform the drug development landscape, facilitating the design of next-generation brain permeable NKCC1-selective inhibitors.

Declarations of competing interest

None.

Acknowledgments

We thank Drs. Peter W. Feit, Thomas Erker, and Markus Kalesse for cooperating with us on the development of novel bumetanide derivatives and prodrugs and synthesizing these compounds for our in vitro and in vivo experiments. Furthermore, we thank Dr. Biff Forbush for the discussion on potential binding sites of bumetanide in NKCC1/2, Dr. Claudio Rivera and MSc. Tommi Ala-Kurikka for critical reading of previous versions of this review, and Dr. Pavel Uvarov for providing Fig. 14. W. Löscher's research has been supported by the Deutsche Forschungsgemeinschaft (Bonn, Germany). K. Kaila's work is supported by the Academy of Finland and the Sigrid Jusélius Foundation.

Appendix A. Supplementary data

Supplementary data to this article can be found online at https://doi.org/10.1016/j.neuropharm.2021.108910.

References

Akiyama, K., Miyashita, T., Matsubara, A., Mori, N., 2010. The detailed localization pattern of Na+/K+/2Cl- cotransporter type 2 and its related ion transport system in the rat endolymphatic sac. J. Histochem. Cytochem. 58, 759–763.

Ala-Kurikka, T., Pospelov, A.S., Summanen, M., Alafuzoff, A., Kurki, S., Voipio, J., Kaila, K., 2021. A physiologically-validated rat model of term birth asphyxia with seizure generation after, not during, brain hypoxia. Epilepsia 62, 908–919.

Allen, N.J., Barres, B.A., 2005. Signaling between glia and neurons: focus on synaptic plasticity. Curr. Opin. Neurobiol. 15, 542–548.

Alshahrani, S., Alvarez-Leefmans, F.J., Di Fulvio, M., 2012. Expression of the Slc12a1 gene in pancreatic beta-cells: molecular characterization and in silico analysis. Cell. Physiol. Biochem. 30, 95–112.

Alterio, V., Esposito, D., Monti, S.M., Supuran, C.T., De Simone, G., 2018. Crystal structure of the human carbonic anhydrase II adduct with 1-(4-sulfamoylphenyl-ethyl)-2,4,6-triphenylpyridinium perchlorate, a membrane-impermeant, isoform selective inhibitor. J. Enzym. Inhib. Med. Chem. 33, 151–157.

Alvarez-Leefmans, F.J., 2012. Intracellular chloride regulation. In: Sperelakis, N. (Ed.), Cell Physiology Sourcebook, fourth ed., Essentials of Membrane Biophysics. Academic Press, London, pp. 221–259.

Auer, T., Schreppel, P., Erker, T., Schwarzer, C., 2020a. Impaired chloride homeostasis in epilepsy: molecular basis, impact on treatment, and current treatment approaches. Pharmacol. Ther. 205, 107422.

Auer, T., Schreppel, P., Erker, T., Schwarzer, C., 2020b. Functional characterization of novel bumetanide derivatives for epilepsy treatment. Neuropharmacology 162, 107754.

Bankir, L., Bichet, D.G., Morgenthaler, N.G., 2017. Vasopressin: physiology, assessment and osmosensation. J. Intern. Med. 282, 284–297.

Barmashenko, G., Hefft, S., Aertsen, A., Kirschstein, T., Köhling, R., 2011. Positive shifts of the $GABA_A$ receptor reversal potential due to altered chloride homeostasis is widespread after status epilepticus. Epilepsia 52, 1570–1578.

Ben Ari, Y., Cherubini, E., Corradetti, R., Gaiarsa, J.L., 1989. Giant synaptic potentials in immature rat CA3 hippocampal neurones. J. Physiol. 416, 303–325.

Ben Ari, Y., Gaiarsa, J.L., Tyzio, R., Khazipov, R., 2007. GABA: a pioneer transmitter that excites immature neurons and generates primitive oscillations. Physiol. Rev. 87, 1215–1284.

Ben Ari, Y., 2017. NKCC1 chloride importer antagonists attenuate many neurological and psychiatric disorders. Trends Neurosci. 40, 536–554.

Bertling, E., Blaesse, P., Seja, P., Kremneva, E., Gateva, G., Virtanen, M.A., Summanen, M., Spoljaric, I., Uvarov, P., Blaesse, M., Paavilainen, V.O., Vutskits, L., Kaila, K., Hotulainen, P., Ruusuvuori, E., 2021. Carbonic anhydrase seven bundles filamentous actin and regulates dendritic spine morphology and density. EMBO Rep. 22, e50145.

Blaesse, P., Airaksinen, M.S., Rivera, C., Kaila, K., 2009. Cation-chloride cotransporters and neuronal function. Neuron 61, 820–838.

Borgogno, M., Savardi, A., Manigrasso, J., Turci, A., Portioli, C., Ottonello, G., Bertozzi, S.M., Armirotti, A., Contestabile, A., Cancedda, L., De Vivo, M., 2021. Design, synthesis, in vitro and in vivo characterization of selective NKCC1 inhibitors for the treatment of core symptoms in down syndrome. J. Med. Chem. 64, 10203–10229.

Brandt, C., Nozadze, M., Heuchert, N., Rattka, M., Löscher, W., 2010. Disease-modifying effects of phenobarbital and the NKCC1 inhibitor bumetanide in the pilocarpine model of temporal lobe epilepsy. J. Neurosci. 30, 8602–8612.

Brandt, C., Seja, P., Töllner, K., Römermann, K., Hampel, P., Kalesse, M., Kipper, A., Feit, P.W., Lykke, K., Toft-Bertelsen, T.L., Paavilainen, P., Spoljaric, I., Puskarjov, M., Macaulay, N., Kaila, K., Löscher, W., 2018. Bumepamine, a brain-permeant benzylamine derivative of bumetanide, does not inhibit NKCC1 but is more potent to enhance phenobarbital's anti-seizure efficacy. Neuropharmacology 143, 186–204.

Brickley, S.G., Revilla, V., Cull-Candy, S.G., Wisden, W., Farrant, M., 2001. Adaptive regulation of neuronal excitability by a voltage-independent potassium conductance. Nature 409, 88–92.

Brown, A.S., Hooton, J., Schaefer, C.A., Zhang, H., Petkova, E., Babulas, V., Perrin, M., Gorman, J.M., Susser, E.S., 2004. Elevated maternal interleukin-8 levels and risk of schizophrenia in adult offspring. Am. J. Psychiatr. 161, 889–895.

Burckhardt, G., 2012. Drug transport by organic anion transporters (OATs). Pharmacol. Ther. 136, 106–130.

Carta, F., Supuran, C.T., 2013. Diuretics with carbonic anhydrase inhibitory action: a patent and literature review (2. Expert Opin. Ther. Pat. 23, 681–691.

Chavan, S.S., Pavlov, V.A., Tracey, K.J., 2017. Mechanisms and therapeutic relevance of neuro-immune communication. Immunity 46, 927–942.

Chen, H., Kintner, D.B., Jones, M., Matsuda, T., Baba, A., Kiedrowski, L., Sun, D., 2007. AMPA-mediated excitotoxicity in oligodendrocytes: role for Na(+)-K(+)-Cl(-) co-transport and reversal of Na(+)/Ca(2+) exchanger. J. Neurochem. 102, 1783–1795.

Chesler, M., 2003. Regulation and modulation of pH in the brain. Physiol. Rev. 83, 1183–1221.

Chew, T.A., Orlando, B.J., Zhang, J., Latorraca, N.R., Wang, A., Hollingsworth, S.A., Chen, D.H., Dror, R.O., Liao, M., Feng, L., 2019. Structure and mechanism of the cation-chloride cotransporter NKCC1. Nature 572, 488–492.

Chi, G., Ebenhoch, R., Man, H., Tang, H., Tremblay, L.E., Reggiano, G., Qiu, X., Bohstedt, T., Liko, I., Almeida, F.G., Garneau, A.P., Wang, D., McKinley, G., Moreau, C.P., Bountra, K.D., Abrusci, P., Mukhopadhyay, S.M.M., Fernandez-Cid, A., Slimani, S., Lavoie, J.L., Burgess-Brown, N.A., Tehan, B., DiMaio, F., Jazayeri, A., Isenring, P., Robinson, C.V., Dürr, K.L., 2021. Phospho-regulation, nucleotide binding and ion access control in potassium-chloride cotransporters. EMBO J. 40, e107294.

Cleary, R.T., Sun, H., Huynh, T., Manning, S.M., Li, Y., Rotenberg, A., Talos, D.M., Kahle, K.T., Jackson, M., Rakhade, S.N., Berry, G., Jensen, F.E., 2013. Bumetanide enhances phenobarbital efficacy in a rat model of hypoxic neonatal seizures. PLoS One 8, e57148.

Cohen, I., Navarro, V., Clemenceau, S., Baulac, M., Miles, R., 2002. On the origin of interictal activity in human temporal lobe epilepsy in vitro. Science 298, 1418–1421.

Cohen, M., 1981. Pharmacology of bumetanide. J. Clin. Pharmacol. 21, 537–542.

Cohen, M.R., Hinsch, E., Vergona, R., Ryan, J., Kolis, S.J., Schwartz, M.A., 1976. A comparative diuretic and tissue distribution study of bumetanide and furosemide in the dog. J. Pharmacol. Exp. Therapeut. 197, 697–702.
Dargaei, Z., Bang, J.Y., Mahadevan, V., Khademullah, C.S., Bedard, S., Parfitt, G.M., Kim, J.C., Woodin, M.A., 2018. Restoring GABAergic inhibition rescues memory deficits in a Huntington's disease mouse model. Proc. Natl. Acad. Sci. U. S. A 115, E1618–E1626.
Dawidowski, B., Gä^{3}rniak, A., Podwalski, P., Lebiecka, Z., Misiak, B., Samochowiec, J., 2021. The role of cytokines in the pathogenesis of schizophrenia. J. Clin. Med. 10.
Dehaye, J.P., Nagy, A., Premkumar, A., Turner, R.J., 2003. Identification of a functionally important conformation-sensitive region of the secretory Na+-K+-2Cl-cotransporter (NKCC1). J. Biol. Chem. 278, 11811–11817.
Deidda, G., Parrini, M., Naskar, S., Bozarth, I.F., Contestabile, A., Cancedda, L., 2015. Reversing excitatory $GABA_AR$ signaling restores synaptic plasticity and memory in a mouse model of Down syndrome. Nat. Med. 21, 318–326.
Delpire, E., Gagnon, K.B., 2018. Na(+) -K(+) -2Cl(-) cotransporter (NKCC) physiological function in nonpolarized cells and transporting epithelia. Comp. Physiol. 8, 871–901.
Delpire, E., Gagnon, K.B., 2019. Elusive role of the Na-K-2Cl cotransporter in the choroid plexus. Am. J. Physiol. Cell Physiol. 316, C522–C524.
Delpire, E., 2021. Advances in the development of novel compounds targeting cation-chloride cotransporter physiology. Am. J. Physiol. Cell Physiol. 320, C324–C340.
Ding, D., Liu, H., Qi, W., Jiang, H., Li, Y., Wu, X., Sun, H., Gross, K., Salvi, R., 2016. Ototoxic effects and mechanisms of loop diuretics. J. Otolaryngol. 11, 145–156.
Dityatev, A., Rusakov, D.A., 2011. Molecular signals of plasticity at the tetrapartite synapse. Curr. Opin. Neurobiol. 21, 353–359.
Divorty, N., Mackenzie, A.E., Nicklin, S.A., Milligan, G., 2015. G protein-coupled receptor 35: an emerging target in inflammatory and cardiovascular disease. Front. Pharmacol. 6, 41.
Donkin, J.J., Vink, R., 2010. Mechanisms of cerebral edema in traumatic brain injury: therapeutic developments. Curr. Opin. Neurol. 23, 293–299.
Donovan, M.D., O'Brien, F.E., Boylan, G.B., Cryan, J.F., Griffin, B.T., 2015. The effect of organic anion transporter 3 inhibitor probenecid on bumetanide levels in the brain: an integrated in vivo microdialysis study in the rat. J. Pharm. Pharmacol. 67, 501–510.
Donovan, M.D., Schellekens, H., Boylan, G.B., Cryan, J.F., Griffin, B.T., 2016. In vitro bidirectional permeability studies identify pharmacokinetic limitations of NKCC1 inhibitor bumetanide. Eur. J. Pharmacol. 770, 117–125.
Dzhala, V.I., Talos, D.M., Sdrulla, D.A., Brumback, A.C., Mathews, G.C., Benke, T.A., Delpire, E., Jensen, F.E., Staley, K.J., 2005. NKCC1 transporter facilitates seizures in the developing brain. Nat. Med. 11, 1205–1213.
Erker, T., Brandt, C., Töllner, K., Schreppel, P., Twele, F., Schidlitzki, A., Löscher, W., 2016. The bumetanide prodrug BUM5, but not bumetanide, potentiates the antiseizure effect of phenobarbital in adult epileptic mice. Epilepsia 57, 698–705.
Feit, P.W., 1971. Aminobenzoic acid diuretics. 2. 4-Substituted-3-amino-5-sulfamylbenzoic acid derivatives. J. Med. Chem. 14, 432–439.
Feit, P.W., 1981. Bumetanide–the way to its chemical structure. J. Clin. Pharmacol. 21, 531–536.
Feit, P.W., 1990. Bumetanide: historical background, taxonomy and chemistry. In: Bumetanide, A.F.Lant (Ed.), Camforth. Marius Press, , U.K., pp. 1–13
Felmlee, M.A., Jones, R.S., Rodriguez-Cruz, V., Follman, K.E., Morris, M.E., 2020. Monocarboxylate transporters (SLC16): function, regulation, and role in health and disease. Pharmacol. Rev. 72, 466–485.
Flatman, P.W., Creanor, J., 1999. Regulation of Na+-K+-2Cl- cotransport by protein phosphorylation in ferret erythrocytes. J. Physiol. 517 (Pt 3), 699–708.
Forbush III, B., Palfrey, H.C., 1983. [3H]bumetanide binding to membranes isolated from dog kidney outer medulla. Relationship to the Na,K,Cl co-transport system. J. Biol. Chem. 258, 11787–11792.
Frey, H.-H., Popp, C., Löscher, W., 1979. Influence of inhibitors of the high affinity GABA uptake on seizures thresholds in mice. Neuropharmacology 18, 581–590.
Frey, H.-H., 1979. Pharmacology of bumetanide. Postgrad. Med. J. 61 (Suppl. 6), 14–18.
Frey, H.-H., Löscher, W., 1980. Cetyl GABA: effect of convulsant thresholds in mice and acute toxicity. Neuropharmacology 19, 217–220.
Frizzell, R.A., Field, M., Schultz, S.G., 1979. Sodium-coupled chloride transport by epithelial tissues. Am. J. Physiol. 236, F1–F8.
Frost, S.C., McKenna, R., 2014. Carbonic Anhydrase: Mechanism, Regulation, Links to Disease, and Industrial Applications. Springer, Heidelberg.
Furihata, T., Anzai, N., 2017. Functional expression of organic ion transporters in astrocytes and their potential as a drug target in the treatment of central nervous system diseases. Biol. Pharm. Bull. 40, 1153–1160.
Gagnon, K.B., Delpire, E., 2013. Physiology of SLC12 transporters: lessons from inherited human genetic mutations and genetically engineered mouse knockouts. Am. J. Physiol. Cell Physiol. 304, C693–C714.
Gagnon, M., Bergeron, M.J., Lavertu, G., Castonguay, A., Tripathy, S., Bonin, R.P., Perez-Sanchez, J., Boudreau, D., Wang, B., Dumas, L., Valade, I., Bachand, K., Jacob-Wagner, M., Tardif, C., Kianicka, I., Isenring, P., Attardo, G., Coull, J.A., de Koninck, Y., 2013. Chloride extrusion enhancers as novel therapeutics for neurological diseases. Nat. Med. 19, 1524–1528.
Gill, S., Gill, R., Wen, Y., Enderle, T., Roth, D., Liang, D., 2017. A high-throughput screening assay for NKCC1 cotransporter using nonradioactive rubidium flux technology. Assay Drug Dev. Technol. 15, 167–177.
Glykys, J., Dzhala, V., Egawa, K., Kahle, K.T., Delpire, E., Staley, K., 2017. Chloride dysregulation, seizures, and cerebral edema: a relationship with therapeutic potential. Trends Neurosci. 40, 276–294.
Gómez-Correa, G., Zepeda, A., 2020. Chronic bumetanide infusion alters young neuron morphology in the dentate gyrus without affecting contextual fear memory. Front. Neurosci. 14, 514.
Gregoriades, J.M.C., Madaris, A., Alvarez, F.J., Alvarez-Leefmans, F.J., 2019. Genetic and pharmacological inactivation of apical Na(+)-K(+)-2Cl(-) cotransporter 1 in choroid plexus epithelial cells reveals the physiological function of the cotransporter. Am. J. Physiol. Cell Physiol. 316, C525–C544.
Gumireddy, K., Li, A., Kossenkov, A.V., Sakurai, M., Yan, J., Li, Y., Xu, H., Wang, J., Zhang, P.J., Zhang, L., Showe, L.C., Nishikura, K., Huang, Q., 2016. The mRNA-edited form of GABRA3 suppresses GABRA3-mediated Akt activation and breast cancer metastasis. Nat. Commun. 7, 10715.
Haglund, M.M., Hochman, D.W., 2005. Furosemide and mannitol suppression of epileptic activity in the human brain. J. Neurophysiol. 94, 907–918.
Halladay, S.C., Carter, D.E., Sipes, I.G., 1978. A relationship between the metabolism of bumetanide and its diuretic activity in the rat. Drug Metab. Dispos. 6, 45–49.
Hampel, P., Römermann, K., Macaulay, N., Löscher, W., 2018. Azosemide is more potent than bumetanide and various other loop diuretics to inhibit the sodium-potassium-chloride-cotransporter human variants hNKCC1A and hNKCC1B. Sci. Rep. 8, 9877.
Hampel, P., Römermann, K., Gramer, M., Löscher, W., 2021a. The Search for Brain-Permeant NKCC1 Inhibitors for the Treatment of Seizures: Pharmacokinetic-Pharmacodynamic Modelling of NKCC1 Inhibition by Azosemide, Torasemide, and Bumetanide in Mouse Brain. Epilepsy Behav, p. 107616.
Hampel, P., Römermann, K., Gailus, B., Johne, M., Gericke, B., Kaczmarek, E., Löscher, W., 2021b. Effects of the NKCC1 Inhibitors Bumetanide, Azosemide, and Torasemide Alone or in Combination with Phenobarbital on Seizure Threshold in Epileptic and Nonepileptic Mice. Neuropharmacology *in press*.
Hampel, P., Johne, M., Gailus, B., Vogel, A., Schidlitzki, A., Gericke, B., Töllner, K., Theilmann, W., Käufer, C., Römermann, K., Kaila, K., Löscher, W., 2021c. Deletion of the Na-K-2Cl cotransporter NKCC1 results in a more severe epileptic phenotype in the intrahippocampal kainate mouse model of temporal lobe epilepsy. Neurobiol. Dis. 152, 105297.
Hannaert, P., Alvarez-Guerra, M., Pirot, D., Nazaret, C., Garay, R.P., 2002. Rat NKCC2/NKCC1 cotransporter selectivity for loop diuretic drugs. Naunyn-Schmiedeberg's Arch. Pharmacol. 365, 193–199.
Hasannejad, H., Takeda, M., Taki, K., Shin, H.J., Babu, E., Jutabha, P., Khamdang, S., Aleboyeh, M., Onozato, M.L., Tojo, A., Enomoto, A., Anzai, N., Narikawa, S., Huang, X.L., Niwa, T., Endou, H., 2004. Interactions of human organic anion transporters with diuretics. J. Pharmacol. Exp. Therapeut. 308, 1021–1029.
Hasegawa, M., Kusuhara, H., Adachi, M., Schuetz, J.D., Takeuchi, K., Sugiyama, Y., 2007. Multidrug resistance-associated protein 4 is involved in the urinary excretion of hydrochlorothiazide and furosemide. J. Am. Soc. Nephrol. 18, 37–45.
Henneberger, C., Bard, L., Panatier, A., Reynolds, J.P., Kopach, O., Medvedev, N.I., Minge, D., Herde, M.K., Anders, S., Kraev, I., Heller, J.P., Rama, S., Zheng, K., Jensen, T.P., Sanchez-Romero, I., Jackson, C.J., Janovjak, H., Ottersen, O.P., Nagelhus, E.A., Oliet, S.H.R., Stewart, M.G., Nägerl, U.V., Rusakov, D.A., 2020. LTP induction boosts glutamate spillover by driving withdrawal of perisynaptic Astroglia. Neuron 108, 919–936.
Hesdorffer, D.C., Stables, J.P., Hauser, W.A., Annegers, J.F., Cascino, G., 2001. Are certain diuretics also anticonvulsants? Ann. Neurol. 50, 458–462.
Hochman, D.W., 2012. The extracellular space and epileptic activity in the adult brain: explaining the antiepileptic effects of furosemide and bumetanide. Epilepsia 53 (Suppl. 1), 18–25.
Hochman, D., Haglund, M., 2009. Evidence that bumetanide suppresses epileptiform activity in adult primate cortex independent of effects on GABA-A signalling. In: American Epilepsy Society 63th Annual Meeting Abstracts Online Abst. 3.035.
Hochman, D.W., Partridge, J.J., 2006. Methods and Compositions for the Treatment of Neuropsychiatric Disorders with Bumetanide and Furosemide Analogs [United States Patent US 20060089350A1].
Hochman, D.W., Partridge, J.J., 2007. Methods and Compositions Using NKCC Cotransporter Inhibitors for the Treatment of Neuropsychiatric and Addictive Disorders [International Patent WO2007047698A2].
Hodes, G.E., Kana, V., Menard, C., Merad, M., Russo, S.J., 2015. Neuroimmune mechanisms of depression. Nat. Neurosci. 18, 1386–1393.
Hollocks, M.J., Howlin, P., Papadopoulos, A.S., Khondoker, M., Simonoff, E., 2014. Differences in HPA-axis and heart rate responsiveness to psychosocial stress in children with autism spectrum disorders with and without co-morbid anxiety. Psychoneuroendocrinology 46, 32–45.
Hooper, A., Paracha, R., Maguire, J., 2018. Seizure-induced activation of the HPA axis increases seizure frequency and comorbid depression-like behaviors. Epilepsy Behav. 78, 124–133.
Huang, H., Song, S., Banerjee, S., Jiang, T., Zhang, J., Kahle, K.T., Sun, D., Zhang, Z., 2019a. The WNK-SPAK/OSR1 kinases and the cation-chloride cotransporters as therapeutic targets for neurological diseases. Aging Dis 10, 626–636.
Huang, H., Bhuiyan, M.I.H., Jiang, T., Song, S., Shankar, S., Taheri, T., Li, E., Schreppel, P., Hintersteininger, M., Yang, S.S., Lin, S.H., Molyneaux, B.J., Zhang, Z., Erker, T., Sun, D., 2019b. A novel Na(+)-K(+)-Cl(-) cotransporter 1 inhibitor STS66* reduces brain damage in mice after ischemic stroke. Stroke 50, 1021–1025.
Hubbard, J.A., Szu, J.I., Binder, D.K., 2018. The role of aquaporin-4 in synaptic plasticity, memory and disease. Brain Res. Bull. 136, 118–129.
Huberfeld, G., Wittner, L., Clemenceau, S., Baulac, M., Kaila, K., Miles, R., Rivera, C., 2007. Perturbed chloride homeostasis and GABAergic signaling in human temporal lobe epilepsy. J. Neurosci. 27, 9866–9873.
Huggins, D.J., Sherman, W., Tidor, B., 2012. Rational approaches to improving selectivity in drug design. J. Med. Chem. 55, 1424–1444.
Hung, C.M., Peng, C.K., Wu, C.P., Huang, K.L., 2018. Bumetanide attenuates acute lung injury by suppressing macrophage activation. Biochem. Pharmacol. 156, 60–67.

Hübner, C.A., Stein, V., Hermans-Borgmeyer, I., Meyer, T., Ballanyi, K., Jentsch, T.J., 2001a. Disruption of KCC2 reveals an essential role of K-Cl cotransport already in early synaptic inhibition. Neuron 30, 515–524.
Hübner, C.A., Lorke, D.E., Hermans-Borgmeyer, I., 2001b. Expression of the Na-K-2Cl-cotransporter NKCC1 during mouse development. Mech. Dev. 102, 267–269.
Iffland, P.H., Grant, G.A., Janigro, D., 2014. Mechanisms of cerebral edema leading to early seizures after traumatic brain injury. In: Lo, E.H., Lok, J., Ning, M., Whalen, M. (Eds.), Vascularmechanisms in CNS Trauma, Springer Series in Translational Stroke Research, 5. Springer, New York, pp. 29–45.
Inoue, M., Uriu, T., Otani, H., Hara, M., Omori, K., Inagaki, C., 1989. Intracerebroventricular injection of ethacrynic acid induces status epilepticus. Eur. J. Pharmacol. 166, 101–106.
Isenring, P., Jacoby, S.C., Forbush III, B., 1998a. The role of transmembrane domain 2 in cation transport by the Na-K-Cl cotransporter. Proc. Natl. Acad. Sci. U. S. A 95, 7179–7184.
Isenring, P., Jacoby, S.C., Chang, J., Forbush, B., 1998b. Mutagenic mapping of the Na-K-Cl cotransporter for domains involved in ion transport and bumetanide binding. J. Gen. Physiol. 112, 549–558.
Ismail, F.Y., Shapiro, B.K., 2019. What are neurodevelopmental disorders? Curr. Opin. Neurol. 32, 611–616.
Javaheri, S., Davis, C., Rogers, D.H., 1993. Ionic composition of cisternal CSF in acute respiratory acidosis: lack of effect of large dose bumetanide. J. Neurochem. 61, 1525–1529.
Jefferys, J.G., 1995. Nonsynaptic modulation of neuronal activity in the brain: electric currents and extracellular ions. Physiol. Rev. 75, 689–723.
Jenkinson, S., Schmidt, F., Rosenbrier, R.L., Delaunois, A., Valentin, J.P., 2020. A practical guide to secondary pharmacology in drug discovery. J. Pharmacol. Toxicol. Methods 105, 106869.
Johne, M., Römermann, K., Hampel, P., Gailus, B., Theilmann, W., Ala-Kurikka, T., Kaila, K., Löscher, W., 2021a. Phenobarbital and midazolam suppress neonatal seizures in a non-invasive rat model of birth asphyxia while bumetanide is ineffective. Epilepsia 62, 920–934.
Johne, M., Käufer, C., Römermann, K., Gailus, B., Gericke, B., Löscher, W., 2021b. A combination of phenobarbital and the bumetanide derivative bumepamine prevents neonatal seizures and subsequent hippocampal neurodegeneration in a rat model of birth asphyxia. Epilepsia 62, 1460–1471.
Kahle, K.T., Staley, K.J., Nahed, B.V., Gamba, G., Hebert, S.C., Lifton, R.P., Mount, D.B., 2008. Roles of the cation-chloride cotransporters in neurological disease. Nat. Clin. Pract. Neurol. 4, 490–503.
Kahle, K.T., Simard, J.M., Staley, K.J., Nahed, B.V., Jones, P.S., Sun, D., 2009. Molecular mechanisms of ischemic cerebral edema: role of electroneutral ion transport. Physiology. (Bethesda.) 24, 257–265.
Kahle, K.T., Deeb, T.Z., Puskarjov, M., Silayeva, L., Liang, B., Kaila, K., Moss, S.J., 2013. Modulation of neuronal activity by phosphorylation of the K-Cl cotransporter KCC2. Trends Neurosci. 36, 726–737.
Kahle, K.T., Khanna, A., Clapham, D.E., Woolf, C.J., 2014. Therapeutic restoration of spinal inhibition via druggable enhancement of potassium-chloride cotransporter KCC2-mediated chloride extrusion in peripheral neuropathic pain. JAMA Neurol. 71, 640–645.
Kaila, K., 1994. Ionic basis of $GABA_A$ receptor channel function in the nervous system. Prog. Neurobiol. 42, 489–537.
Kaila, K., Price, T.J., Payne, J.A., Puskarjov, M., Voipio, J., 2014a. Cation-chloride cotransporters in neuronal development, plasticity and disease. Nat. Rev. Neurosci. 15, 637–654.
Kaila, K., Ruusuvuori, E., Seja, P., Voipio, J., Puskarjov, M., 2014b. GABA actions and ionic plasticity in epilepsy. Curr. Opin. Neurobiol. 26, 34–41.
Kaila, K., Trevelyan, A., Raimondo, J., Ala-Kurikka, T., Huberfeld, G., Avoli, M., De Curtis, M., 2022. $GABA_A$-receptor signaling and ionic plasticity in the generation and spread of seizures. In: Noebels, J.L., Avoli, M., Rogawski, M.A., Vezzani, A., Delgado-Escueta, A.V. (Eds.), Jasper's Basic Mechanisms of the Epilepsies, fifth ed. Oxford University Press, Oxford.
Kakigi, A., Nishimura, M., Takeda, T., Taguchi, D., Nishioka, R., 2009. Expression of aquaporin1, 3, and 4, NKCC1, and NKCC2 in the human endolymphatic sac. Auris Nasus Larynx 36, 135–139.
Kang, S.K., Markowitz, G.J., Kim, S.T., Johnston, M.V., Kadam, S.D., 2015. Age- and sex-dependent susceptibility to phenobarbital-resistant neonatal seizures: role of chloride co-transporters. Front. Cell. Neurosci. 9, 173.
Karimy, J.K., Zhang, J., Kurland, D.B., Theriault, B.C., Duran, D., Stokum, J.A., Furey, C. G., Zhou, X., Mansuri, M.S., Montejo, J., Vera, A., DiLuna, M.L., Delpire, E., Alper, S. L., Gunel, M., Gerzanich, V., Medzhitov, R., Simard, J.M., Kahle, K.T., 2017. Inflammation-dependent cerebrospinal fluid hypersecretion by the choroid plexus epithelium in posthemorrhagic hydrocephalus. Nat. Med. 23, 997–1003.
Kaya, B., Donas, C., Wuggenig, P., Díaz, O.E., Morales, R.A., Melhem, H., Hernández, P. P., Kaymak, T., Das, S., Hruz, P., Franc, Y., Geier, F., Ayata, C.K., Villablanca, E.J., Niess, J.H., 2020. Lysophosphatidic acid-mediated GPR35 signaling in CX3CR1(+) macrophages regulates intestinal homeostasis. Cell Rep. 32, 107979.
Kharod, S.C., Carter, B.M., Kadam, S.D., 2018. Pharmaco-resistant neonatal seizures: critical mechanistic insights from a chemoconvulsant model. Dev. Neurobiol. 78, 1117–1130.
Kharod, S.C., Kang, S.K., Kadam, S.D., 2019. Off-label use of bumetanide for brain disorders: an overview. Front. Neurosci. 13, 310.
Ko, M.C., Lee, M.C., Tang, T.H., Amstislavskaya, T.G., Tikhonova, M.A., Yang, Y.L., Lu, K. T., 2018. Bumetanide blocks the acquisition of conditioned fear in adult rats. Br. J. Pharmacol. 175, 1580–1589.
Kobayashi, Y., Ohbayashi, M., Kohyama, N., Yamamoto, T., 2005. Mouse organic anion transporter 2 and 3 (mOAT2/3[Slc22a7/8]) mediates the renal transport of bumetanide. Eur. J. Pharmacol. 524, 44–48.
Korpi, E.R., Kuner, T., Seeburg, P.H., Lã¼ddens, H., 1995. Selective antagonist for the cerebellar granule cell-specific gamma-aminobutyric acid type A receptor. Mol. Pharmacol. 47, 283–289.
Koumangoye, R., Bastarache, L., Delpire, E., 2021. NKCC1: Newly Found as a Human Disease-Causing Ion Transporter. Function, vol. 2. Oxf), p. zqaa028.
Kourdougli, N., Pellegrino, C., Renko, J.M., Khirug, S., Chazal, G., Kukko-Lukjanov, T.K., Lauri, S.E., Gaiarsa, J.L., Zhou, L., Peret, A., Castren, E., Tuominen, R.K., Crepel, V., Rivera, C., 2017. Depolarizing gamma-aminobutyric acid contributes to glutamatergic network rewiring in epilepsy. Ann. Neurol. 81, 251–265.
Köhling, R., Lucke, A., Straub, H., Speckmann, E.J., Tuxhorn, I., Wolf, P., Pannek, H., Oppel, F., 1998. Spontaneous sharp waves in human neocortical slices excised from epileptic patients. Brain 121 (Pt 6), 1073–1087.
Kursan, S., McMillen, T.S., Beesetty, P., Dias-Junior, E., Almutairi, M.M., Sajib, A.A., Kozak, J.A., Aguilar-Bryan, L., Di Fulvio, M., 2017. The neuronal K(+)Cl(-) co-transporter 2 (Slc12a5) modulates insulin secretion. Sci. Rep. 7, 1732.
Kusuhara, H., Sugiyama, Y., 2004. Efflux transport systems for organic anions and cations at the blood-CSF barrier. Adv. Drug Deliv. Rev. 56, 1741–1763.
Kusuhara, H., Sugiyama, Y., 2005. Active efflux across the blood-brain barrier: role of the solute carrier family. NeuroRx 2, 73–85.
Lemon, N., Canepa, E., Illies, M.A., Fossati, S., 2021. Carbonic anhydrases as potential targets against neurovascular unit dysfunction in Alzheimer's disease and stroke. Front. Aging Neurosci. 13, 772278.
Lemonnier, E., Ben Ari, Y., 2010. The diuretic bumetanide decreases autistic behaviour in five infants treated during 3 months with no side effects. Acta Paediatr. 99, 1885–1888.
Lemonnier, E., Degrez, C., Phelep, M., Tyzio, R., Josse, F., Grandgeorge, M., Hadjikhani, N., Ben Ari, Y., 2012. A randomised controlled trial of bumetanide in the treatment of autism in children. Transl. Psychiatry 2, e202.
Lemonnier, E., Villeneuve, N., Sonie, S., Serret, S., Rosier, A., Roue, M., Brosset, P., Viellard, M., Bernoux, D., Rondeau, S., Thummler, S., Ravel, D., Ben Ari, Y., 2017. Effects of bumetanide on neurobehavioral function in children and adolescents with autism spectrum disorders. Transl. Psychiatry 7, e1056.
Li, Y., Cleary, R., Kellogg, M., Soul, J.S., Berry, G.T., Jensen, F.E., 2011. Sensitive isotope dilution liquid chromatography/tandem mass spectrometry method for quantitative analysis of bumetanide in serum and brain tissue. J Chromatogr. B Analyt. Technol. Biomed. Life Sci. 879, 998–1002.
Löscher, W., Frey, H.-H., Reiche, R., Schultz, D., 1983. High anticonvulsant potency of y-aminobutyric acid(GABA)mimetic drugs in gerbils with genetically determined epilepsy. J. Pharmacol. Exp. Therapeut. 226, 839–844.
Löscher, W., 1985. Anticonvulsant action in the epileptic gerbil of novel inhibitors of GABA uptake. Eur. J. Pharmacol. 110, 103–108.
Löscher, W., 2002. Basic pharmacology of valproate: a review after 35 years of clinical use for the treatment of epilepsy. CNS Drugs 16, 669–694.
Löscher, W., Potschka, H., 2005. Drug resistance in brain diseases and the role of drug efflux transporters. Nat. Rev. Neurosci. 6, 591–602.
Löscher, W., Rogawski, M.A., 2012. How theories evolved concerning the mechanism of action of barbiturates. Epilepsia 53 (Suppl. 8), 12–25.
Löscher, W., Puskarjov, M., Kaila, K., 2013. Cation-chloride cotransporters NKCC1 and KCC2 as potential targets for novel antiepileptic and antiepileptogenic treatments. Neuropharmacology 69, 62–74.
Löscher, W., Friedman, A., 2020. Structural, molecular and functional alterations of the blood-brain barrier during epileptogenesis and epilepsy: a cause, consequence or both? Int. J. Mol. Sci. 21, 591.
Löscher, W., Kaila, K., 2021. Bumetanide and neonatal seizures: fiction vs. reality. Epilepsia 62, 941–946.
Lu, K.T., Wu, C.Y., Cheng, N.C., Wo, Y.Y., Yang, J.T., Yen, H.H., Yang, Y.L., 2006. Inhibition of the Na+ -K+ -2Cl- -cotransporter in choroid plexus attenuates traumatic brain injury-induced brain edema and neuronal damage. Eur. J. Pharmacol. 548, 99–105.
Lu, K.T., Cheng, N.C., Wu, C.Y., Yang, Y.L., 2008. NKCC1-mediated traumatic brain injury-induced brain edema and neuron death via Raf/MEK/MAPK cascade. Crit. Care Med. 36, 917–922.
Luo, L., Wang, J., Ding, D., Hasan, M.N., Yang, S.S., Lin, S.H., Schreppel, P., Sun, B., Yin, Y., Erker, T., Sun, D., 2020. Role of NKCC1 activity in glioma K(+) homeostasis and cell growth: new insights with the bumetanide-derivative STS66. Front. Physiol. 11, 911.
Lykke, K., Töllner, K., Römermann, K., Feit, P.W., Erker, T., Macaulay, N., Löscher, W., 2015. Structure-activity relationships of bumetanide derivatives: correlation between diuretic activity in dogs and inhibition of human NKCC2 variant A. Br. J. Pharmacol. 172, 4469–4480.
Lykke, K., Töllner, K., Feit, P.W., Erker, T., Macaulay, N., Löscher, W., 2016. The search for NKCC1-selective drugs for the treatment of epilepsy: structure-function relationship of bumetanide and various bumetanide derivatives in inhibiting the human cation-chloride cotransporter NKCC1A. Epilepsy Behav. 59, 42–49.
Mackenzie, A.E., Milligan, G., 2017. The emerging pharmacology and function of GPR35 in the nervous system. Neuropharmacology 113, 661–671.
Maguire, J., Salpekar, J.A., 2013. Stress, seizures, and hypothalamic-pituitary-adrenal axis targets for the treatment of epilepsy. Epilepsy Behav. 26, 352–362.
Mahadevan, V., Woodin, M.A., 2020. A historical overview of chloride transporter research. In: Tang, Y. (Ed.), Neuronal Chloride Transporters in Health and Disease. Academic Press, San Diego, pp. 1–17.
Marder, E., Goaillard, J.M., 2006. Variability, compensation and homeostasis in neuron and network function. Nat. Rev. Neurosci. 7, 563–574.

Marguet, S.L., Le Schulte, V.T., Merseburg, A., Neu, A., Eichler, R., Jakovcevski, I., Ivanov, A., Hanganu-Opatz, I.L., Bernard, C., Morellini, F., Isbrandt, D., 2015. Treatment during a vulnerable developmental period rescues a genetic epilepsy. Nat. Med. 21, 1436–1444.
Markadieu, N., Delpire, E., 2014. Physiology and pathophysiology of SLC12A1/2 transporters. Pflügers Archiv 466, 91–105.
Metz, J.T., Hajduk, P.J., 2010. Rational approaches to targeted polypharmacology: creating and navigating protein-ligand interaction networks. Curr. Opin. Chem. Biol. 14, 498–504.
Migliati, E., Meurice, N., DuBois, P., Fang, J.S., Somasekharan, S., Beckett, E., Flynn, G., Yool, A.J., 2009. Inhibition of aquaporin-1 and aquaporin-4 water permeability by a derivative of the loop diuretic bumetanide acting at an internal pore-occluding binding site. Mol. Pharmacol. 76, 105–112.
Migliati, E.R., Amiry-Moghaddam, M., Froehner, S.C., Adams, M.E., Ottersen, O.P., Bhardwaj, A., 2010. Na(+)-K (+)-2Cl (-) cotransport inhibitor attenuates cerebral edema following experimental stroke via the perivascular pool of aquaporin-4. Neurocritical Care 13, 123–131.
Miller, A.H., Haroon, E., Felger, J.C., 2017. The immunology of behavior-exploring the role of the immune system in brain health and illness. Neuropsychopharmacology 42, 1–4.
Mokgokong, R., Wang, S., Taylor, C.J., Barrand, M.A., Hladky, S.B., 2014. Ion transporters in brain endothelial cells that contribute to formation of brain interstitial fluid. Pflügers Archiv 466, 887–901.
Murakami, Y., Kohyama, N., Kobayashi, Y., Ohbayashi, M., Ohtani, H., Sawada, Y., Yamamoto, T., 2005. Functional characterization of human monocarboxylate transporter 6 (SLC16A5). Drug Metab. Dispos. 33, 1845–1851.
Murata, Y., Colonnese, M.T., 2020. GABAergic interneurons excite neonatal hippocampus in vivo. Sci. Adv. 6, eaba1430.
Nabel, C., Schweda, F., Riegger, G.A., KrÃ¤mer, B.K., Kurtz, A., 1999. Chloride channel blockers attenuate the inhibition of renin secretion by angiotensin II. Pflügers Archiv 438, 694–699.
Nguyen, M., Pace, A.J., Koller, B.H., 2007. Mice lacking NKCC1 are protected from development of bacteremia and hypothermic sepsis secondary to bacterial pneumonia. J. Exp. Med. 204, 1383–1393.
Nielsen, O.B.T., Feit, P.W., 1978. Structure-activity relationships of aminobenzoic acid diuretics and related compounds. In: Am. Chem. Soc. Symp. Ser., Diuretic Agents, 83, pp. 12–23.
Nishimura, M., Kakigi, A., Takeda, T., Takeda, S., Doi, K., 2009. Expression of aquaporins, vasopressin type 2 receptor, and Na+(-)K+(-)Cl(-) cotransporters in the rat endolymphatic sac. Acta Otolaryngol. 129, 812–818.
Norlander, A.E., Saleh, M.A., Pandey, A.K., Itani, H.A., Wu, J., Xiao, L., Kang, J., Dale, B. L., Goleva, S.B., Laroumanie, F., Du, L., Harrison, D.G., Madhur, M.S., 2017. A salt-sensing kinase in T lymphocytes, SGK1, drives hypertension and hypertensive end-organ damage. JCI. Insight. 2.
O'Toole, K.K., Hooper, A., Wakefield, S., Maguire, J., 2014. Seizure-induced disinhibition of the HPA axis increases seizure susceptibility. Epilepsy Res. 108, 29–43.
Oh, S.W., Han, S.Y., 2015. Loop Diuretics in Clinical Practice, vol. 13. Electrolyte Blood Press, pp. 17–21.
Olsen, U.B., 1977. The pharmacology of bumetanide. Acta Pharmacol. Toxicol. (Copenh) 41, 1–29.
Palfrey, H.C., Feit, P.W., Greengard, P., 1980. cAMP-stimulated cation cotransport in avian erythrocytes: inhibition by "loop" diuretics. Am. J. Physiol. 238, C139–C148.
Panet, R., Eliash, M., Pick, M., Atlan, H., 2002. Na(+)/K(+)/Cl(-) cotransporter activates mitogen-activated protein kinase in fibroblasts and lymphocytes. J. Cell. Physiol. 190, 227–237.
Pardridge, W.M., Hochman, D.W., 2017. BUMETANIDE ANALOGS, COMPOSITIONS and METHODS of USE. United States Patent US 9, 682,928 B2.
Pavlov, V.A., Chavan, S.S., Tracey, K.J., 2018. Molecular and functional neuroscience in immunity. Annu. Rev. Immunol. 36, 783–812.
Payne, J.A., Xu, J.C., Haas, M., Lytle, C.Y., Ward, D., Forbush III, B., 1995. Primary structure, functional expression, and chromosomal localization of the bumetanide-sensitive Na-K-Cl cotransporter in human colon. J. Biol. Chem. 270, 17977–17985.
Peón, A., Naulaerts, S., Ballester, P.J., 2017. Predicting the reliability of drug-target interaction predictions with maximum coverage of target space. Sci. Rep. 7, 3820.
Perry, J.S.A., Morioka, S., Medina, C.B., Iker, E.J., Barron, B., Raymond, M.H., Lucas, C. D., Onengut-Gumuscu, S., Delpire, E., Ravichandran, K.S., 2019. Interpreting an apoptotic corpse as anti-inflammatory involves a chloride sensing pathway. Nat. Cell Biol. 21, 1532–1543.
Pospelov, A.S., Puskarjov, M., Kaila, K., Voipio, J., 2020. Endogenous bain-sparing responses in brain pH and *P*O2 in a rodent model of birth asphyxia. Acta Physiol. 229, e13467.
Pospelov, A.S., Ala-Kurikka, T., Kurki, S., Voipio, J., Kaila, K., 2021. Carbonic anhydrase inhibitors suppress seizures in a rat model of birth asphyxia. Epilepsia 62, 1971–1984.
Pressler, R.M., Boylan, G.B., Marlow, N., Blennow, M., Chiron, C., Cross, J.H., De Vries, L. S., Hallberg, B., Hellstrom-Westas, L., Jullien, V., Livingstone, V., Mangum, B., Murphy, B., Murray, D., Pons, G., Rennie, J., Swarte, R., Toet, M.C., Vanhatalo, S., Zohar, S., 2015. Bumetanide for the treatment of seizures in newborn babies with hypoxic ischaemic encephalopathy (NEMO): an open-label, dose finding, and feasibility phase 1/2 trial. Lancet Neurol. 14, 469–477.
Puskarjov, M., Kahle, K.T., Ruusuvuori, E., Kaila, K., 2014. Pharmacotherapeutic targeting of cation-chloride cotransporters in neonatal seizures. Epilepsia 55, 806–818.
Quon, T., Lin, L.C., Ganguly, A., Tobin, A.B., Milligan, G., 2020. Therapeutic opportunities and challenges in targeting the Orphan G protein-coupled receptor GPR35. ACS Pharmacol. Transl. Sci. 3, 801–812.
Rao, K.V., Reddy, P.V., Curtis, K.M., Norenberg, M.D., 2011. Aquaporin-4 expression in cultured astrocytes after fluid percussion injury. J. Neurotrauma 28, 371–381.
Rao, M.S., Gupta, R., Liguori, M.J., Hu, M., Huang, X., Mantena, S.R., Mittelstadt, S.W., Blomme, E.A.G., Van Vleet, T.R., 2019. Novel computational approach to predict off-target interactions for small molecules. Front Big. Data 2, 25.
Rautio, J., Laine, K., Gynther, M., Savolainen, J., 2008. Prodrug approaches for CNS delivery. AAPS J. 10, 92–102.
Rautio, J., KÃ¤rkkÃ¤inen, J., Sloan, K.B., 2017. Prodrugs - recent approvals and a glimpse of the pipeline. Eur. J. Pharmaceut. Sci. 109, 146–161.
Raveendran, V.A., Pressey, J.C., Woodin, M.A., 2020. A novel small molecule targets NKCC1 to restore synaptic inhibition. Trends Pharmacol. Sci. 41, 897–899.
Rivera, C., Voipio, J., Payne, J.A., Ruusuvuori, E., Lahtinen, H., Lamsa, K., Pirvola, U., Saarma, M., Kaila, K., 1999. The K+/Cl- co-transporter KCC2 renders GABA hyperpolarizing during neuronal maturation. Nature 397, 251–255.
Rivera, C., Li, H., Thomas-Crusells, J., Lahtinen, H., Viitanen, T., Nanobashvili, A., Kokaia, Z., Airaksinen, M.S., Voipio, J., Kaila, K., Saarma, M., 2002. BDNF-induced TrkB activation down-regulates the K+-Cl- cotransporter KCC2 and impairs neuronal Cl- extrusion. J. Cell Biol. 159, 747–752.
Roush, G.C., Kaur, R., Ernst, M.E., 2014. Diuretics: a review and update. J. Cardiovasc. Pharmacol. Therapeut. 19, 5–13.
Roy, A.S., Sawrav, S.S., Hossain, S., Johura, F.T., Ahmed, F., Hami, I., Islam, K., Al Reza, H., Bhuiyan, M.I.H., Bahadur, N.M., Rahaman, M., 2021. *In silico* identification of potential inhibitors with higher potency than bumetanide targeting NKCC1: an important ion cotransporter to treat neurological disorders. Informatics in Medicine Unlocked (IMU) *in Press*.
Römermann, K., Fedrowitz, M., Hampel, P., Kaczmarek, E., Töllner, K., Erker, T., Sweet, D.H., Löscher, W., 2017. Multiple blood-brain barrier transport mechanisms limit bumetanide accumulation, and therapeutic potential, in the mammalian brain. Neuropharmacology 117, 182–194.
Russell, J.M., 2000. Sodium-potassium-chloride cotransport. Physiol. Rev. 80, 211–276.
Ruusuvuori, E., Kaila, K., 2014. Carbonic anhydrases and brain pH in the control of neuronal excitability. Subcell. Biochem. 75, 271–290.
Saidijam, M., Karimi, D.F., Sohrabi, S., Patching, S.G., 2018. Efflux proteins at the blood-brain barrier: review and bioinformatics analysis. Xenobiotica 48, 506–532.
Savardi, A., Borgogno, M., Narducci, R., La Sala, G., Ortega, J.A., Summa, M., Armirotti, A., Bertorelli, R., Contestabile, A., De Vivo, M., Cancedda, L., 2020. Discovery of a small molecule drug candidate for selective NKCC1 inhibition in brain disorders. Chem 6, 2073–2096.
Savardi, A., Borgogno, M., De Vivo, M., Cancedda, L., 2021. Pharmacological tools to target NKCC1 in brain disorders. Trends Pharmacol. Sci. 42, 1009–1034.
Schäfer, A.M., Meyer zu Schwabedissen, H.E., Grube, M., 2021. Expression and function of organic anion transporting polypeptides in the human brain: physiological and pharmacological implications. Pharmaceutics 13.
Schlatter, E., Greger, R., Weidtke, C., 1983. Effect of "high ceiling" diuretics on active salt transport in the cortical thick ascending limb of Henle's loop of rabbit kidney. Correlation of chemical structure and inhibitory potency. Pflügers Archiv 396, 210–217.
Schulte, J.T., Wierenga, C.J., Bruining, H., 2018. Chloride transporters and GABA polarity in developmental, neurological and psychiatric conditions. Neurosci. Biobehav. Rev. 90, 260–271.
Schwartz, M.A., 1981. Metabolism of bumetanide. J. Clin. Pharmacol. 21, 555–563.
Schwartzkroin, P.A., Baraban, S.C., Hochman, D.W., 1998. Osmolarity, ionic flux, and changes in brain excitability. Epilepsy Res. 32, 275–285.
Sedmak, G., Jovanov-Milosevic, N., Puskarjov, M., Ulamec, M., Kruslin, B., Kaila, K., Judas, M., 2016. Developmental expression patterns of KCC2 and functionally associated molecules in the human brain. Cerebr. Cortex 26, 4574–4589.
Shekarabi, M., Zhang, J., Khanna, A.R., Ellison, D.H., Delpire, E., Kahle, K.T., 2017. WNK kinase signaling in ion homeostasis and human disease. Cell Metabol. 25, 285–299.
Simard, J.M., Kahle, K.T., Gerzanich, V., 2010. Molecular mechanisms of microvascular failure in central nervous system injury–synergistic roles of NKCC1 and SUR1/TRPM4. J. Neurosurg. 113, 622–629.
Sipilä, S.T., Huttu, K., Soltesz, I., Voipio, J., Kaila, K., 2005. Depolarizing GABA acts on intrinsically bursting pyramidal neurons to drive giant depolarizing potentials in the immature hippocampus. J. Neurosci. 25, 5280–5289.
Sipilä, S.T., Schuchmann, S., Voipio, J., Yamada, J., Kaila, K., 2006. The cation-chloride cotransporter NKCC1 promotes sharp waves in the neonatal rat hippocampus. J. Physiol. 573, 765–773.
Sipilä, S.T., Huttu, K., Yamada, J., Afzalov, R., Voipio, J., Blaesse, P., Kaila, K., 2009. Compensatory enhancement of intrinsic spiking upon NKCC1 disruption in neonatal hippocampus. J. Neurosci. 29, 6982–6988.
Sivakumaran, S., Maguire, J., 2016. Bumetanide reduces seizure progression and the development of pharmacoresistant status epilepticus. Epilepsia 57, 222–232.
Somasekharan, S., Tanis, J., Forbush, B., 2012. Loop diuretic and ion-binding residues revealed by scanning mutagenesis of transmembrane helix 3 (TM3) of Na-K-Cl cotransporter (NKCC1). J. Biol. Chem. 287, 17308–17317.
Song, S., Luo, L., Sun, B., Sun, D., 2020. Roles of glial ion transporters in brain diseases. Glia 68, 472–494.
Soul, J.S., Bergin, A.M., Stopp, C., Hayes, B., Singh, A., Fortuno, C.R., O'Reilly, D., Krishnamoorthy, K., Jensen, F.E., Rofeberg, V., Dong, M., Vinks, A.A., Wypij, D., Staley, K.J., 2021. A pilot randomized, controlled,double-blind trial of bumetanide to treat neonatal seizures. Ann. Neurol. 89, 327–340.
Spoljaric, A., Seja, P., Spoljaric, I., Virtanen, M.A., Lindfors, J., Uvarov, P., Summanen, M., Crow, A.K., Hsueh, B., Puskarjov, M., Ruusuvuori, E., Voipio, J.,

Deisseroth, K., Kaila, K., 2017. Vasopressin excites interneurons to suppress hippocampal network activity across a broad span of brain maturity at birth. Proc. Natl. Acad. Sci. U. S. A 114, E10819–E10828.
Spoljaric, I., Spoljaric, A., Mavrovic, M., Seja, P., Puskarjov, M., Kaila, K., 2019. KCC2-Mediated Cl(-) extrusion modulates spontaneous hippocampal network events in perinatal rats and mice. Cell Rep. 26, 1073–1081.
Spratt, E.G., Nicholas, J.S., Brady, K.T., Carpenter, L.A., Hatcher, C.R., Meekins, K.A., Furlanetto, R.W., Charles, J.M., 2012. Enhanced cortisol response to stress in children in autism. J. Autism Dev. Disord. 42, 75–81.
Sprengers, J.J., van Andel, D.M., Zuithoff, N.P.A., Keijzer-Veen, M.G., Schulp, A.J.A., Scheepers, F.E., Lilien, M.R., Oranje, B., Bruining, H., 2021. Bumetanide for core symptoms of autism spectrum disorder (BAMBI): a single center, double-blinded, participant-randomized, placebo-controlled, phase-2 superiority trial. J. Am. Acad. Child Adolesc. Psychiatry 60, 865–876.
Stamboulian-Platel, S., Legendre, A., Chabrol, T., Platel, J.C., Pernot, F., Duveau, V., Roucard, C., Baudry, M., Depaulis, A., 2016. Activation of GABA(A) receptors controls mesiotemporal lobe epilepsy despite changes in chloride transporters expression: in vivo and in silico approach. Exp. Neurol. 284, 11–28.
Supuran, C.T., 2021. Emerging role of carbonic anhydrase inhibitors. Clin. Sci. (Lond) 135, 1233–1249.
Szklarczyk, D., Santos, A., von Mering, C., Jensen, L.J., Bork, P., Kuhn, M., 2016. STITCH 5: augmenting protein-chemical interaction networks with tissue and affinity data. Nucleic Acids Res. 44 (D1), D380–D384.
Taubes, A., Nova, P., Zalocusky, K.A., Kost, I., Bicak, M., Zilberter, M.Y., Hao, Y., Yoon, S. Y., Oskotsky, T., Pineda, S., Chen, B., Jones, E.A.A., Choudhary, K., Grone, B., Balestra, M.E., Chaudhry, F., Paranjpe, I., De Freitas, J., Koutsodendris, N., Chen, N., Wang, C., Chang, W., An, A., Glicksberg, B.S., Sirota, M., Huang, Y., 2021. Experimental and Real-World Evidence Supporting the Computational Repurposing of Bumetanide for *APOE4*-Related Alzheimer's Disease. Nature Aging *in press*.
Temperini, C., Cecchi, A., Scozzafava, A., Supuran, C.T., 2008. Carbonic anhydrase inhibitors. Sulfonamide diuretics revisited–old leads for new applications? Org. Biomol. Chem. 6, 2499–2506.
Thapar, A., Cooper, M., Rutter, M., 2017. Neurodevelopmental disorders. Lancet Psychiatr. 4, 339–346.
Theilmann, W., Brandt, C., Bohnhorst, B., Winstroth, A.-M., Das, A.M., Gramer, M., Kipper, A., Kalesse, M., Löscher, W., 2020. Hydrolytic Biotransformation of the Bumetanide Ester Prodrug DIMAEB to Bumetanide by Esterases in Neonatal Human and Rat Serum and Neonatal Rat Brain – A New Treatment Strategy for Neonatal Seizures? Epilepsia *in press*.
Tóth, K., Lénárt, N., Szabadits, E., Pósfai, B., Fekete, R., Cserép, C., Alatshan, A., Benkó, S., Hübner, C.M., Kaila, K., Környei, Z., Dénes, A., 2021. Microglial NKCC1 shapes microglial phenotype, cerebral inflammatory responses and brain injury. bioRxiv, 427597.
Töllner, K., Brandt, C., Töpfer, M., Brunhofer, G., Erker, T., Gabriel, M., Feit, P.W., Lindfors, J., Kaila, K., Löscher, W., 2014. A novel prodrug-based strategy to increase effects of bumetanide in epilepsy. Ann. Neurol. 75, 550–562.
Töllner, K., Brandt, C., Erker, T., Löscher, W., 2015a. Bumetanide is not capable of terminating status epilepticus but enhances phenobarbital efficacy in different rat models. Eur. J. Pharmacol. 746, 78–88.
Töllner, K., Brandt, C., Römermann, K., Löscher, W., 2015b. The organic anion transport inhibitor probenecid increases brain concentrations of the NKCC1 inhibitor bumetanide. Eur. J. Pharmacol. 746, 167–173.
Töpfer, M., Töllner, K., Brandt, C., Twele, F., Bröer, S., Löscher, W., 2014. Consequences of inhibition of bumetanide metabolism in rodents on brain penetration and effects of bumetanide in chronic models of epilepsy. Eur. J. Neurosci. 39, 673–687.
Tracey, K.J., 2002. The inflammatory reflex. Nature 420, 853–859.
van Andel, D.M., Sprengers, J.J., Oranje, B., Scheepers, F.E., Jansen, F.E., Bruining, H., 2020. Effects of bumetanide on neurodevelopmental impairments in patients with tuberous sclerosis complex: an open-label pilot study. Mol. Autism. 11, 30.
Van Vleet, T.R., Liguori, M.J., Lynch III, J.J., Rao, M., Warder, S., 2019. Screening strategies and methods for better off-target liability prediction and identification of small-molecule pharmaceuticals. SLAS. Discov. 24, 1–24.
Vandebroek, A., Yasui, M., 2020. Regulation of AQP4 in the central nervous system. Int. J. Mol. Sci. 21.
Vanhatalo, S., Palva, J.M., Andersson, S., Rivera, C., Voipio, J., Kaila, K., 2005. Slow endogenous activity transients and developmental expression of K+-Cl- cotransporter 2 in the immature human cortex. Eur. J. Neurosci. 22, 2799–2804.
Vargas, D.L., Nascimbene, C., Krishnan, C., Zimmerman, A.W., Pardo, C.A., 2005. Neuroglial activation and neuroinflammation in the brain of patients with autism. Ann. Neurol. 57, 67–81.
Vibat, C.R., Holland, M.J., Kang, J.J., Putney, L.K., O'Donnell, M.E., 2001. Quantitation of Na+-K+-2Cl- cotransport splice variants in human tissues using kinetic polymerase chain reaction. Anal. Biochem. 298, 218–230.
Vijay, N., Morris, M.E., 2014. Role of monocarboxylate transporters in drug delivery to the brain. Curr. Pharmaceut. Des. 20, 1487–1498.
Virtanen, M.A., Uvarov, P., Hübner, C.A., Kaila, K., 2020. NKCC1, an elusive molecular target in brain development: making sense of the existing data. Cells 9.
Virtanen, M.A., Uvarov, P., Mavrovic, M., Poncer, J.C., Kaila, K., 2021. The multifaceted roles of KCC2 in cortical development. Trends Neurosci. 44, 378–392.
Wallace, B.K., Foroutan, S., O'Donnell, M.E., 2011. Ischemia-induced stimulation of Na-K-Cl cotransport in cerebral microvascular endothelial cells involves AMP kinase. Am. J. Physiol. Cell Physiol. 301, C316–C326.
Wanaski, S., Partridge, J.J., Collins, S., 2010. Preparation of Bumetanide, Furosemide, Piretanide, Azosemide, and Torsemide Analogs and Therapeutic Compositions Containing Same for Treating Disorders Involving the Na+K+Cl- Cotransporter and $GABA_A$ Receptors. [International Patent WO2010085352A2.
Wanaski, S., Collins, S., Kincaid, J., 2012. Arylsulfonamide Derivatives as Sodium-Potassium-Chloride Cotransporter Inhibitors and Their Preparation, Compositions, and Methods of Use. [International Patent WO2012018635A2.
Wang, F., Wang, X., Shapiro, L.A., Cotrina, M.L., Liu, W., Wang, E.W., Gu, S., Wang, W., He, X., Nedergaard, M., Huang, J.H., 2017. NKCC1 up-regulation contributes to early post-traumatic seizures and increased post-traumatic seizure susceptibility. Brain Struct. Funct. 222, 1543–1556.
Wang, S., Zhang, X.Q., Song, C.G., Xiao, T., Zhao, M., Zhu, G., Zhao, C.S., 2015. In vivo effects of bumetanide at brain concentrations incompatible with NKCC1 inhibition on newborn DGC structure and spontaneous EEG seizures following hypoxia-induced neonatal seizures. Neuroscience 286, 203–215.
Ward, A., Heel, R.C., 1984. Bumetanide. A review of its pharmacodynamic and pharmacokinetic properties and therapeutic use. Drugs 28, 426–464.
Wargo, K.A., Banta, W.M., 2009. A comprehensive review of the loop diuretics: should furosemide be first line? Ann. Pharmacother. 43, 1836–1847.
Wilhelm, I., Nyul-Toth, A., Suciu, M., Hermenean, A., Krizbai, I.A., 2016. Heterogeneity of the blood-brain barrier. Tissue Barriers 4, e1143544.
Xu, J.C., Lytle, C., Zhu, T.T., Payne, J.A., Benz Jr., E., Forbush III, B., 1994. Molecular cloning and functional expression of the bumetanide-sensitive Na-K-Cl cotransporter. Proc. Natl. Acad. Sci. U. S. A 91, 2201–2205.
Yamazaki, Y., Abe, Y., Fujii, S., Tanaka, K.F., 2021. Oligodendrocytic Na^+-K^+-Cl^- co-transporter 1activity facilitates axonal conduction and restoresplasticity in the adult mouse brain. Nature Comm. 12, 5146.
Yang, X., Wang, Q., Cao, E., 2020. Structure of the human cation-chloride cotransporter NKCC1 determined by single-particle electron cryo-microscopy. Nat. Commun. 11, 1016.
Yang, Y., Fu, A., Wu, X., Reagan, J.D., 2012. GPR35 is a target of the loop diuretic drugs bumetanide and furosemide. Pharmacology 89, 13–17.
Zeisel, A., Hochgerner, H., Lönnerberg, P., Johnsson, A., Memic, F., van der, Z.J., Häring, M., Braun, E., Borm, L.E., La Manno, G., Codeluppi, S., Furlan, A., Lee, K., Skene, N., Harris, K.D., Hjerling-Leffler, J., Arenas, E., Ernfors, P., Marklund, U., Linnarsson, S., 2018. Molecular architecture of the mouse nervous system. Cell 174, 999–1014.
Zhang, J., Bhuiyan, M.I.H., Zhang, T., Karimy, J.K., Wu, Z., Fiesler, V.M., Zhang, J., Huang, H., Hasan, M.N., Skrzypiec, A.E., Mucha, M., Duran, D., Huang, W., Pawlak, R., Foley, L.M., Hitchens, T.K., Minnigh, M.B., Poloyac, S.M., Alper, S.L., Molyneaux, B.J., Trevelyan, A.J., Kahle, K.T., Sun, D., Deng, X., 2020a. Modulation of brain cation-Cl(-) cotransport via the SPAK kinase inhibitor ZT-1a. Nat. Commun. 11, 78.
Zhang, J., Cordshagen, A., Medina, I., Nothwang, H.G., Wisniewski, J.R., Winklhofer, M., Hartmann, A.M., 2020b. Staurosporine and NEM mainly impair WNK-SPAK/OSR1 mediated phosphorylation of KCC2 and NKCC1. PLoS One 15, e0232967.
Zhang, M., Cui, Z., Cui, H., Cao, Y., Zhong, C., Wang, Y., 2016. Astaxanthin alleviates cerebral edema by modulating NKCC1 and AQP4 expression after traumatic brain injury in mice. BMC Neurosci. 17, 60.
Zhang, S., Zhou, J., Zhang, Y., Liu, T., Friedel, P., Zhuo, W., Somasekharan, S., Roy, K., Zhang, L., Liu, Y., Meng, X., Deng, H., Zeng, W., Li, G., Forbush, B., Yang, M., 2021. The structural basis of function and regulation of neuronal cotransporters NKCC1 and KCC2. Commun. Biol. 4, 226.
Zhou, M.S., Nasir, M., Farhat, L.C., Kook, M., Artukoglu, B.B., Bloch, M.H., 2021. Meta-analysis: pharmacologic treatment of restricted and repetitive behaviors in autism spectrum disorders. J. Am. Acad. Child Adolesc. Psychiatry 60, 35–45.
Zhu, J.X., Xue, H., Ji, T., Xing, Y., 2011. Cellular localization of NKCC2 and its possible role in the Cl- absorption in the rat and human distal colonic epithelia. Transl. Res. 158, 146–154.